arXiv:1008.3933v2 [cond-mat.quant-gas] 20 Mar 2012

Chapter 9
The Unitary Fermi Gas: From Monte Carlo to Density Functionals

Aurel Bulgac, Michael McNeil Forbes and Piotr Magierski

Abstract In this chapter, we describe three related studies of the universal physics of two-component unitary Fermi gases with resonant short-ranged interactions. First we discuss an ab initio auxiliary field quantum Monte Carlo technique for calculating thermodynamic properties of the unitary gas from first principles. We then describe in detail a Density Functional Theory (DFT) fit to these thermodynamic properties: the Superfluid Local Density Approximation (SLDA) and its Asymmetric (ASLDA) generalization. We present several applications, including vortex structure, trapped systems, and a supersolid Larkin-Ovchinnikov (FFLO/LOFF) state. Finally, we discuss the time-dependent extension to the density functional (TDDFT) which can describe quantum dynamics in these systems, including non-adiabatic evolution, superfluid to normal transitions and other modes not accessible in traditional frameworks such as a Landau-Ginzburg, Gross-Pitaevskii, or quantum hydrodynamics.

Aurel Bulgac
Department of Physics, University of Washington, Seattle, WA, USA,
e-mail: bulgac@uw.edu

Michael McNeil Forbes
Institute for Nuclear Theory and Department of Physics,
University of Washington, Seattle, WA, USA,
T-2, Los Alamos National Laboratory, Los Alamos, NM, USA
e-mail: mforbes@uw.edu

Piotr Magierski
Faculty of Physics, Warsaw University of Technology, Warsaw, Poland,
e-mail: Piotr.Magierski@if.pw.edu.pl

Contents

9 The Unitary Fermi Gas: From Monte Carlo to Density Functionals . 1
Aurel Bulgac, Michael McNeil Forbes and Piotr Magierski
9.1 Introduction 2
9.2 The Quantum Monte Carlo Approach 5
9.2.1 From the Physical Problem to the Lattice Formulation . . . 5
9.2.2 Effective Hamiltonian 6
9.2.3 The Hubbard-Stratonovich Transformation 7
9.2.4 Stabilization of the Algorithm for Small Temperatures . . . 13
9.2.5 Finite Size Scaling 15
9.2.6 Results: the Energy and the Entropy 16
9.2.7 Response to External Probes and the Spectral Function . . 20
9.2.8 The Pairing Gap, Pseudogap, and Critical Temperature . . 22
9.2.9 Describing Trapped Systems with Quantum Monte Carlo Results 25
9.3 Density Functional Theory for the Unitary Fermi Gas 28
9.3.1 The Energy Density Functional 30
9.3.2 Determining the SLDA and ASLDA Energy Density Functionals 36
9.3.3 Using the SLDA and ASLDA 44
9.4 Time-Dependent Superfluid Local Density Approximation 48
9.4.1 Time-Dependent Equations for the Quasiparticle Wave Functions 48
9.4.2 Galilean Invariance 49
9.4.3 The Excitation of the Pairing Higgs Mode 52
9.4.4 Generation and Dynamics of Vortices 56
9.5 Concluding Remarks 60
References 61
9.6 Appendix 68
9.6.1 Formal Description of the DFT 68
9.6.2 Single Particle Hamiltonian 70

9.1 Introduction

The question of how pairing correlations between two types of fermions develop with interaction strength has fascinated physicists for decades, beginning with the papers of Eagles [1] and Leggett [2], and followed by many others [3, 4, 5, 6]. These initial studies focused on the inter-species pairing gap at various temperatures as the pairing interaction varied throughout the entire BCS–BEC crossover from weak to strong attraction.

Eagles and Leggett [1, 2] solved the Bardeen-Cooper-Schrieffer (BCS) mean-field equations only in the particle-particle (pairing) channel: The prevailing attitude

(influenced by electronic systems) was that the pairing gap is much smaller than the self-energy (exponentially suppressed in weak-coupling), and that the presence or absence of pairing correlations was a tiny effect compared to the background density which determined the self-energy. Subsequent improvements to the theory focused only on a more accurate description of the pairing channel [3, 4, 5, 6, 7, 8, 9, 10, 11], neglecting the so called "Hartree-Fock" contributions to the total energy of such a system.

However, even in the weak coupling limit ($a < 0$ and $k_F|a| \ll 1$ where the Fermi energy $\varepsilon_F = p_F^2/2m$, the Fermi momentum $p_F = \hbar k_F = \hbar(3\pi^2 n)^{1/3}$, n is the total density, and a is the two-body s-wave scattering length)—which was rather thoroughly studied in the 1950's [12, 13]—it was evident that the "Hartree-Fock" and higher order particle-hole contributions dominate in the total energy. These contributions can be described perturbatively in terms of the small parameter $k_F a$ (in both BCS and BEC limits). In the BCS limit, for example, the leading contributions enter at linear order $\propto \varepsilon_F k_F a$ while the particle-particle pairing contributions are exponentially suppressed $\propto \varepsilon_F \exp(\pi/k_F a)$.

Despite neglecting the dominant particle-hole contributions, these mean-field studies correctly captured many of the *qualitative* features of the BCS–BEC crossover. This can be partially attributed to the fact that the particle-particle channel correctly accounts for the two-body bound state that dominates in the extreme BEC limit at strong attraction (however, higher order effects—describing the dimer-dimer interaction for example—are not correct [14, 15, 16, 17]).

At unitarity, the majority of the interaction energy is due to the particle-hole channel: see [18] where the energy of the normal state at $T = 0$ was evaluated for the first time and the discussion in Sec. 9.2.6. In particular—above the critical temperature T_c, for example—the total energy of the normal phase exceeds the ground state energy by only about 20% or so [19]: This means that the condensation energy gained by the particle-particle pairing interaction is a relatively small contribution to the total interaction energy. A quantitative description of unitary physics must thus include these "Hartree-Fock" contributions and go beyond the simple mean-field models used initially to study the crossover.

In 1999, G. F. Bertsch [20] emphasized the special role played by the problem of a two-species Fermi gas at unitarity with large scattering length. In the crust of neutron stars one can find a situation where the scattering length a of the interaction is anomalously large compared to the other length scales, the average interparticle separation $n^{-1/3}$, and the range r_0 of the interaction: $r_0 \ll n^{-1/3} \ll |a|$. Since the Fermi momentum is small ($k_F r_0 \ll 1$), the neutrons effectively interact only in the relative s-partial wave, and the ground state energy should be some function of the physical parameters defining the system $E_{gs} = f(N,V,r_0,a,\hbar,m)$, where N is the particle number contained in a volume V of the system. In the formal limit of $k_F r_0 \to 0$ and $1/k_F a \to 0$ this function simplifies:

$$E_{gs} = f(N,V,\hbar,m) = \frac{3}{5}\varepsilon_F N \xi, \tag{9.1}$$

and all the non-perturbative effects are described by a single dimensionless constant: ξ (often referred to as the Bertsch parameter). At finite temperatures the total energy of the system becomes a slightly more complicated function, since now it depends also on the temperature T:

$$E(T) = f(N,V,T,\hbar,m) = \frac{3}{5}\varepsilon_F N\xi\left(\frac{T}{\varepsilon_F}\right). \tag{9.2}$$

The Bertsch parameter (along with all other thermodynamic properties) becomes a "universal" function of the dimensionless variable T/ε_F [21].

In 1999 it was not yet clear whether this limit existed: One might expect such a system to collapse, since the naïve coupling constant $g = 4\pi\hbar^2 a/m$ is infinite at unitarity. Baker [22, 23, 24] provided the first clue that this system was actually stable. Carlson and collaborators [18] subsequently calculated the energy of this system, proving that it was stable, and showing that the superfluid paring gap was very large. Meanwhile, using a Feshbach resonance to induce an extremely large scattering length, J. E. Thomas and his collaborators [25] produce for the first time a quantum degenerate unitary gas of cold-atoms in a trap, thus providing experimental evidence that this system is indeed stable.

There has since been an explosion in both theoretical and experimental studies of resonant Fermi gases near the unitary regime (see for example the reviews [26, 27, 28, 29, 30]). On one hand, cold-atom experiments can simulate other systems of interest; for example, dilute superfluid neutron matter which can only exist in the crust of neutron stars, various condensed matter systems (the unitary gas exhibits a pseudogap that might shed light on the pseudogap in high-temperature superconductors), and quantum systems with extremely low viscosity similar to quark-gluon plasmas observed in ultra-relativistic heavy-ion collisions. On the other hand, the simplicity of the system provides an excellent vehicle through which the plethora of many-body techniques can be put to rigorous test, including both traditional approaches, as well as modern developments such as the ε-expansion and AdS/CFT correspondence [31, 32].

We shall not provide a cursory review of current theoretical techniques, but will instead focus on a couple of theoretical methods that have produced a large reliable set of information about the properties of unitary Fermi gases. The first approach is an ab initio Quantum Monte Carlo (QMC) method that has accurately evaluated many properties of these systems, and has been confirmed by experiments. The second approach is Density Functional Theory (DFT), which is in principle, an exact approach commonly used for describing "normal" systems (no superfluidity). We show how to extend the DFT to describe both superfluid systems and time-dependent phenomena, and how the DFT allows us to address phenomena that are essentially impossible to describe within a QMC approach.

9.2 The Quantum Monte Carlo Approach

9.2.1 From the Physical Problem to the Lattice Formulation

Atomic collisions in a trap occur at very low relative velocities (due to the diluteness of the gas) and this fact allows us to restrict the description to using the lowest partial waves only. In practice, the s-wave scattering phase shift fully determines the properties of a unitary Fermi gas, for which $r_0 \ll n^{-1/3} \ll |a|$. The detailed physics of the collision is more complicated since atoms are not point-like objects and can appear in various configurations. Roughly speaking, these can be associated with various valence electronic configurations. For example, atoms with a single valence electron (such as ^{6}Li) can form two possible electronic configurations in a binary system: a singlet and a triplet configuration. The inter-atomic potential describing a singlet configuration corresponds to the symmetric spatial wave function. It admits the existence of a bound state and corresponds to the closed (inaccessible) scattering channel. The triplet channel, on the other hand, is open and shallow: due to large (mainly electronic) magnetic moment, its energy can be easily tuned with respect to the closed singlet channel threshold by adjusting an external magnetic field. This allows experimentalists to use a Feshbach resonance to tune the effective interaction in the open channel to virtually any value: in particular, experiments with dilute clouds of cold atoms can directly probe the unitary regime.

A typical Hamiltonian describing the two channel atom-atom collision is of the form [33, 34, 35, 36, 37]:

$$\boldsymbol{H} = \frac{p^2}{2M_r} + \sum_{i=1}^{2}(V_i^{hf} + V_i^Z) + V^c + V^d, \tag{9.3}$$

where M_r is the reduced mass of two atoms, $V^{hf} = a_{hf}\mathbf{S}^e \cdot \mathbf{S}^n/\hbar^2$ is a hyperfine interaction term for each atom (with hyperfine constant a_{hf}), and $\mathbf{S}^e$ and $\mathbf{S}^n$ are the total electron spin and the total nuclear spin respectively. The Zeeman term $V^Z = (\gamma_e S_z^e + \gamma_n S_z^p)B$ describes the interaction with the external magnetic field B which is assumed to be parallel to the z-axis. The terms V^c and V^d denote the Coulomb interaction and dipole-dipole magnetic interaction, respectively. The dipole term contributes weakly to the interaction and can be neglected. The Coulomb term distinguishes singlet and triplet channels (due to different symmetry properties of electronic wave function) and produces different interaction potentials in both channels. Consequently, the continuum of the singlet channel lies above the continuum of the incident triplet channel. At very low collision energies, only the singlet channel is open. However the hyperfine interaction couples the singlet and triplet states and consequently, resonant scattering may occur due to the bound state of the singlet potential (see reviews [38, 39, 40] and references therein). An external magnetic field can thus be used as an experimental knob to control the resonance position, effectively altering the atom-atom collision cross-section. In the limit of low collisional energy, the effective scattering length for two colliding atoms is well described by

$$a(B) = a_0 + \frac{C}{B - B_{\rm res}}, \tag{9.4}$$

where a_0 is the triplet channel off-resonant background scattering length, and $C > 0$. The second term results from the coupling to the closed channel, and $B_{\rm res}$ is the value of the magnetic field where the Feshbach resonance occurs. In this way, experiments may realized the unitary Fermi gas by considering dilute systems ($r_0 \ll n^{-1/3}$) and tuning the scattering length (9.4) near the resonance ($n^{-1/3} \ll |a|$).

To determine the thermodynamic properties of an ensemble of fermionic atoms in a non-perturbative manner, we consider the system on a three dimensional (3D) cubic spatial lattice with periodic boundary conditions. The system consists of two species of fermions that we shall denote "a" and "b". In dilute neutron matter these would correspond to the two spin states of the neutrons, while in cold atom experiments these are the two populated hyperfine states. Although there are physical processes that can convert one species to another, for the purposes of the experiments we shall describe, these transitions are highly suppressed and one can consider each species to be independently conserved.

The lattice spacing l and size $L = N_s l$ introduce natural ultraviolet (UV) and infrared (IR) momentum cut-offs given by $\hbar k_c = \pi\hbar/l$ and $\hbar\Lambda_0 = 2\pi\hbar/L$, respectively. The momentum space has the shape of a cubic lattice, but in order to simplify the analysis, we place a spherically symmetric UV cut-off, including only momenta satisfying $k \le k_c \le \pi/l$. In order to minimize the discretization errors, the absolute value of scattering length must be much larger than the lattice spacing: $a \gg l$.

9.2.2 Effective Hamiltonian

As discussed in the introduction, it has by now been well established that the unitary regime exists and is stable. Hence, any sufficiently short-ranged interaction with large scattering length will exhibit the same universal physics. Here we use a contact (zero-range) interaction $V(\mathbf{r}_1 - \mathbf{r}_2) = -g\delta(\mathbf{r}_1 - \mathbf{r}_2)$ regularized by the lattice, which defines a momentum cut-off $\hbar k_c$. (We require all two-body matrix elements to vanish if the relative momentum of the incoming particles exceeds this cutoff.) The second quantized Hamiltonian of this system is

$$\hat{H} = \int \mathrm{d}^3 r \left(- \sum_{\sigma=a,b} \hat{\psi}^+_\sigma(\mathbf{r}) \frac{\hbar^2\nabla^2}{2m} \hat{\psi}_\sigma(\mathbf{r}) + g\hat{n}_a(\mathbf{r})\hat{n}_b(\mathbf{r}) \right), \tag{9.5}$$

where $\hat{n}_\sigma(\mathbf{r}) = \hat{\psi}^+_\sigma(\mathbf{r})\hat{\psi}_\sigma(\mathbf{r})$. Once the cutoff is imposed, the value of the bare coupling g can be tuned to fix the value of the renormalized physical coupling—in this case, the s-wave scattering length a. The relation between a and the coupling constant g can be obtained from T matrix describing two-particle scattering induced by the interaction (9.5) with the s-wave phase shift:

$$k\cot\delta = -\frac{4\pi\hbar^2}{gm} - \frac{2}{\pi}k_c - \frac{k}{\pi}\ln\left|\frac{k_c-k}{k_c+k}\right|. \tag{9.6}$$

The low-momentum expansion of the scattering amplitude reads:

$$f(k) \approx \left[-\mathrm{i}k + \frac{4\pi\hbar^2}{gm} - \frac{2k_c}{\pi} + \frac{2k^2}{\pi k_c} + \mathrm{O}(k^3)\right]^{-1}. \tag{9.7}$$

At low momentum we have $f(k) = [-\mathrm{i}k - 1/a + r_{\mathrm{eff}}k^2/2 + \mathrm{O}(k^3)]^{-1}$, which gives the relation between the bare coupling constant g and the scattering length a at a given momentum cutoff $\hbar k_c$:

$$\frac{1}{g} = \frac{m}{4\pi\hbar^2 a} - \frac{k_c m}{2\pi^2\hbar^2} = \frac{m}{4\pi\hbar^2 a}\left(1 - \frac{2k_c a}{\pi}\right). \tag{9.8}$$

One has to remember, however, that the value of the coupling constant g has been determined for the two body system in its center of mass frame. On the other hand the Hamiltonian (9.5) is supposed to describe an ensemble of fermions in the box. Consequently, only a fraction of interacting pairs have their center of mass at rest with respect to the box. Most of the interaction processes will occur for pairs for which the center of mass velocity is nonzero. It implies that their mutual interaction will be characterized by a slightly different scattering length than (9.8). Consequently, the Hamiltonian will generate a systematic error in the description of interacting fermions. This error will scale as k_F/k_c and in order to minimize its influence one should keep the particle density as small as possible. Another source of systematic error is related to the nonzero effective range, which is generated by the interaction and is independent of the coupling constant $r_{\mathrm{eff}} = 4/(\pi k_c)$. Note however that the choice of k_c described above implies that $r_{\mathrm{eff}} < l$.

9.2.3 The Hubbard-Stratonovich Transformation

Since we are interested in the finite temperature thermodynamic properties of the system, it is natural to use the grand canonical ensemble to evaluate physical quantities. This is equivalent to considering a small portion of volume $V = L^3$ in thermal and chemical equilibrium with the larger system. Consequently we allow for energy and particle exchange between our subsystem and the larger system, fixing only the average values of these quantities in the box. The thermodynamic variables are thus the temperature T, the chemical potential μ, and the volume V. The partition function and average of an observable $\hat{O}$ are calculated according to

$$\begin{aligned} Z(\beta,\mu,V) &= \mathrm{Tr}\left\{\exp[-\beta(\hat{H}-\mu\hat{N})]\right\}, \\ O(\beta,\mu,V) &= \frac{\mathrm{Tr}\,\left\{\hat{O}\exp[-\beta(\hat{H}-\mu\hat{N})]\right\}}{Z(\beta,\mu,V)}, \end{aligned} \tag{9.9}$$

where $\beta = 1/T$ (in this work we will take Boltzmann's constant to be $k_B = 1$ so that temperature is expressed in units of energy). In order to be able to calculate these quantities we first factorize the statistical weight using the Trotter formula:

$$\exp[-\beta(\hat{H}-\mu\hat{N})] = \prod_{j=1}^{N_\tau} \exp[-\tau(\hat{H}-\mu\hat{N})] \tag{9.10}$$

where $\beta = N_\tau\tau$. The next step is to decompose the exponentials on the right hand side into exponentials that depend separately on the kinetic and potential energy operators. The second order expansion is (higher orders require more effort, see [41, 42, 43, 44]):

$$\begin{aligned}&\exp[-\tau(\hat{H}-\mu\hat{N})]\\ &\quad= \exp\left[-\frac{\tau(\hat{K}-\mu\hat{N})}{2}\right]\exp(-\tau\hat{V})\exp\left[-\frac{\tau(\hat{K}-\mu\hat{N})}{2}\right]+\mathrm{O}(\tau^3),\end{aligned} \tag{9.11}$$

where $\hat{K}$ is the kinetic energy operator, whose dispersion relation, for momenta smaller than the cut-off, is given by $\varepsilon_{\mathbf{k}} = \hbar^2k^2/2m$. Since τ has the dimension of inverse energy, the above approximate representation makes sense only if $\tau_{\max}\|\hat{V}\| \ll 1$ and $\tau_{\max}\|\hat{K}-\mu\hat{N}\| \ll 1$. Since both the interaction and kinetic energies are extensive quantities, this restriction might appear as very strict. However, after performing a Hubbard-Stratonovich transformation (see below), this restriction is considerably eased and both the kinetic and the interaction energies in these inequalities are replaced by the corresponding intensive energies per particle. It is important to note that, because we have used the expansion up to $\mathrm{O}(\tau^3)$, when calculating the partition function the error becomes $\mathrm{O}(\tau^2)$. Indeed, the statistical weight involves a product of N_τ factors and is given by the following expression:

$$\begin{aligned}&\exp[-\beta(\hat{H}-\mu\hat{N})] = \exp\left[-\frac{\tau(\hat{K}-\mu\hat{N})}{2}\right]\\ &\quad\times\left(\prod_{j=1}^{N_\tau}\exp[-\tau\hat{V}]\exp[-\tau(\hat{K}-\mu\hat{N})]\right)\exp\left[+\frac{\tau(\hat{K}-\mu\hat{N})}{2}\right]+\mathrm{O}(\tau^2)\end{aligned} \tag{9.12}$$

Note also that this approach does not depend on the choice of dispersion relation in the kinetic energy term. However various choices of representation of derivatives on the lattice may lead to different discretization errors [45]. In our case we shall consider the kinetic energy operator in momentum space, $\varepsilon(k) = \hbar^2k^2/2m$, which minimizes the discretization errors.

In order to efficiently evaluate the term containing the interaction, one has to replace it by the sum (or integral) of one body terms. This can be done with the Hubbard-Stratonovich transformation [46]. The transformation is not unique, and we take advantage of this freedom to ensure an efficient summation (or integration) scheme. In our case, due to the simplicity of the interaction term, a discrete Hubbard-Stratonovich transformation can be applied, similar to that in [47]:

$$\exp[-g\tau\hat{n}_a(\mathbf{r})\hat{n}_b(\mathbf{r})] = \frac{1}{2}\sum_{\sigma(\mathbf{r},\tau_j)=\pm 1}[1+A\sigma(\mathbf{r},\tau_j)\hat{n}_a(\mathbf{r})][1+A\sigma(\mathbf{r},\tau_j)\hat{n}_b(\mathbf{r})], \tag{9.13}$$

where $A=\sqrt{\exp(-g\tau)-1}$, τ_j labels the location on the imaginary time axis, $j=1,\ldots,N_\tau$, and $\sigma(\mathbf{r},\tau_j)$ is a field that can take values ± 1 at each point on the space-time lattice. This identity can be proved simply by evaluating both sides at $\hat{n}_{\{a,b\}}(\mathbf{r})=0,1$. This discrete Hubbard-Stratonovich transformation is sensible only for $A<1$, which means that the imaginary time step cannot exceed $|g|^{-1}\log 2$. The advantages of this transform is discussed, for example, in [47, 45].

Taking all this into account, the grand canonical partition function becomes

$$Z(\beta,\mu,V) = \mathrm{Tr}\left\{\exp[-\beta(\hat{H}-\mu\hat{N})]\right\} = \int\prod_{\mathbf{r},\tau_j}\mathscr{D}\sigma(\mathbf{r},\tau_j)\mathrm{Tr}\,\hat{\mathscr{U}}(\{\sigma\}), \tag{9.14}$$

where we define

$$\hat{\mathscr{U}}(\{\sigma\}) = \prod_{j=1}^{N_\tau}\hat{\mathscr{W}}_j(\{\sigma\}) \tag{9.15}$$

and

$$\begin{aligned}\hat{\mathscr{W}}_j(\{\sigma\}) &= \exp\left[-\frac{\tau(\hat{K}-\mu\hat{N})}{2}\right]\\ &\times\left(\prod_{\mathbf{i}}[1+A\sigma(\mathbf{r},\tau_j)\hat{n}_a(\mathbf{r})][1+A\sigma(\mathbf{r},\tau_j)\hat{n}_b(\mathbf{r})]\right)\exp\left[-\frac{\tau(\hat{K}-\mu\hat{N})}{2}\right].\end{aligned} \tag{9.16}$$

Since $\sigma(\mathbf{r},\tau)$ is discrete, the integration is in fact a summation:

$$\int\prod_{\mathbf{r},\tau_j}\mathscr{D}\sigma(\mathbf{r},\tau_j) \equiv \sum_{\{\sigma\}}\frac{1}{2^{N_s^3N_\tau}}\sum_{\{\sigma(\mathbf{r},\tau_1)\}=\pm 1}\sum_{\{\sigma(\mathbf{r},\tau_2)\}=\pm 1}\cdots\sum_{\{\sigma(\mathbf{r},\tau_{N_\tau})\}=\pm 1}, \tag{9.17}$$

where

$$\sum_{\{\sigma(\mathbf{r},\tau_j)\}=\pm 1} = \sum_{\sigma((1,0,0),\tau_j)=\pm 1}\sum_{\sigma((2,0,0),\tau_j)=\pm 1}\cdots\sum_{\sigma((N_s,N_s,N_s),\tau_j)=\pm 1}. \tag{9.18}$$

In a shorthand notation we will write

$$\hat{\mathscr{U}}(\{\sigma\}) = \mathrm{T}_\tau\exp\left\{-\int\mathrm{d}\tau[\hat{h}(\{\sigma\})-\mu\hat{N}]\right\},$$

where T_τ stands for an imaginary time ordering operator and $\hat{h}(\{\sigma\})$ is a resulting σ-dependent one-body Hamiltonian. It is crucial to note that $\hat{\mathscr{U}}(\{\sigma\})$ can be expressed as a product of two operators which describe the imaginary time evolution of two species of fermions:

$$\hat{\mathscr{U}}(\{\sigma\}) = \hat{\mathscr{U}}_b(\{\sigma\})\hat{\mathscr{U}}_a(\{\sigma\}), \tag{9.19a}$$

$$\hat{\mathscr{U}}_b(\{\sigma\}) = \prod_{j=1}^{N_\tau} \hat{\mathscr{W}}_{jb}(\{\sigma\}), \qquad \hat{\mathscr{U}}_a(\{\sigma\}) = \prod_{j=1}^{N_\tau} \hat{\mathscr{W}}_{ja}(\{\sigma\}). \tag{9.19b}$$

As we only consider unpolarized systems, for which $\mu_a = \mu_b = \mu$, the operators for both species a and b are identical.

The expectation values of operators take the form:

$$O(\beta,\mu,V) = \frac{\mathrm{Tr}\,\left\{\hat{O}\exp[-\beta(\hat{H}-\mu\hat{N})]\right\}}{Z(\beta,\mu,V)} = \\ = \int \frac{\prod_{\mathbf{i}j}\mathscr{D}\sigma(\mathbf{r},\tau_j)\mathrm{Tr}\,\hat{\mathscr{U}}(\{\sigma\})}{Z(\beta,\mu,V)} \frac{\mathrm{Tr}\,\hat{O}\hat{\mathscr{U}}(\{\sigma\})}{\mathrm{Tr}\,\hat{\mathscr{U}}(\{\sigma\})}, \tag{9.20}$$

where we have introduced $\mathrm{Tr}\,\hat{\mathscr{U}}(\{\sigma\})$ for convenience: in the numerator it represents the probability measure used in our simulations (see below), and in the denominator it serves the purpose of moderating the variations of $\mathrm{Tr}\,\hat{O}\hat{\mathscr{U}}(\{\sigma\})$ as a function of the auxiliary field σ.

All of the above traces over Fock space acquire very simple forms [48, 49], and can be easily evaluated. In particular, $\mathrm{Tr}\,\hat{\mathscr{U}}(\{\sigma\})$ can be written as

$$\mathrm{Tr}\,\hat{\mathscr{U}}(\{\sigma\}) = \det[1+\mathscr{U}(\{\sigma\})] = \det[1+\mathscr{U}_b(\{\sigma\})]\det[1+\mathscr{U}_a(\{\sigma\})], \tag{9.21}$$

where $\mathscr{U}$ (without the hat) is the representation of $\hat{\mathscr{U}}$ in the single-particle Hilbert space. The second equality is a result of the decomposition (9.19) and is easy to prove by expanding both sides. For symmetric (unpolarized) systems the chemical potentials $\mu_a = \mu_b$ are the same for both species of fermion, so it follows that $\det[1+\mathscr{U}_b(\{\sigma\})] = \det[1+\mathscr{U}_a(\{\sigma\})]$. This implies that $\mathrm{Tr}\,\hat{\mathscr{U}}(\{\sigma\})$ is positive, i.e., that there is no fermion sign problem. Indeed, this allows to define a positive definite probability measure:

$$P(\{\sigma\}) = \frac{\mathrm{Tr}\,\hat{\mathscr{U}}(\{\sigma\})}{Z(\beta,\mu,V)} = \frac{\{\det[1+\mathscr{U}_a(\{\sigma\})]\}^2}{Z(\beta,\mu,V)} \\ = \frac{1}{Z(\beta,\mu,V)}\exp(2\,\mathrm{tr}\,(\log[1+\mathscr{U}_a(\{\sigma\})])) \tag{9.22}$$

where the exponent in the last equation defines the negative of the so-called effective action. The positive definite probability measure is crucial for Monte Carlo (MC) treatment, allowing for statistical sampling of the σ space. When considering the polarized system, the sign problem inevitably occurs, making the Monte Carlo procedure very difficult. The sign problem appears also when more complicated forms of interaction are applied. In such a case one can sometimes cure the problem by properly choosing the Hubbard-Stratonovich transformation [50].

The many-fermion problem is thus reduced to an Auxiliary Field Quantum Monte Carlo problem (AFQMC), to which the standard Metropolis algorithm can be applied,

using (9.22) as a probability measure. Before moving on to the details of our Monte Carlo algorithm, we briefly discuss the expressions used to compute a few specific thermal averages.

Let us consider the one body operator

$$\hat{O} = \sum_{s,t=b,a} \int \mathrm{d}^3\mathbf{r}_1 d^3\mathbf{r}_2 \hat{\psi}_s^+(\mathbf{r}_1) O_{st}(\mathbf{r}_1,\mathbf{r}_2) \hat{\psi}_t(\mathbf{r}_2) \tag{9.23}$$

From (9.20) it follows that

$$\langle \hat{O} \rangle = \sum_{\{\sigma\}} P(\{\sigma\}) \frac{\mathrm{Tr}\, \hat{O}\hat{\mathscr{U}}(\{\sigma\})}{\mathrm{Tr}\, \hat{\mathscr{U}}(\{\sigma\})} = \sum_{\{\sigma\}} P(\{\sigma\}) \frac{\mathrm{Tr}\, \hat{O}\hat{\mathscr{U}}(\{\sigma\})}{\det[1+\mathscr{U}(\{\sigma\})]}. \tag{9.24}$$

The calculation of the last term requires the evaluation of

$$\mathrm{Tr}\left[\hat{\psi}_s^+(\mathbf{r}_1)\hat{\psi}_t(\mathbf{r}_2)\hat{\mathscr{U}}(\{\sigma\})\right] = \delta_{st} \det[1+\mathscr{U}(\{\sigma\})]^2 n_s(\mathbf{r}_1,\mathbf{r}_2,\{\sigma\}) \tag{9.25}$$

where s and t run over both species (a or b), and

$$n_s(\mathbf{r}_1,\mathbf{r}_2,\{\sigma\}) = \sum_{\mathbf{k}_1,\mathbf{k}_2 \le k_c} \varphi_{\mathbf{k}_1}(\mathbf{r}_1) \left[\frac{\mathscr{U}_s(\{\sigma\})}{1+\mathscr{U}_s(\{\sigma\})}\right]_{\mathbf{k}_1,\mathbf{k}_2} \varphi^*_{\mathbf{k}_2}(\mathbf{r}_2) \tag{9.26}$$

Here $\varphi_{\mathbf{k}}(\mathbf{r}) = \exp(i\mathbf{k}\cdot\mathbf{r})/L^{3/2}$ are the single-particle orbitals on the lattice with periodic boundary conditions, and hence quantized momenta $\mathbf{k} = 2\pi\mathbf{n}/L$. This holds for any 1-body operator $\hat{O}$, if $\mathscr{U}$ is a product of exponentials of 1-body operators, as is the case once the Hubbard-Stratonovich transformation is performed. It is then obvious that the momentum representation of the one-body density matrix has the form

$$n_s(\mathbf{k}_1,\mathbf{k}_2,\{\sigma\}) = \left[\frac{\mathscr{U}_s(\{\sigma\})}{1+\mathscr{U}_s(\{\sigma\})}\right]_{\mathbf{k}_1,\mathbf{k}_2} \tag{9.27}$$

which, for a non-interacting homogeneous Fermi gas, is diagonal and equal to the occupation number probability $1/(\exp[\beta(\varepsilon_{\mathbf{k}}-\mu)]+1)$ of a state with the energy $\varepsilon_{\mathbf{k}} = \hbar^2k^2/(2m)$.

Summarizing, the expectation value of any one-body operator may be calculated by summing over samples of the auxiliary field $\sigma(\mathbf{r},\tau_j)$:

$$\langle \hat{O} \rangle = \int \prod_{\mathbf{r},\tau_j} \mathscr{D}\sigma(\mathbf{r},\tau_j) P(\{\sigma\}) \sum_{\mathbf{r}_1,\mathbf{r}_2} \sum_{s=a,b} O_{ss}(\mathbf{r}_1,\mathbf{r}_2) n_s(\mathbf{r}_1,\mathbf{r}_2,\{\sigma\}) \tag{9.28}$$

In particular, the kinetic energy can be calculated according to:

$$\langle \hat{K} \rangle = \int \frac{\prod_{\mathbf{r},\tau_j} \mathscr{D}\sigma(\mathbf{r},\tau_j) \mathrm{Tr}\, \mathscr{U}(\{\sigma\})}{Z(\beta,\mu,V)} \frac{\mathrm{Tr}\, \hat{K}\mathscr{U}(\{\sigma\})}{\mathrm{Tr}\, \mathscr{U}(\{\sigma\})}$$
$$= \int \prod_{\mathbf{r},\tau_j} \mathscr{D}\sigma(\mathbf{r},\tau_j) P(\{\sigma\}) \sum_{\mathbf{k}}^{k\leq k_c} \sum_{s=a,b} \left[n_s(\mathbf{k},\mathbf{k},\{\sigma\}) \frac{\hbar^2 \mathbf{k}^2}{2m} \right] \quad (9.29)$$

Analogously, for a generic two-body operator:

$$\hat{O} = \sum_{s,t,u,v=b,a} \int \mathrm{d}^3\mathbf{r}_1' \mathrm{d}^3\mathbf{r}_2' \mathrm{d}^3\mathbf{r}_1 \mathrm{d}^3\mathbf{r}_2 \hat{\psi}_s^+(\mathbf{r}_1') \hat{\psi}_t^+(\mathbf{r}_2') O_{stuv}(\mathbf{r}_1',\mathbf{r}_2',\mathbf{r}_1,\mathbf{r}_2) \hat{\psi}_v(\mathbf{r}_2) \hat{\psi}_u(\mathbf{r}_1). \quad (9.30)$$

In order to calculate $\langle \hat{O} \rangle$ one needs to evaluate the expression

$$\mathrm{Tr}\left[\hat{\psi}_s^+(\mathbf{r}_1') \hat{\psi}_t^+(\mathbf{r}_2') \hat{\psi}_v(\mathbf{r}_2) \hat{\psi}_u(\mathbf{r}_1) \hat{\mathscr{U}}(\{\sigma\}) \right]$$
$$= (\det[1+\mathscr{U}(\{\sigma\})])^2 \Big(\delta_{su}\delta_{tv} n_s(\mathbf{r}_1',\mathbf{r}_1,\{\sigma\}) n_t(\mathbf{r}_2',\mathbf{r}_2,\{\sigma\})$$
$$- \delta_{sv}\delta_{tu} n_s(\mathbf{r}_1',\mathbf{r}_2,\{\sigma\}) n_t(\mathbf{r}_2',\mathbf{r}_1,\{\sigma\}) \Big). \quad (9.31)$$

Hence, for the expectation value of the two body operator we get

$$\langle \hat{O} \rangle = \int \prod_{\mathbf{r},\tau_j} \mathscr{D}\sigma(\mathbf{r},\tau_j) P(\{\sigma\})$$
$$\times \sum_{\mathbf{r}_1',\mathbf{r}_2',\mathbf{r}_1,\mathbf{r}_2} \sum_{s,t=a,b} \Big[O_{stst}(\mathbf{r}_1',\mathbf{r}_2',\mathbf{r}_1,\mathbf{r}_2) n_s(\mathbf{r}_1',\mathbf{r}_1,\{\sigma\}) n_t(\mathbf{r}_2',\mathbf{r}_2,\{\sigma\})$$
$$- O_{stts}(\mathbf{r}_1',\mathbf{r}_2',\mathbf{r}_1,\mathbf{r}_2) n_s(\mathbf{r}_1',\mathbf{r}_2,\{\sigma\}) n_t(\mathbf{r}_2',\mathbf{r}_1,\{\sigma\}) \Big]. \quad (9.32)$$

In particular, the expectation value of the interaction energy reads:

$$\langle \hat{V} \rangle = -g \int \prod_{\mathbf{r},\tau_j} \mathscr{D}\sigma(\mathbf{r},\tau_j) P(\{\sigma\}) \sum_{\mathbf{r}} n_a(\mathbf{r},\mathbf{r},\{\sigma\}) n_b(\mathbf{r},\mathbf{r},\{\sigma\}) \quad (9.33)$$

It should be noted that in the symmetric system ($\mu_a = \mu_b$)

$$n_a(\mathbf{r},\mathbf{r}',\{\sigma\}) = n_b(\mathbf{r},\mathbf{r}',\{\sigma\}). \quad (9.34)$$

Hence,

$$\langle \hat{V} \rangle = -g \int \prod_{\mathbf{r},\tau_j} \mathscr{D}\sigma(\mathbf{r},\tau_j) P(\{\sigma\}) \sum_{\mathbf{r}} [n_a(\mathbf{r},\mathbf{r},\{\sigma\})]^2 \quad (9.35)$$

It is useful to introduce the correlation function

$$g_2(\mathbf{r}) = \left(\frac{2}{N}\right)^2 \int \mathrm{d}^3\mathbf{r}_1 \mathrm{d}^3\mathbf{r}_2 \langle \psi_a^\dagger(\mathbf{r}_1+\mathbf{r})\psi_b^\dagger(\mathbf{r}_2+\mathbf{r})\psi_b(\mathbf{r}_2)\psi_a(\mathbf{r}_1)\rangle$$
$$= \left(\frac{2}{N}\right)^2 \int \prod_{\mathbf{r},\tau_j} \mathscr{D}\sigma(\mathbf{r},\tau_j) P(\{\sigma\})$$
$$\times \int \mathrm{d}^3\mathbf{r}_1 \mathrm{d}^3\mathbf{r}_2 n_a(\mathbf{r}_1+\mathbf{r},\mathbf{r}_1,\{\sigma\}) n_b(\mathbf{r}_2+\mathbf{r},\mathbf{r}_2,\{\sigma\}), \tag{9.36}$$

(where N is the average particle number) which is normalized in such a way that for a non-interacting homogeneous Fermi gas $g_2(\mathbf{r}) = 3j_1(k_F r)/(k_F r)$ and $g_2(0) = 1$.

9.2.4 Stabilization of the Algorithm for Small Temperatures

Once we have written the observables as in (9.20), the next step is to sum over all possible configurations of $\sigma(\mathbf{r},\tau_j)$. This is still an impossible task, as for example, a lattice size $N_x^3 \times N_\tau$ (where typically $N_x = 8$ and $N_\tau \simeq 1000$), requires performing the sum over the $2^{N_x^3 \times N_\tau}$ points in configuration space. It is in these cases that a Monte Carlo approach becomes essential. By generating $\mathscr{N}$ independent samples of the field $\sigma(\mathbf{r},\tau_j)$ with probability given by (9.22), and adding up the values of the integrand at those samples, one can estimate averages of observables with $\mathrm{O}(1/\sqrt{\mathscr{N}})$ accuracy.

The standard Metropolis algorithm is used to generate the samples. Namely, at every MC step, the sign of σ is changed at random locations of the space-time lattice (see [19, 45, 51] for details). This procedure allows to probe the sigma space, in order to collect the set of statistically uncorrelated samples.

In order to compute the probability of a given σ configuration, it is necessary to find the matrix elements of $\mathscr{U}$, which entails applying it to a complete set of single-particle wave-functions. For the latter we chose plane waves (with momenta $\hbar k \leq \hbar k_c$). This choice is particularly convenient because one can compute the overlap of any given function with the whole basis of plane waves by performing a single Fast Fourier Transform (FFT) on that function [45].

The procedure described above requires many matrix multiplications to calculate $\mathscr{U}$. In particular at low temperatures the number of matrix multiplications grows rapidly and the matrices have elements that vary over a large range of magnitudes. To avoid numerical instabilities it is necessary to separate the scales when multiplying the matrices, and a more costly but robust algorithm such as the Singular Value Decomposition (SVD) is required. In this section we follow the same approach developed in [48] to introduce the SVD to our calculations.

Let us write the matrix $\mathscr{U}(\{\sigma\})$ more explicitly:

$$\mathscr{U}(\{\sigma\}) = \prod_{j=1}^{N_\tau} \mathscr{W}_j(\{\sigma\}) = \mathscr{W}_{N_\tau}\mathscr{W}_{N_\tau-1}\cdots\mathscr{W}_2\mathscr{W}_1, \tag{9.37}$$

where the $\mathscr{W}_k(\{\sigma\})$ are $N \times N$ matrices, for a single-particle basis of dimension N. Let us then define

$$\begin{aligned} \mathscr{U}_0 &= 1 \\ \mathscr{U}_1 &= \mathscr{W}_1 \\ \mathscr{U}_2 &= \mathscr{W}_2\mathscr{W}_1 \\ &\vdots \\ \mathscr{U}_n &= \mathscr{W}_n\mathscr{W}_{n-1}\cdots\mathscr{W}_1 = \mathscr{W}_n\mathscr{U}_{n-1}. \end{aligned} \tag{9.38}$$

To separate the scales one decomposes the matrix $\mathscr{U}_{n-1}$ before multiplying it by $\mathscr{W}_n$ to get $\mathscr{U}_n$. This process begins as follows

$$\begin{aligned} \mathscr{U}_0 &= 1 \\ \mathscr{U}_1 &= \mathscr{W}_1 = \mathscr{S}_1\mathscr{D}_1\mathscr{V}_1 \\ \mathscr{U}_2 &= \mathscr{W}_2\mathscr{W}_1 = (\mathscr{W}_2\mathscr{S}_1\mathscr{D}_1)\mathscr{V}_1 = \mathscr{S}_2\mathscr{D}_2\mathscr{V}_2\mathscr{V}_1 \end{aligned} \tag{9.39}$$

where $\mathscr{S}_1$ and $\mathscr{V}_1$ are orthogonal matrices (not necessarily inverses of each other), and $\mathscr{D}_1$ is a diagonal positive matrix containing the singular values of $\mathscr{U}_1$. The idea is that the actual multiplication should be done by first computing the factor in parenthesis in the last equation. This factor is then decomposed into $\mathscr{S}_2\mathscr{D}_2\mathscr{V}_2$, in preparation for the multiplication by $\mathscr{W}_3$, and so on. A generic step in this process looks like:

$$\mathscr{U}_n = \mathscr{W}_n\mathscr{U}_{n-1} = \mathscr{W}_n\mathscr{S}_{n-1}\mathscr{D}_{n-1}\mathscr{V}_{n-1}\mathscr{V}_{n-2}\cdots\mathscr{V}_1, \tag{9.40}$$

so that in the end

$$\mathscr{U}_{N_\tau} = \mathscr{U}(\{\sigma\}) = \mathscr{S}_{N_\tau}\mathscr{D}_{N_\tau}\mathscr{V}_{N_\tau}\mathscr{V}_{N_\tau-1}\cdots\mathscr{V}_1 = \mathscr{S}\mathscr{D}\mathscr{V}, \tag{9.41}$$

where we have decomposed the full product in the last step. Calculating the determinant, and therefore of the probability measure, is straightforward if we perform one final more SVD in the following chain of identities:

$$\begin{aligned} \det(1+\mathscr{U}(\{\sigma\})) &= \det(1+\mathscr{S}\mathscr{D}\mathscr{V}) = \det(\mathscr{S}(\mathscr{S}^\dagger\mathscr{V}^\dagger+\mathscr{D})\mathscr{V}) \\ &= \det(\mathscr{S}\ \tilde{\mathscr{S}}\tilde{\mathscr{D}}\tilde{\mathscr{V}}\ \mathscr{V}) = \det(\mathscr{S}\ \tilde{\mathscr{S}})\det(\tilde{\mathscr{D}})\det(\tilde{\mathscr{V}}\mathscr{V}) \end{aligned} \tag{9.42}$$

For equal densities (the symmetric case) we need this determinant squared, so we only care about the factor in the middle of the last expression: the other two factors have unit magnitude. Indeed, in that case we can write the probability measure as

$$P(\{\sigma\}) = \exp\left(\sum_{i=1}^{M}\log\tilde{d}_i\right) \tag{9.43}$$

where $\tilde{d}_i > 0$ are the elements in the diagonal of $\tilde{\mathscr{D}}$, and M is the dimension of the single particle Hilbert space. The number of SVD's required to stabilize the

calculation grows as we increase β. In our calculations we have made limited use of the SVD, ranging from 2 decompositions at the highest T to 8 decompositions at low T's.

9.2.5 Finite Size Scaling

The Monte Carlo calculations are performed in a box of finite size with a finite average number of particles. We are interested, however, in the thermodynamic limit $N \to \infty, V \to \infty$ and $N/V = \text{const}$, so we need to consider the finite size scaling of the system so we can properly relate the values calculated in the box to their thermodynamic counterparts. This becomes particularly important in the vicinity of phase transitions where the correlation length ξ_{corr} characterizing the non-local degree of correlation of a system diverges:

$$\xi_{\text{corr}} \propto |t|^{-\nu}, \tag{9.44}$$

where $t = 1 - T/T_c$, T_c is the critical temperature, and ν is a universal critical exponent. For the $U(1)$ universality class, (which contains superfluid phase transitions), this exponent is well-known: $\nu = 0.671$.

When dealing with systems that have a finite size L^3, the theory of the renormalization group (RG) predicts a very specific behavior for the correlation functions close enough to the transition temperature (see e.g. [52]). In particular, the two-body density matrix $K(L,T)$ that gives the order parameter for off-diagonal long-range order, scales as

$$R(L,T) = L^{1+\eta} K(L,T) = f(x)(1 + cL^{-\omega} + \cdots), \tag{9.45}$$

where $\eta = 0.038$ is another universal critical exponent, $f(x)$ is a universal analytic function, $x = (L/\xi_{corr})^{1/\nu}$, and c is a non-universal constant, and $\omega \simeq 0.8$ is the critical exponent of the leading irrelevant field. One should keep in mind that typically one knows neither c nor T_c, but is interested in finding the latter.

In a typical Monte Carlo calculation $K(L,T)$ is computed for various lengths L_i and temperatures T. The procedure to locate the critical point (characterized by scale invariance) involves finding the "crossing" temperatures T_{ij}, for which $R(L_i, T_{ij}) = R(L_j, T_{ij})$ at two given lengths L_i and L_j. Assuming that one is close to the transition (so that the correlation length is large compared to any other scale), one can expand $f(x(|t|)) = f(0) + f'(0) L^{1/\nu} b|t|$ (where we set $\xi_{corr} = b|t|^{-\nu}$), and derive the relation

$$|T_c - T_{ij}| = \kappa g(L_i, L_j), \tag{9.46}$$

where

$$g(L_i, L_j) = L_j^{-(\omega + 1/\nu)} \left[\frac{\left(\frac{L_j}{L_i}\right)^{\omega} - 1}{1 - \left(\frac{L_i}{L_j}\right)^{1/\nu}} \right] \tag{9.47}$$

and $\kappa = cT_c f(0)/bf'(0)$. If there were no non-universal corrections to scaling (i.e. if $c = 0$), then $\kappa = 0$ and $T_c = T_{ij}$, which means that, upon scaling by the appropriate factor (as above) all the curves $K(L,T)$ corresponding to different L's would cross exactly at T_c. In general these corrections are present, and it is therefore necessary to perform a linear fit of T_{ij} vs. $g(L_i,L_j)$ and extrapolate to infinite L in order to determine the true T_c [45].

9.2.6 Results: the Energy and the Entropy

The results of our Monte Carlo simulations are shown in Figs. 9.1 and 9.2 [19, 51, 45]. The Monte Carlo autocorrelation length was estimated (by computing the autocorrelation function of the total energy) to be approximately 200 Metropolis steps at $T \approx 0.2\varepsilon_F$. Therefore, the statistical errors are of the order of the size of the symbols in the figure. The chemical potential was chosen so as to have a total of about 45 particles for the 8^3 lattice. We have also performed calculations for particle numbers ranging from 30 to 80, for lattice sizes 8^3 and 10^3, and various temperatures: in all cases, the results agree to within the aforementioned errors.

According to the theory [53, 54] the asymptotic behavior in the limit of large momenta $n(k) \propto C(k_F/k)^n$ should at all temperatures be governed by the same exponent, namely $n = 4$. This is consistent with a value of the exponent $n = 4.5(5)$ extracted from the MC data. Both the energy 9.1 and the entropy 9.2 exhibit a definite transition between low and a high temperature regimes separated by a characteristic temperature T_0:

$$T_0 = 0.23(2)\varepsilon_F. \tag{9.48}$$

We shall discuss the relation between T_0, the superfluid critical temperature T_c, and the pair breaking temperature T^* in Sec. 9.2.8. First we focus on the low temperature limit.

At $T = 0$, several interesting quantities describe the symmetric unitary system: one is the energy as expressed through the Bertsch parameter $\xi = E_{SF}/E_{FG}$; related is the somewhat fictitious energy of the interacting normal state $\xi_N = E_N/E_{FG}$; finally, there is the pairing gap $\Delta = \eta\varepsilon_F$. The $T = 0$ value of these quantities have been obtained to high precision by other groups using the variational fixed-node Monte Carlo techniques [18, 55, 56, 57]. Unlike our approach, these $T = 0$ techniques suffer from a sign problem that is overcome by using a fixed-node constraint: This formally provides only an upper bound on the energy. Our result $\xi = 0.37(5)$ (see Table 9.1 agrees with these variational bounds, $\xi = 0.44(1)$ [18, 55], $\xi = 0.42(1)$ [56, 57], and with more recently quoted AFQMC results $\xi = 0.40(1)$ [58, 59]. Although not as precise, our method is truly ab initio and hence provide a non-trivial validation of these variational results.

The quantity ξ_N for the normal state—though not precisely defined (since the normal state is not the ground state)—provides a useful description of the physics. For example, in the high temperature regime $T > T_0$, the energy is described well

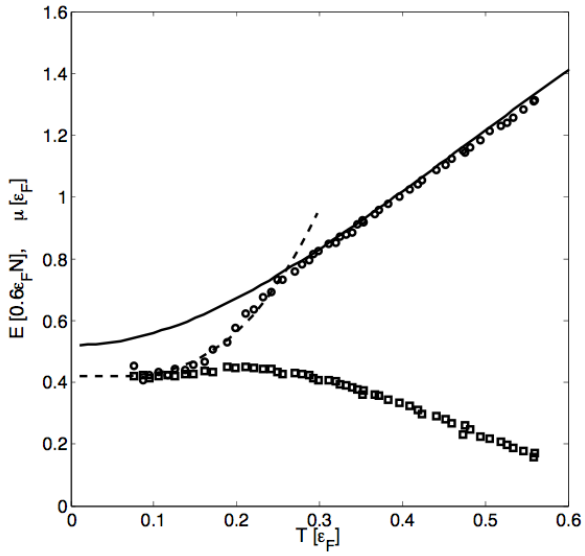

Fig. 9.1 The total energy $E(T)$ with open circles, and the chemical potential $\mu(T)$ with squares, both for the case of an 8^3 lattice. The combined Bogoliubov-Anderson phonon and fermion quasiparticle contributions $E_{\rm ph+qp}(T)$ (Eq. (9.50)) is shown as a dashed line. The solid line represents the energy of a free Fermi gas, with an offset (see text). From [45].

by the energy of a free Fermi gas shifted down by $1-\xi_N$ (shown as a solid line in Fig. 9.1), where $\xi_N = \xi + \delta_\xi \approx 0.52$ can be found by determining what shift is necessary to make the solid curve coincide with the high temperature data (where the gas is expected to become normal).

Taking $\xi \approx 0.4$ this gives the condensation energy $\delta_\xi \approx 0.12$ which is roughly consistent with the estimate

$$\delta_\xi = \frac{\delta E}{\frac{3}{5}\varepsilon_F N} = \frac{5}{8}\left(\frac{\Delta}{\varepsilon_F}\right)^2 \simeq 0.15 \tag{9.49}$$

based on the BCS expression for $\delta E = \frac{3}{8}\frac{\Delta^2}{\varepsilon_F}N$ (see [60]) and the QMC value of the pairing gap where $\Delta \simeq 0.50\varepsilon_F$ [18, 57] and confirmed by us in [61] (which turns out to be very close to the weak-coupling prediction of Gorkov and Melik-Barkhudarov [13, 62]). Our estimate should also be compared with the results $\xi_N \approx 0.54$ of [18, 63] and $\xi_N \approx 0.56$ of [64] obtained by considering only normal state nodal constraints. Finally, a similar result $\xi_N \approx 0.57(2)$ (see Eq. (9.95e)) arises from fitting the SLDA density functional to be discussed in Sec. 9.3.2.1.

At low temperatures, $T < T_0$, temperature dependence of the energy can be accounted for by the elementary excitations present in the superfluid phase: boson-like Bogoliubov-Anderson phonons and fermion-like gapped Bogoliubov quasiparticles.

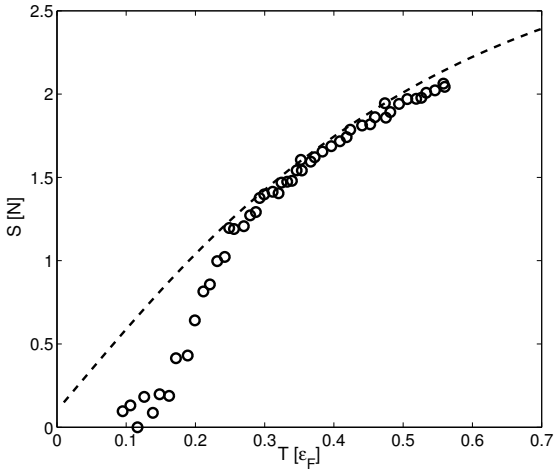

Fig. 9.2 The entropy per particle with circles for 8^3 lattice, and with a dashed line the entropy of a free Fermi gas with a slight vertical offset. The statistical errors are the size of the symbol or smaller. From [45].

Their contributions are given by

$$E_{\mathrm{ph+qp}}(T) = \frac{3}{5}\varepsilon_F N\left[\xi + \frac{\sqrt{3}\pi^4}{16\xi^{3/2}}\left(\frac{T}{\varepsilon_F}\right)^4 + \frac{5}{2}\sqrt{\frac{2\pi\Delta^3 T}{\varepsilon_F^4}}\exp\left(-\frac{\Delta}{T}\right)\right], \quad (9.50)$$

$$\Delta \approx \left(\frac{2}{e}\right)^{7/3}\varepsilon_F \exp\left(\frac{\pi}{2k_F a}\right), \quad (9.51)$$

The sum of the contributions from these excitations is plotted in Fig. 9.1 as a dashed line: Both of these contributions are comparable in magnitude over most of the temperature interval $(T_0/2, T_0)$. Since the above expressions are only approximate for $T \ll T_c$, the agreement with our numerical results may be coincidental.

At $T > T_c$ the system is expected to become normal. If T_0 and T_c are identified, then the fact that the specific heat is essentially that of a normal Fermi liquid $E_F(T)$ above T_0 is somewhat of a surprise: one would expect the presence of a large fraction of non-condensed but unbroken pairs. Indeed, the pair-breaking temperature has been estimated to be $T^* \simeq 0.55\varepsilon_F$, based on fluctuations around the mean-field, see [1, 2, 65, 3, 4, 6, 66]. This implies that for $T_c < T < T^*$ there should be a noticeable fraction of non-condensed pairs. In the next sections we will show that this is indeed the case and that above the superfluid critical temperature, the fermionic spectrum still contains a gap, giving rise to the so-called pseudogap phase.

From the data for the energy E and chemical potential μ, one can compute the entropy S using the unitary relation $PV = \frac{2}{3}E$ (true of a free gas as well) which holds,

where P is the pressure, V is the volume and E is the energy. It is straightforward to show that

$$\frac{S}{N} = \frac{E + PV - \mu N}{NT} = \frac{\xi(x) - \zeta(x)}{x}, \tag{9.52}$$

where $\zeta(x) = \mu/\varepsilon_F$ and $x = T/\varepsilon_F$ determines the entropy per particle in terms of quantities extracted from our simulation. As shown in Fig. 9.2, the entropy also departs from the free gas behavior below T_0.

This data can be used to calibrate the temperature scale at unitarity [19, 51]. Indeed, extending the suggestion of [67], from a known temperature in the BCS limit, the corresponding $S(T_{\rm BCS})$ can be determined. Then, by adiabatically tuning the system to the unitary regime, one can uses $S(T_{\rm BCS}) = S(T_{\rm unitary})$ to determine T at unitarity. (In practice the experimental procedure goes in the opposite direction, namely measurements are performed at unitarity, and then the system is tuned to the deep BCS side, see [68].)

On the other hand, knowledge of the chemical potential as a function of temperature allows for the construction of density profiles by using of the Local Density Approximation (LDA) (see the next section). In turn, this makes it possible to determine $S(E)$ for the system in a trap, fixing the temperature scale via $\partial S/\partial E = 1/T$. Direct comparison with experiment shows remarkable agreement with our data (we discuss this later in Fig. 9.6) [69].

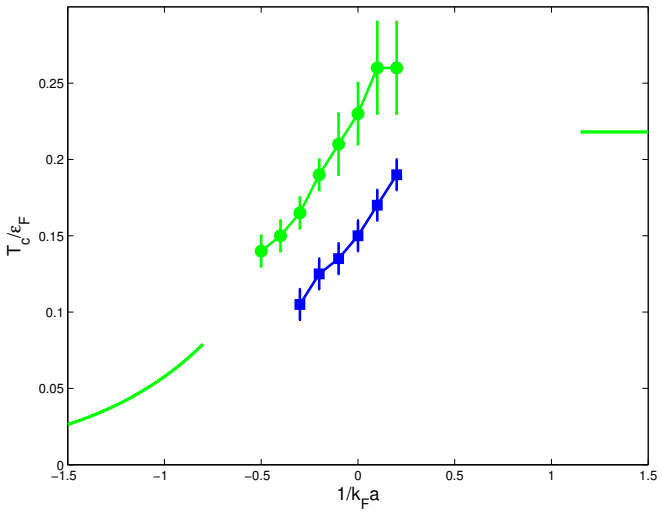

Fig. 9.3 The critical temperature T_c (squares either error bars) and the characteristic temperature T_0 (circles with error bars) around the unitary point determined in QMC and using finite size analysis. On the far left BCS side of the critical point we show (solid green line) the expected BCS critical temperature, including the corrections due to induced interactions [13, 62], and on the far right side of the BEC side of the unitary point we show (solid green line) the expect critical temperature in the BEC limit. For more details see [45].

In the following we present a brief summary of our results near unitarity on both the BCS $a<0$ and BEC $a>0$ sides, (see Fig. 9.3 and Table 9.1). The coupling strength was varied in the range $-0.5 \leq 1/k_F a \leq 0.2$ (where $k_F = (3\pi^2 n)^{1/3}$), limited on the negative (BCS) side by the finite volume V (which becomes comparable to the size of the Cooper pairs), and on the positive (BEC) side by the finite lattice spacing l (which becomes comparable to the size $a = \mathrm{O}(l)$ of the localized dimers, manifesting as poor convergence of observables).

$1/k_F a$	$E(0)/E_F$	T_0	μ_0/ε_F	E_0/E_F	$T_c <$	μ_c/ε_F	E_c/E_F
-0.5	0.60(4)	0.14(1)	0.685(5)	0.77(2)	–	–	–
-0.4	0.59(4)	0.15(1)	0.65(1)	0.75(1)	–	–	–
-0.3	0.55(4)	0.165(10)	0.615(10)	0.735(10)	0.105(10)	0.61(1)	0.64(2)
-0.2	0.51(4)	0.19(1)	0.565(10)	0.725(10)	0.125(10)	0.56(1)	0.61(2)
-0.1	0.42(4)	0.21(2)	0.51(1)	0.71(2)	0.135(10)	0.50(1)	0.54(2)
0	0.37(5)	0.23(2)	0.42(2)	0.68(5)	0.15(1)	0.43(1)	0.45(1)
0.1	0.24(8)	0.26(3)	0.34(1)	0.56(8)	0.17(1)	0.35(1)	0.41(1)
0.2	0.06(8)	0.26(3)	0.22(1)	0.39(8)	0.19(1)	0.21(1)	0.25(1)

Table 9.1 Results for the ground state energy, the characteristic temperature T_0, and the corresponding chemical potential and energy, from the caloric curves $E(T)$ and the upper bounds on the critical temperature T_c from finite size scaling and the corresponding chemical potentials and energies [45].

9.2.7 Response to External Probes and the Spectral Function

In order to get an insight into basic degrees of freedom which contribute to the low energy excitations of the system one has to investigate the response of the system to various external probes. Here we will present the simplest possible probe: adding a particle to the system and calculating the probability amplitude of finding it in a given single particle state. This requires calculating the one-body finite temperature (Matsubara) Green's function [70]:

$$\mathscr{G}(\mathbf{p},\tau) = \frac{1}{Z}\,\mathrm{Tr}\{\exp[-(\beta-\tau)(H-\mu N)]\,\psi^{\dagger}(\mathbf{p})\exp[-\tau(H-\mu N)\psi(\mathbf{p})]\}, \quad (9.53)$$

where $\beta = 1/T$ is the inverse temperature and $\tau > 0$. The trace is performed over the Fock space, and $Z = \mathrm{Tr}\{\exp[-\beta(H-\mu N)]\}$. The spectral weight function $A(\mathbf{p},\omega)$ can be extracted from the finite temperature Green's function using the relation:

$$\mathscr{G}(\mathbf{p},\tau) = -\frac{1}{2\pi}\int_{-\infty}^{\infty} \mathrm{d}\omega A(\mathbf{p},\omega)\frac{\exp(-\omega\tau)}{1+\exp(-\omega\beta)}. \quad (9.54)$$

By definition, $A(\mathbf{p},\omega)$ fulfills the following constraints:

$$A(\mathbf{p},\omega) \geq 0, \qquad \int_{-\infty}^{\infty} \frac{\mathrm{d}\omega}{2\pi} A(\mathbf{p},\omega) = 1. \tag{9.55}$$

Since our study focuses on the symmetric (unpolarized) system and the Hamiltonian is symmetric under $a \leftrightarrow b$, $\mathscr{G}(\mathbf{p},\tau)$ is block diagonal and the species index is suppressed in all formulae. The numerical evaluation of the one-body temperature propagator (9.53) is performed as described above, using a Trotter expansion of $\exp[-\tau(H-\mu N)]$ followed by a Hubbard-Stratonovich transformation and Metropolis importance sampling. Details can be found in [61].

The numerical determination of $A(\mathbf{p},\omega)$ by inverting (9.54) is an ill-posed problem that requires special methods. We have used two, based on completely different approaches. The first approach is the maximum entropy method [71, 72, 73, 74], which is based on Bayes' theorem. Quantum Monte Carlo calculations provide us with a discrete set of values $\tilde{\mathscr{G}}(\mathbf{p},\tau_i)$, where $i = 1,2,\ldots,\mathscr{N}_\tau = 50$. We treat them as normally distributed random numbers around the true values $\mathscr{G}(\mathbf{p},\tau_i)$. The Bayesian strategy consists in maximizing the *posterior probability*

$$P(A|\tilde{G}) \propto P(\tilde{G}|A)P(A) \tag{9.56}$$

of finding the right $A(\mathbf{p},\omega)$ under the condition that $\tilde{\mathscr{G}}(\mathbf{p},\tau_i)$ are known. Here,

$$P(\tilde{G}|A) \propto \exp\left(-\frac{1}{2}\chi^2\right) \tag{9.57}$$

is the *likelihood function*, where

$$\chi^2 = \sum_{i=1}^{\mathscr{N}_\tau} \left[\tilde{\mathscr{G}}(\mathbf{p},\tau_i) - \mathscr{G}(\mathbf{p},\tau_i)\right]^2 / \sigma^2. \tag{9.58}$$

The quantity $\mathscr{G}(\mathbf{p},\tau_i)$ is determined by the spectral weight function in the discretized form of (9.54) at frequencies ω_k. The prior probability $P(A)$, describing our ignorance about the spectral weight function, is defined as $P(A) \propto \exp(\alpha S(\mathscr{M}))$, where $\alpha > 0$ and $S(\mathscr{M})$ is the relative information entropy with respect to the assumed model $\mathscr{M}$:

$$S(\mathscr{M}) = -\sum_k \Delta\omega \left[A(\mathbf{p},\omega_k) - \mathscr{M}(\omega_k) - A(\mathbf{p},\omega_k)\ln\left(\frac{A(\mathbf{p},\omega_k)}{\mathscr{M}(\omega_k)}\right)\right]. \tag{9.59}$$

Hence the maximization of $P(A|\tilde{G})$ leads in practice to the minimization of the quantity $\frac{1}{2}\chi^2 - \alpha S(\mathscr{M})$ with respect to A [61].

The second approach is based on the SVD of the integral kernel $\mathscr{K}$ of (9.54), which can be rewritten in operator form as

$$\mathscr{G}(\mathbf{p},\tau_i) = (\mathscr{K}A)(\mathbf{p},\tau_i). \tag{9.60}$$

The operator $\mathscr{K}$ possesses a singular subspace

$$\mathscr{K}u_i = \lambda_i \mathbf{v}_i, \quad \mathscr{K}^*\mathbf{v}_i = \lambda_i u_i, \tag{9.61}$$

where $\mathscr{K}^*$ denotes the adjoint of $\mathscr{K}$, λ_i are the singular values, and u_i and $\mathbf{v}_i$ are right-singular functions and left-singular vectors respectively. The singular subspace forms a suitable basis for the expansion of the spectral weight function [75, 76, 77], which we can then write as

$$A(\mathbf{p},\omega) = \sum_{i=1}^{r} b_i(\mathbf{p}) u_i(\omega), \qquad b_i(\mathbf{p}) = \frac{1}{\lambda_i}(\mathscr{G}(\mathbf{p}) \cdot \mathbf{v}_i), \tag{9.62}$$

where $(_ \cdot _)$ is a scalar product and r is the rank of the operator $\mathscr{K}\mathscr{K}^*$. Since $\mathscr{G}(\mathbf{p},\tau_i)$ is affected by Monte Carlo errors σ_i, the coefficients b_i carry some uncertainty Δb_i. Each set of expansion coefficients $\tilde{b}_i \in (b_i - \Delta b_i, b_i + \Delta b_i)$ reproduces $\mathscr{G}(\mathbf{p},\tau_i)$ within its error bars. We use this flexibility of choosing the expansion coefficients to produce a solution satisfying constraints (9.55) [78]. The relative advantages of each method will be discussed elsewhere [79].

A sample of calculated spectral weight functions at unitarity are shown in Fig. 9.4. In order to characterize the quasiparticle excitation spectrum we have associated with the maximum of $A(\mathbf{p},\omega)$ the quasiparticle energy $E(\mathbf{p})$:

$$E(\mathbf{p}) = \pm\sqrt{\left(\frac{p^2}{2m^*} + U - \mu\right)^2 + \Delta^2}, \tag{9.63}$$

where the effective mass m^*, the effective potential U, and the "pairing" gap Δ depend on temperature, and μ is an input parameter. In Fig. 9.5 we compare the spectrum of elementary fermionic excitations evaluated in [57], with the one extracted by us from our lowest temperature spectral weight function.

9.2.8 The Pairing Gap, Pseudogap, and Critical Temperature

In order to find the critical temperature for the superfluid-normal transition one has to perform the finite size analysis discussed in the previous section. Following this procedure, our data for the condensate fraction of the unitary Fermi gas indicates that $T_c \lesssim 0.15(1)\varepsilon_F$, considerably lower than the characteristic temperature $T_0 = 0.23(2)$ found by studying the behavior of the energy and the chemical potential (see Fig. 9.3 and Table 9.1). Even though this result for T_c is close to estimates by other groups (see e.g. [80, 81, 82]), it should be pointed out that the experimental data of [68] shows a distinctive feature in the energy versus entropy curve at a temperature close to T_0 (see [69]).

It is notable that both methods (the maximum entropy method and the SVD method) admit a "gapped" spectral function above the critical temperature T_c: a situation commonly called a pseudogap. It characterizes the range of temperatures where the system exists in an exotic state which is neither normal, nor superfluid, and defies a conventional BCS description. Therefore the onset of pairing and superfluidity can occur at different temperatures. On the other hand, the pseudogap is

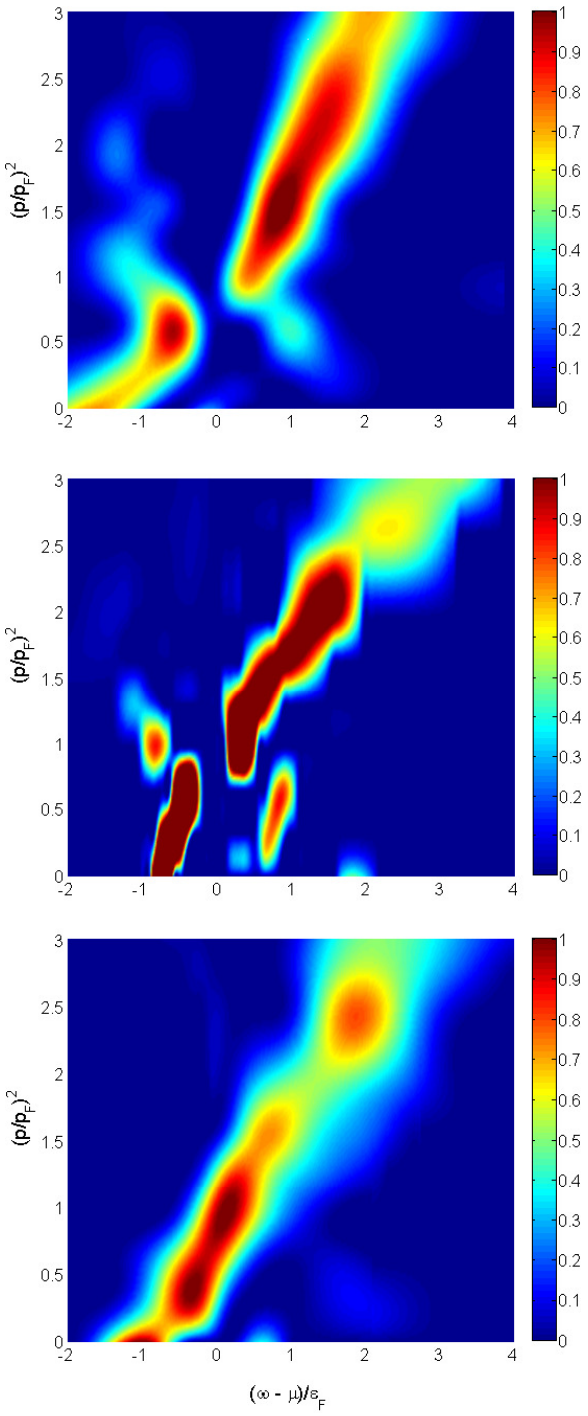

Fig. 9.4 Spectral weight function $A(\mathbf{p},\omega)$ for three temperatures: $T = 0.15\varepsilon_F \approx T_c$ (upper panel), $T = 0.18\varepsilon_F \approx T_c$ (middle panel) and $T = 0.20\varepsilon_F$ (lower panel). The presence of a gap in clearly seen in the upper two panels. From [61].

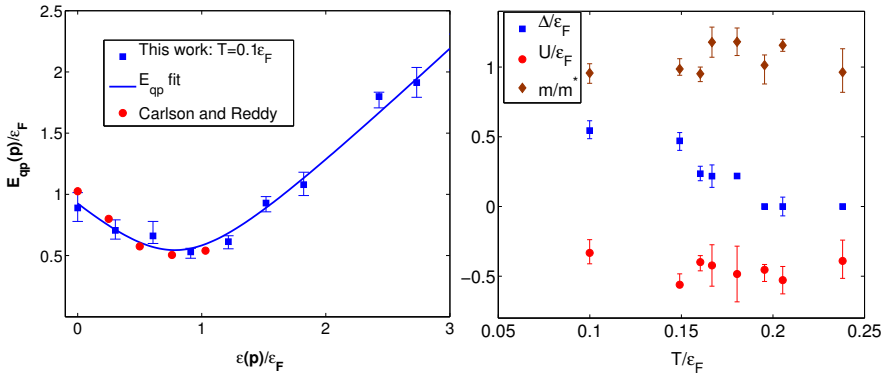

Fig. 9.5 Quantities extracted from the spectral weight function $A(\mathbf{p},\omega)$ at $T = 0.1\varepsilon_F$ at unitarity (from [61]). Left: Quasiparticle energies $E(\mathbf{p})$ (squares). The line corresponds to the fit to (9.63). The circles are the results of Carlson and Reddy [57]. (See also Fig. 9.10 where the same data is used to fit the SLDA density functional.) Right: The single-particle parameters. One should note that while the effective mans and the self-energy show a very weak temperature dependence across the phase transition, the pairing gap halves in value at T_c and vanishes around T_0.

easy to understand in the BEC limit where stable dimers exist well above the critical temperature. This gives rise to a pseudogap phase, where the system share a BCS-like dispersion and a partially gapped density of states, but does not exhibit superfluidity. Several groups have been advocating various aspects of pseudogap physics in the unitary Fermi gas for the past few years [4, 66, 83, 84, 85, 86].

There have been several experimental attempts to extract the pairing gap in ultra-cold dilute Fermi gases [87, 88, 89] and a theoretical explanation of these spectra was given in [90, 91]. It was later shown in [92, 93, 94, 95] that these initial interpretations of the rf-spectra ignored the strong final state interaction effects. Recent experimental measurement of pair condensation in momentum space and a measurement of the single-particle spectral function using an analog to photo-emission spectroscopy, directly probed the pseudogap phase and revealed its existence for $1/(k_F a) \approx 0.15$ [96]. Although this lies on the BEC side, there are indications that the pseudogap persists well into the unitary regime [97, 98].

Our calculations show that the spectral function reveals the presence of a gap in the spectrum up to about $T^* \approx 0.20\varepsilon_F$ (see Fig. 9.5), and a two peak structure around the Fermi level at temperatures above T_c [61, 99]. We note that T^* is close to T_0 (not surprising in hindsight), the temperature at which the caloric curve $E(T)$ has a shoulder [19, 51] (called T_0 in [45]).

9.2.9 Describing Trapped Systems with Quantum Monte Carlo Results

The Monte Carlo calculations presented above assume that the system is uniform. In experiment, however, this condition is not fulfilled since atoms are trapped in an external potential which induces inhomogeneity of density distribution. Most of the atomic trapping potentials used in these experiments can be approximated rather well with harmonic potential wells. Such potentials can be shown to satisfy the virial theorem at unitarity, namely $E(T,N) = 2N\langle U\rangle = 3m\omega_z^2\langle z^2\rangle$ [100], and therefore simply measuring the spatial shape of the cloud allows for a unique determination of the unitary gas energy at any temperature. One of the main goals is therefore to provide a link between the results of experiment [68] and the available finite temperature QMC calculations.

At unitarity $(1/k_F a = 0)$ the pressure of a homogeneous unitary gas is determined by a universal convex function $h_T(z)$:

$$\mathscr{P}(T,\mu) = \frac{2}{5}\beta\left[T h_T\left(\frac{\mu}{T}\right)\right]^{5/2}, \qquad \beta = \frac{1}{6\pi^2}\left(\frac{2m}{\hbar^2}\right)^{3/2}, \tag{9.64}$$

where T and μ are the temperature and the chemical potential, respectively. $\mathscr{P}(T,\mu)$ is a convex function of its arguments (second law of thermodynamics) if and only if $h_T(z)$ is convex. One can show [101] that thermodynamic stability implies positivity $h_T(z) \geq 0$, monotonicity $h_T'(z) \geq 0$, and convexity $h_T''(z) \geq 0$. Remembering that the grand canonical potential is $\Omega(V,T,\mu) = -V\mathscr{P}(T,\mu)$ one can show that the energy of the system reads: $E = 3\mathscr{P}V/2$, where V is the volume of the system. As it was mentioned before, this relation between energy and pressure is identical in form to the one corresponding to non-interacting particles. In the high-temperature limit $\mu \to -\infty$ and $\mathscr{P}(T,\mu)$ tends from above to the free Fermi gas pressure. In the low-temperature limit $\mathscr{P}(T,\mu)$ tends from above to $\mathscr{P}(0,\xi\varepsilon_F) = 4\beta\varepsilon_F^{5/2}\xi/5$.

Standard manipulations show that all the thermodynamic potentials for the unitary Fermi gas can be expressed in terms of a single function of one variable, a property known as universality [19, 21, 51, 80, 81]. This property was incorporated in our interpolation. At high temperatures we notice that our results smoothly approach the corresponding free Fermi gas results with some offsets for the energy, chemical potential and entropy [19, 51].

At this point we assume that the Local Density Approximation (LDA) can be used to describe the properties of an atomic cloud in a trap. We will neglect the gradient corrections as one can show that for the mostly-harmonic traps used in typical experiments the role of the gradient corrections is relatively small [69], as the average interparticle distance, and thus the Fermi wave length, is much smaller than the harmonic oscillator length.

In this approach, the grand canonical thermodynamic potential for a unitary Fermi gas confined by an external potential $U(\mathbf{r})$ is a functional of the local density $n(\mathbf{r})$ given by

$$\Omega = \int \mathrm{d}^3\mathbf{r}\left[\frac{3}{5}\varepsilon_F(\mathbf{r})\varphi(x)n(\mathbf{r}) + U(\mathbf{r})n(\mathbf{r}) - \lambda n(\mathbf{r})\right], \tag{9.65}$$

where

$$x = \frac{T}{\varepsilon_F(\mathbf{r})}, \quad \varepsilon_F(\mathbf{r}) = \frac{\hbar^2}{2m}[3\pi^2 n(\mathbf{r})]^{2/3}, \tag{9.66}$$

and we have used the universal form for the free energy per particle F/N in the unitary regime:

$$\frac{F}{N} = \frac{E-TS}{N} = \frac{3}{5}\varepsilon_F\varphi(x) = \frac{3}{5}\varepsilon_F[\xi(x) - x\sigma(x)], \tag{9.67}$$

where for a homogeneous system $\xi(x) = 5E/3\varepsilon_F N$, $\sigma(x) = S/N$ is the entropy per particle and $x = T/\varepsilon_F$. The overall chemical potential λ and the temperature T are constant throughout the system. The density profile will depend on the shape of the trap as dictated by $\delta\Omega/\delta n(\mathbf{r}) = 0$, which results in:

$$\frac{\delta\Omega}{\delta n(\mathbf{r})} = \frac{\delta(F-\lambda N)}{\delta n(\mathbf{r})} = \mu(x(\mathbf{r})) + U(\mathbf{r}) - \lambda = 0. \tag{9.68}$$

At a given T and λ, (9.66) and (9.68) completely determine the density profile $n(\mathbf{r})$ (and consequently both $E(T,N)$ and $S(T,N)$) in a given trap for a given total particle number. The only experimental input we have used is the particle number, the trapping potential and the scattering length at $B = 1200$ G, taken from [68]. The potential was assumed to be an 'isotropic' Gaussian, as suggested by the experimental group [68], although it is not entirely clear to us to what extent this is accurate, especially in the axial direction. We have approximated the properties of the atomic cloud at $B = 840$ G with those at unitarity ($B = 834$ G), where we have MC data. For $B = 840$ G and for the parameters of the Duke experiment [68] one obtains $1/k_F a = -0.06$, using data of [102], if the Fermi momentum corresponds to the central density of the cloud at $T = 0$.

Our results for the entropy of the cloud and the density profiles for several temperatures, are shown in Figs. 9.6 and 9.7. In all the figures the temperature is measured in natural units of $\varepsilon_F(0)$, corresponding to the actual central density of the cloud at that specific temperature. In [68, 103] the temperature is expressed in units of the Fermi energy at $T = 0$ in a harmonic trap: $\varepsilon_F^{ho} = \hbar\Omega(3N)^{1/3}$. It is clear from Fig. 9.7 that the central density decreases with T and that the superfluid core disappears at $T_c = 0.23(2)\varepsilon_F(0)$, which translates into $T_c = 0.27(3)\varepsilon_F^{ho}$ to be compared to $T_c = 0.29(2)\varepsilon_F^{ho}$ of [68]. There is a noticeable systematic difference between theory and experiment at high energies, see Fig. 9.6. This discrepancy can be attributed to the fact that the experiment was performed slightly off resonance, on the BCS side, where $1/k_F a = -0.06$.

Recently a couple of new experiments have been published, one by the Paris group [104] and another by the Tokyo group [105]. Using new techniques these groups were able to extract directly from cloud images the pressure as a function of the fugacity. While the Paris group has observed a very good agreement with our

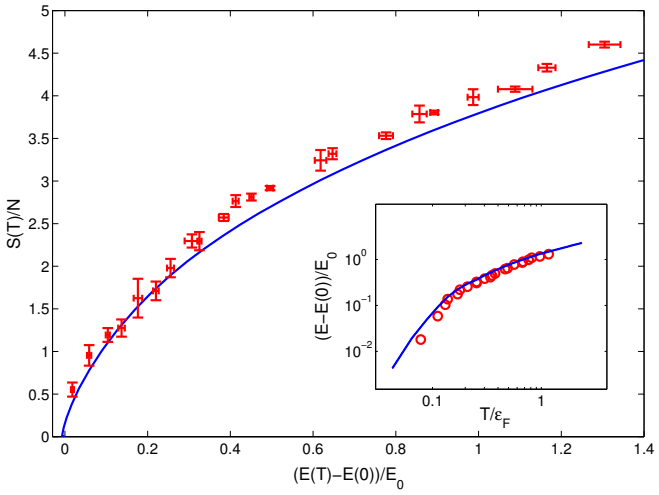

Fig. 9.6 Entropy as a function of energy for the unitary Fermi gas in the Duke trap [68]: experiment (points with error bars) and present work (solid curve), where $E_0 = N\varepsilon_F^{HO}$. Inset: log-log plot of $E(T)$ as results from our calculations and as derived from experimental data [68]. The temperature is units of the corresponding Fermi energy at the center of the trap: $\varepsilon_F(0)$. From [69].

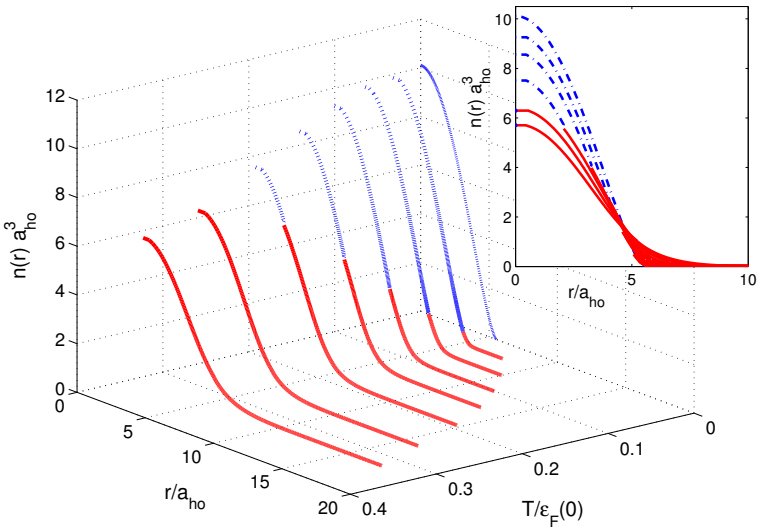

Fig. 9.7 The radial (along shortest axis) density profiles of the Duke cloud at various temperatures, as determined theoretically using the QMC results [19, 51]. The dotted blue line shows the superfluid part of the cloud, for which $x(\mathbf{r}) = T/\varepsilon_F(\mathbf{r}) \leq 0.23$. The solid red line shows the part of the system that is locally normal. Here $a_{ho}^2 = \hbar/m\omega_{max}$. From [69].

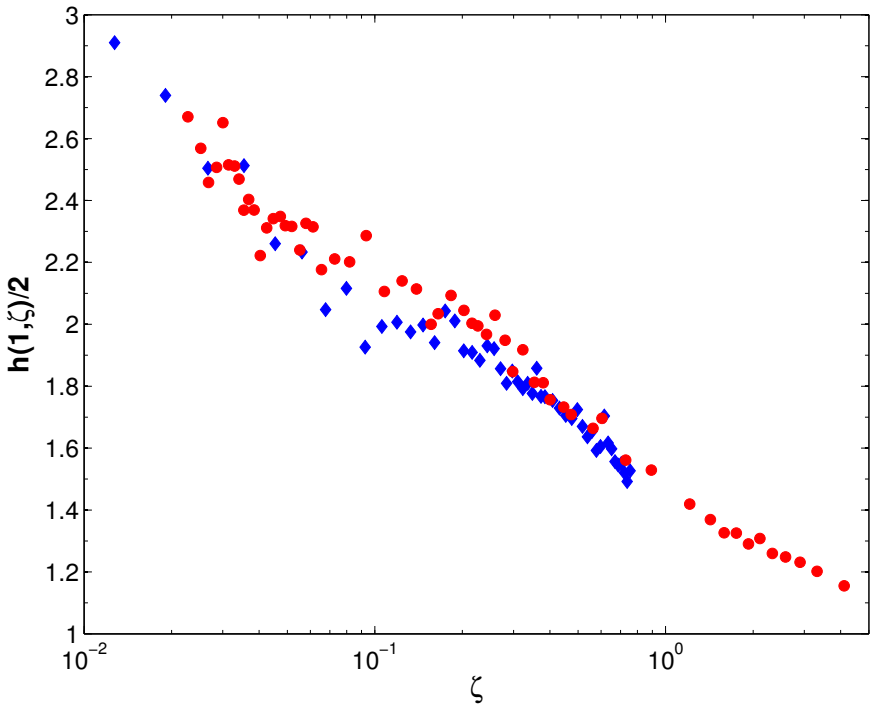

Fig. 9.8 The comparison between the ration of the pressure versus fugacity of a unitary Fermi gas and the pressure of a free Fermi gas: measured in [106] (red filled circles) and calculated in QMC in [69] (blue filled diamonds).

QMC results, see Fig. 9.8, they have also noticed that the results of the Tokyo group show systematic differences [106].

One can summarize that so far the bulk of the theoretical predictions obtained in ab initio QMC have been confirmed experimentally with impressive accuracy in most cases, often at a level of a few percent, which is the accuracy of both theoretical calculations and of many experimental results as well. The emergence of a pseudogap in the unitary gas is a fascinating new feature, but still in its infancy both theoretically and experimentally.

9.3 Density Functional Theory for the Unitary Fermi Gas

The idea of Density Functional Theory (DFT) originated with Hohenberg and Kohn [107] and Kohn and Sham [108] (see the monographs [109, 110] for an overview) where they proved that the ground state energy and the density of a system of interacting fermions in an *arbitrary* external potential $V_{\rm ext}(\mathbf{r})$ may be found by

minimizing a functional

$$E[n(\mathbf{r})] + \int \mathrm{d}^3\mathbf{r}\, V_{\mathrm{ext}}(\mathbf{r}) n(\mathbf{r}). \tag{9.69}$$

The utility of this approach is that the functional $E[n(\mathbf{r})]$ depends only on the interactions of the system and is independent of the external potential. Thus, if we were able to deduce $E[n(\mathbf{r})]$ for the unitary Fermi gas, then by simply minimizing a single functional, we could determine the ground state in any external potential, including arbitrary trapping geometries and optical lattices.

The challenge is that the Hohenberg-Kohn theorem is an existence theorem. The exact form of the functional $E[n(\mathbf{r})]$ is unknown, and in general it may be extremely complicated and highly non-local. In problems that are under perturbative control, the functional can be formally derived (see [111]), but in highly non-perturbative problems such as the unitary gas, one must choose a physically motivated approximate functional and check its accuracy.

Our strategy is thus:

1. Postulate simple functional forms capturing the relevant physics with a small number of parameters.
2. Use ab initio results to fix these parameters.
3. Validate the functional with different ab initio and experimental results.
4. Make interesting and verifiable physical predictions.

The computational cost of minimizing the density functional is much less than solving for many-body wavefunctions, and one may consider substantially larger systems, untenable with ab initio methods. This allows one to make direct contact with typical mesoscopic experiments for example. In this way, one may view the density functional as a bridge between microscopic and mesoscopic physics.

As we have noted, although DFT is exact in principle, for non-trivial systems we must postulate a form for the functional. Nevertheless, it provides a substantial improvement to the ad hoc mean-field methods typically employed to study the properties of large non-perturbative many-body systems. Without a program for systematically correcting the functional, the DFT approach will not be the final word. However, judging from the success of the approach in quantum chemistry, and from the results presented here, we expect that without too much effort one should be able to obtain percent level accuracy for a wide range of systems, which should be sufficient for quite some time.

The qualitative success of the Eagles-Leggett [1, 2] mean-field model describing the BCS–BEC crossover suggests a functional description of the unitary Fermi gas in terms of quasi-particle fermionic states (see (9.76)). As discussed in Sec. 9.1, although the BdG approximation is quite successful, it is quantitatively inaccurate as it describes *all* interaction effects through the condensation energy (pairing) alone, completely omitting the "Hartree-Fock" contribution which dominates the energetics. To see this, consider the typical local interaction $g a^\dagger b^\dagger b a$ between species a (spin up) and species b (spin down). The mean-field approximation retains the pairing term $g\langle a^\dagger b^\dagger\rangle\langle b a\rangle = g\nu^\dagger\nu$ and the Hartree term $g\langle a^\dagger a\rangle\langle b^\dagger b\rangle = g n_a n_b$. (The other

quadratic Fock term $\langle a^\dagger b\rangle \langle b^\dagger a\rangle$ has zero expectation.) The problem arises upon renormalization: As discussed below, the anomalous density ν is formally divergent, and regularization requires taking the coupling $g \to 0$ to keep the gap parameter $\Delta = -g\nu$ finite. Since the densities remain finite, the Hartree contribution $g n_a n_b \to 0$ vanishes.

In weak coupling, one can carefully take the zero-range limit while summing ladders [12, 70], obtaining the well known form $a n_a n_b$ of the Hartree interaction, which is clearly invalid in the unitary limit $|a| \to \infty$. In particular, for the symmetric phase $n_a = n_b = n$, there is no additional length scale, and so we must have a dependence $\sim n^{5/3}$ as dictated by dimensional analysis. This physics—the dominant contribution to the energetics (see the discussion below (9.49))—is completely missing from the BdG (mean-field) approach and is one of the main deficiencies we hope to overcome within an improved DFT description.

We shall first discuss an improved local DFT for symmetric systems $n_a = n_b = n$: the Superfluid Local Density Approximation (SLDA). This is a generalization of the Kohn-Sham Local Density Approximation (LDA) to includes pairing effects and subsumes the BdG form, adding an $n^{5/3}$ Hartree interaction term.

We subsequently extent the SLDA to study asymmetric systems $n_a \neq n_b$ through the use of the Asymmetric SLDA (ASLDA) functional that subsumes the SLDA. The approach of both these approximations is to introduce as few parameters as possible that are consistent with the scaling and symmetries of the problem, then to determine the coefficients of these terms by matching to ab initio properties in the thermodynamic limit. The form of the functionals is described in Sec. 9.3.1, the fitting of the parameters is discussed in Sec. 9.3.2, and some physical applications are presented in Sec. 9.3.3.

9.3.1 The Energy Density Functional

We start with the most restrictive conditions of a cold ($T = 0$) symmetric ($n_a = n_b$, $m_a = m_b$) unitary ($|a| = \infty$) Fermi gas. As discussed in Sec. 9.1, the only dimensionful scale in the problem is the density n, so dimensional analysis provides significant constraints on the form of the functional and thermodynamic functions, allowing us to postulate a simple functional form characterized by only three dimensionless parameters. Relaxing any of these conditions will introduce additional dimensionless parameters. In particular, we consider the dimensionless polarization $p = (n_a - n_b)/(n_a + n_b)$ to formulate ASLDA [101, 112]. The generalized ASLDA functional promotes the dimensionless parameters to dimensionless functions of this asymmetry parameter p.

9.3.1.1 Local Density Approximation (LDA)

In general, the energy functional might be a highly non-local and extremely complicated object. One major simplification is to assume that the functional is local and can be represented by a function of various types of densities. This amounts to introducing the energy density $\mathscr{E}$ which is a function (as opposed to a functional) of the local densities and their derivatives (referred to as gradient corrections):

$$E_{KS} = \int \mathrm{d}^3\mathbf{r}\, \mathscr{E}_{KS}[n(\mathbf{r}), \tau(\mathbf{r}), \nabla n(\mathbf{r}), \dots] + U(\mathbf{r})n(\mathbf{r}) + \cdots, \tag{9.70}$$

where $U(\mathbf{r})$ represents an external (trapping) potential. This local density approximation (LDA) has met with remarkable success in quantum chemistry applications [113, 109, 110].

The simplest function contains a single term $E \propto n^{5/3}$. This—along with gradient corrections—has been explored in [114, 115], and, while it can model the energetics of the symmetric gas, it does not include information about pairing correlations. The extensions we describe here include both kinetic terms and an anomalous pairing density.

9.3.1.2 Densities and Currents

The first task is to construct the densities and currents. In the SLDA, we consider five types of densities: the standard particle densities $n_a(\mathbf{r}) \propto \langle a^\dagger(\mathbf{r})a(\mathbf{r})\rangle$ and $n_b(\mathbf{r}) \propto \langle b^\dagger(\mathbf{r})b(\mathbf{r})\rangle$, the kinetic densities $\tau_a(\mathbf{r}) \propto \langle a^\dagger(\mathbf{r})\Delta a(\mathbf{r})\rangle$ and $\tau_b(\mathbf{r}) \propto \langle b^\dagger(\mathbf{r})\Delta b(\mathbf{r})\rangle$, and an anomalous density $\nu(\mathbf{r}) \propto \langle a(\mathbf{r})b(\mathbf{r})\rangle$. When considering time dependence (Sec. 9.4), we must also include the currents $\mathbf{j}_a(\mathbf{r}) \propto \langle a^\dagger(\mathbf{r})\nabla a(\mathbf{r})\rangle$ and $\mathbf{j}_b(\mathbf{r}) \propto \langle b^\dagger(\mathbf{r})\nabla b(\mathbf{r})\rangle$ to restore Galilean invariance as discussed in Sec. 9.4.2. In principle, these densities may be non-local, but to simplify the functional we wish to consider only local quantities. The local form of the anomalous density ν leads to UV divergences that we must regularize as we discuss in Sec. 9.3.1.4.

The formal analysis proceeds with a four-component formalism discussed in Sec. 9.6.2, but the symmetries of the cold atom systems allow everything to be expressed in terms of two-component wavefunctions (see Appendix 9.6)

$$\psi_n(\mathbf{r}) = \begin{pmatrix} u_n(\mathbf{r}) \\ v_n(\mathbf{r}) \end{pmatrix} \tag{9.71}$$

with energy E_n. The densities and currents are constructed from these as

$$
\begin{aligned}
n_a(\mathbf{r}) &= \sum_n |u_n(\mathbf{r})|^2 f_\beta(E_n), \qquad n_b(\mathbf{r}) = \sum_n |v_n(\mathbf{r})|^2 f_\beta(-E_n), \\
\tau_a(\mathbf{r}) &= \sum_n |\nabla u_n(\mathbf{r})|^2 f_\beta(E_n), \quad \tau_b(\mathbf{r}) = \sum_n |\nabla v_n(\mathbf{r})|^2 f_\beta(-E_n),
\end{aligned} \tag{9.72a}
$$

$$
\begin{aligned}
\nu(\mathbf{r}) &= \frac{1}{2}\sum_n u_n(\mathbf{r}) v_n^*(\mathbf{r}) \Big(f_\beta(-E_n) - f_\beta(E_n) \Big), \\
\mathbf{j}_a(\mathbf{r}) &= \frac{\mathrm{i}}{2}\sum_n [u_n^*(\mathbf{r})\nabla u_n(\mathbf{r}) - u_n(\mathbf{r})\nabla u_n^*(\mathbf{r})]\, f_\beta(E_n), \\
\mathbf{j}_b(\mathbf{r}) &= \frac{\mathrm{i}}{2}\sum_n [v_n^*(\mathbf{r})\nabla v_n(\mathbf{r}) - v_n(\mathbf{r})\nabla v_n^*(\mathbf{r})]\, f_\beta(-E_n),
\end{aligned} \tag{9.72b}
$$

where $f_\beta(E_n) = 1/(\exp(\beta E_n)+1)$ is the Fermi distribution and $\beta = 1/T$ is the inverse temperature. Even though we shall only discuss the zero temperature limit of SLDA it is convenient for numerical purposes to introduce a very small temperature (much smaller than any other energy scale in the system) so that $\mathscr{E}(\mu)$ is a smooth function.

9.3.1.3 Functional Form

Our functionals generically include a kinetic term and a pairing term of the form

$$
\mathscr{E} = \frac{\hbar^2}{m}\left(\frac{\tau_a+\tau_b}{2}\right) + g\nu^\dagger\nu + \cdots, \tag{9.73}
$$

along with additional density dependent terms, where all of the densities and currents $n(\mathbf{r})$ etc. are functions of position but have no non-local structure. (Note that here and in many of the following formulae we suppress the explicit dependence on position $\mathbf{r}$.) In the superfluid, this local approximation has formal difficulties since the anomalous density $\nu(\mathbf{r},\mathbf{r}') \sim \sum u_n(\mathbf{r}) v_n^*(\mathbf{r}') \sim |\mathbf{r}-\mathbf{r}'|^{-1}$ diverges for small $|\mathbf{r}-\mathbf{r}'|$ if the pairing field is taken to be a multiplicative operator $\Delta(\mathbf{r})$. The kinetic energy densities $\tau_{a,b}(\mathbf{r})$ diverge as well. A proper local formulation thus requires regularization [116] as discussed in Sec. 9.3.1.4. We introduce an energy cutoff E_c—$\nu_c(\mathbf{r}) \sim \sum_{|E|<E_c} u_n(\mathbf{r}) v_n^*(\mathbf{r})$—and a cutoff dependent effective interaction g_{eff} such that

$$
\Delta = -g\nu = -g_{\text{eff}}\nu_c \tag{9.74}
$$

is finite and independent of the cutoff as $E_c \to \infty$. Once this is done, we can write the functional as

$$
\mathscr{E} = \frac{\hbar^2}{m}\left(\frac{\tau_a+\tau_b}{2}\right) - \Delta^\dagger\nu + \cdots. \tag{9.75}
$$

Note that ν is still formally divergent, but will cancel with a similar divergence in the kinetic piece such that the energy density is finite. The full forms of the local functionals considered here are thus:

Bogoliubov de-Gennes (BdG) [117]:

$$\mathscr{E}_{\mathrm{BdG}} = \frac{\hbar^2\tau_a}{2m_a} + \frac{\hbar^2\tau_b}{2m_b} + g\nu^\dagger\nu. \tag{9.76}$$

For homogeneous systems, this is equivalent to the Eagles-Leggett mean-field theory where the parameters here represent the bare parameters (elsewhere we shall only consider $m_a = m_b = m$) and the coupling constant is tuned to reproduce the vacuum two-body scattering length a. Note the absence of a self-energy: all of the interaction effects are modelled through the pairing interaction. One unphysical consequence is that the normal state is described as completely non-interacting in this model. While this may capture some qualitative features of the theory, and provides a rigorous variational bound on the energy, it cannot be trusted for quantitative results beyond the rather poor variational upper bound.

SLDA:

$$\mathscr{E}_{\mathrm{SLDA}} = \frac{\hbar^2}{m}\left(\frac{\alpha}{2}(\tau_a+\tau_b) + \beta\frac{3}{10}(3\pi^2)^{2/3}(n_a+n_b)^{5/3}\right) + g\nu^\dagger\nu. \tag{9.77}$$

This may be thought of as the unitary generalization of the symmetric BdG functional for symmetric matter $n_a = n_b = n_+/2$ to include a self-energy term $n_+^{5/3}$ (whose form is fixed by simple dimensional analysis) and an effective mass $m_{\mathrm{eff}} = m/\alpha$. The three parameters here α, β, and the pairing interaction g must be fixed by matching to experiments or ab initio calculations as discussed in Sec. 9.3.2.1. Since g is formally zero in the large coupling limit, we characterize it with a dimensionless constant γ such that $g_{\mathrm{eff}}^{-1} = (n_a+n_b)^{1/3}/\gamma - \Lambda$ where Λ is the cutoff discussed in Sec. 9.3.1.4.

ASLDA:

$$\mathscr{E}_{\mathrm{ASLDA}} = \frac{\hbar^2}{m}\left(\alpha_a(n_a,n_b)\frac{\tau_a}{2} + \alpha_b(n_a,n_b)\frac{\tau_b}{2} + D(n_a,n_b)\right) + g\nu^\dagger\nu. \tag{9.78}$$

Here we allow for polarization $n_a \neq n_b$ and so we must generalize the parameters such as the effective masses and self-interaction to be functions of the local polarization $p = (n_a - n_b)/(n_a + n_b)$. Dimensional analysis restricts these $\alpha_{a,b}(\lambda n_a, \lambda n_b) = \alpha(n_a, n_b)$ and $D(\lambda n_a, \lambda n_b) = \lambda^{5/3} D(n_a, n_b)$ so that we need only to parametrize functions of the single variable p as discussed in Sec. 9.3.2.1.

To fully define these functionals, we must now regularize the pairing interaction g (Sec. 9.3.1.4) and then specify the values and functional forms of the parameters and parametric functions (Sec. 9.3.2).

9.3.1.4 Regularization

As formulated, the local theory is ultraviolet divergent due to the well known behaviour of the anomalous density:

$$\nu(\mathbf{r},\mathbf{r}') \sim \sum_n u_n(\mathbf{r})v_n^*(\mathbf{r}') \propto \frac{1}{|\mathbf{r}-\mathbf{r}'|}. \tag{9.79}$$

There are many ways of dealing with this. For example, physical potentials are always non-local, and the non-locality naturally regulates the theory. However, in the unitary gas, the non-local (range of the interaction) is much smaller than any other length scale in the system and the stability of the system (see Sec. 9.1) indicates that the low-energy large-distance physics should be independent of the short-range details.

As a result, one can choose any sort of regularization scheme that is convenient and obtain the universal results with an appropriate limiting procedure. In the homogeneous case, one can use a variety of techniques: some interesting choices include dimensional regularization [118] and selective distribution functions [119]. The most straightforward is to use a momentum cutoff, but for inhomogeneous systems, momentum is not a good quantum number. Instead, an energy cutoff E_c suffices. All quantities—especially the divergent anomalous density—can be computed from states with energies below this cutoff:

$$\nu_c = \sum_{|E_n|<E_c} u_n v_n^* \frac{f_\beta(E_n) - f_\beta(-E_n)}{2}. \tag{9.80}$$

(To improve the behaviour, we actually use a smooth cutoff so that discontinuities are not introduced when levels cross in and out of the sum during the self-consistent iterations.)

To better understand the nature of these divergences, consider the ultraviolet limit where the length scale is much smaller than any other scale in the system. In this limit, the semi-classical Thomas-Fermi approximation may be applied locally. The linear divergences in both the symmetric combination of the kinetic energy and in the anomalous density have the form

$$\tau_+(k) = \tau_a(k) + \tau_b(k) \to \frac{2(m^*)^2\Delta^\dagger\Delta}{\hbar^4 k^2}, \qquad \nu(k) \to \frac{m^*\Delta}{\hbar^2 k^2}, \tag{9.81}$$

where the average effective mass $m^* = m/\alpha_+ = 2m/(\alpha_a+\alpha_b)$ enters explicitly through the equations of motion. From this it is clear that the combination

$$\frac{\hbar^2\tau_+}{2m^*} - \Delta^\dagger\nu = \frac{\hbar^2}{m}\left(\frac{\alpha_a\tau_a}{2} + \frac{\alpha_b\tau_b}{2}\right) + g\nu^\dagger\nu$$

remains finite if we regularize the theory such that the gap parameter remains finite for all values of the cutoff

$$\Delta = -g_{\text{eff}}\nu_c. \tag{9.82}$$

When regularizing the BdG equations (9.76), we hold fixed the vacuum two-body scattering length,

$$\frac{m}{4\pi\hbar^2 a} = \frac{1}{g} + \frac{1}{2}\int \frac{\mathrm{d}^3\mathbf{k}}{(2\pi)^3}\frac{1}{\frac{\hbar^2k^2}{2m} + \mathrm{i}0^+} \tag{9.83}$$

where $\fint$ is the principal value integral. This may be easily derived from the pseudo-potential approach (see for example [120, 121] or for higher partial waves [122, 123]).

In the other DFTs (9.77) and (9.78), g does not represent the physical interaction, but is simply another parameter of the theory. Thus, we define a similar regularization scheme by introducing a finite function $\tilde{C}(n_a, n_b)$ that must be fit in order to characterize the pairing interaction and correlations.[1]

$$\tilde{C}(n_a,n_b) = -\frac{\alpha_+ \nu}{\Delta} + \frac{1}{2}\fint \frac{\mathrm{d}^3\mathbf{k}}{(2\pi)^3} \frac{1}{\dfrac{\hbar^2 k^2}{2m} - \dfrac{\mu_+}{\alpha_+} + \mathrm{i}0^+} = \frac{\alpha_+}{g_{\text{eff}}} + \Lambda. \tag{9.84}$$

This differs from (9.83) in two ways: 1) we have included a factor of the effective mass parameter α_+ to ensure that the divergences (9.81) cancel and, 2) we have shifted the pole of the integral by the average local chemical potential $\mu_+ = (\mu_a - V_a + \mu_b + V_b)/2$ to improve convergence. As pointed out in [116], the shift does not change the integral in the limit of infinite cutoff, but greatly improves the convergence if a cutoff is used. Given a fixed momentum cutoff $k < k_c$, the integral Λ in the second term can be performed exactly

$$\Lambda = \frac{m}{\hbar^2}\frac{k_c}{2\pi^2}\left\{1 - \frac{k_0}{2k_c}\ln\frac{k_c+k_0}{k_c-k_0}\right\} \tag{9.85}$$

where $\hbar^2 k_0^2/(2m) = \mu_+/\alpha_+$ defines the location of the pole. In general, translational invariance is not preserved, and so we must use the fixed energy cutoff $|E(k)| < E_c$ that enters (9.80) rather than a momentum cutoff as the latter is not a good quantum number. To relate the two we used the local quasiparticle dispersion relationship:

$$\frac{\hbar^2}{2m}\alpha_+(\mathbf{r})k_0^2(\mathbf{r}) - \mu_+(\mathbf{r}) = 0, \tag{9.86a}$$

$$\frac{\hbar^2}{2m}\alpha_+(\mathbf{r})k_c^2(\mathbf{r}) - \mu_+(\mathbf{r}) = E_c. \tag{9.86b}$$

This defines a position-dependent momentum cutoff $k_c(\mathbf{r})$ and effective coupling constant $g(\mathbf{r})$ that can be used to regulate the anomalous density at any point in space:

$$\Lambda(\mathbf{r}) = \frac{m}{\hbar^2}\frac{k_c(\mathbf{r})}{2\pi^2}\left\{1 - \frac{k_0(\mathbf{r})}{2k_c(\mathbf{r})}\ln\frac{k_c(\mathbf{r})+k_0(\mathbf{r})}{k_c(\mathbf{r})-k_0(\mathbf{r})}\right\}, \tag{9.87a}$$

$$\frac{\alpha_+(\mathbf{r})}{g_{\text{eff}}(\mathbf{r})} = \tilde{C}\Big(n_a(\mathbf{r}), n_b(\mathbf{r})\Big) - \Lambda(\mathbf{r}), \tag{9.87b}$$

$$\Delta(\mathbf{r}) = -g_{\text{eff}}(\mathbf{r})\nu_c(\mathbf{r}). \tag{9.87c}$$

[1] We have changed notations slightly from [124] using $\tilde{C}(n_a,n_b) = \alpha_+ C(n_a,n_b)$ which simplifies the equations because, in the limit of infinite cutoff, Λ is independent of any densities and functional parameters.

Varying the functional with respect to the occupation numbers (see Appendix 9.6.1 for a formal description) allows us to derive the self-consistency conditions. Recall that the functional has the form

$$\alpha_-(n_a,n_b)\frac{\hbar^2\tau_-}{2m}+\alpha_+(n_a,n_b)\left(\frac{\hbar^2\tau_+}{2m}+\frac{g_{\rm eff}}{\alpha_+}\nu_c^\dagger\nu_c\right)+\frac{\hbar^2}{m}D(n_a,n_b), \tag{9.88}$$

and that, in the limit of infinite cutoff, Λ has no dependence on the functional parameters so that[2]

$$\mathrm{d}\tilde{C}=\mathrm{d}\left(\frac{\alpha_+}{g_{\rm eff}}\right) \qquad \Longrightarrow \qquad \mathrm{d}\left(\frac{g_{\rm eff}}{\alpha_+}\right)=-\left(\frac{g_{\rm eff}}{\alpha_+}\right)^2\mathrm{d}\tilde{C}. \tag{9.89}$$

Thus, we have the following equations:

$$\begin{pmatrix} K_a-\mu_a+V_a & \Delta^\dagger \\ \Delta & -K_b+\mu_b-V_b \end{pmatrix}\begin{pmatrix} u_n \\ v_n \end{pmatrix}=E_n\begin{pmatrix} u_n \\ v_n \end{pmatrix}$$

where

$$\begin{aligned}
K_a u &= -\frac{\hbar^2}{2m}\nabla_i\big(\alpha_a(n_a,n_b)\nabla_i u\big)\\
K_b v &= -\frac{\hbar^2}{2m}\nabla_i\big(\alpha_b(n_a,n_b)\nabla_i v\big)\\
V_a &= \frac{\partial\alpha_-(n_a,n_b)}{\partial n_a}\frac{\hbar^2\tau_-}{2m}+\frac{\partial\alpha_+(n_a,n_b)}{\partial n_a}\left(\frac{\hbar^2\tau_+}{2m}-\frac{\Delta^\dagger\nu}{\alpha_+(n_a,n_b)}\right)\\
&\quad-\frac{\partial\tilde{C}(n_a,n_b)}{\partial n_a}\frac{\Delta^\dagger\Delta}{\alpha_+}+\frac{\hbar^2}{m}\frac{\partial D(n_a,n_b)}{\partial n_a}+U_a(\mathbf{r}),\\
\alpha_\pm(n_a,n_b) &= \tfrac{1}{2}[\alpha_a(n_a,n_b)\pm\alpha_b(n_a,n_b)],\\
\tau_\pm &= \tau_a\pm\tau_b.
\end{aligned}$$

and similarly with $a\leftrightarrow b$.

9.3.2 Determining the SLDA and ASLDA Energy Density Functionals

Unless one has perturbative control over the theory, one cannot in general determine the correct functional from first principles. Instead, the functional must be treated as a model incorporating the most relevant physics for the application at hand. As such, one must determine some parameters in order to make predictions about other

[2] There is a small correction due to the residual density dependence of Λ at finite cutoff but in practice this is insignificant.

properties of the system. Here we use properties of homogeneous matter in the thermodynamic limit to determine the parameters of our functional, and then use the functional to compute the properties of non-uniform systems such as trapped gases. Our hope is that the single particle states in the self-consistent approach will provide a good description of the finite size (shell) effects missing in the Thomas Fermi approximation.

Fortunately, the thermodynamic functions describing the unitary Fermi gas are tightly constrained [101], and have both calculational and experimental verification. We shall now describe how to use these constraints to determine the form of the dimensionless parameters describing the functional.

9.3.2.1 Homogeneous Matter

A simple Thomas-Fermi calculation can be employed to describe states of homogeneous matter by exploiting the translational invariance of the system. This allows us to fix all non-gradient terms in the functional. The only remaining term—the effective mass—must be fixed by other means and we use the quasiparticle properties to determine this coefficient.

NORMAL PHASE

The energy-density for the normal phase of homogeneous matter has the form

$$\mathscr{E}[n_a,n_b] = \frac{\hbar^2}{m}\frac{\left(6\pi^2(n_a+n_b)\right)^{5/3}}{20\pi^2}G(p), \qquad p=\frac{n_a-n_b}{n_a+n_b}\in[-1,1]. \tag{9.90a}$$

where

$$G(p) = \alpha(p)\left(\frac{1+p}{2}\right)^{5/3} + \alpha(-p)\left(\frac{1-p}{2}\right)^{5/3} + 2^{-2/3}\beta(p) \tag{9.90b}$$

and $\beta(p)$ is defined through

$$D(n_a,n_b) = \frac{\left(6\pi^2(n_a+n_b)\right)^{5/3}}{20\pi^2}2^{-2/3}\beta(p). \tag{9.90c}$$

The function $G(p)$ will be the main function that enters our numerical formulae.[3]

We shall define the dimensionless function $G(p)$ by fitting a simple even polynomial to the Monte-Carlo data tabulated for $f[p(x)]$.[4] From this, the function $D(n_a,n_b)$

[3] In our previous calculations [125, 124], we used a more complicated parametrization: the present form $G(p)$ is just as good and much simpler and we advocate its use instead.

[4] $G(p)$ is related to the other dimensionless functions $f(x)$ and $g(x)$ discussed in the literature as:

may be directly expressed in terms of the inverse effective mass $\alpha(p)$, which may be independently parametrized:

$$D(n_a,n_b) = \frac{\left(6\pi^2(n_a+n_b)\right)^{5/3}}{20\pi^2}\left[G(p) - \alpha(p)\left(\frac{1+p}{2}\right)^{5/3} - \alpha(-p)\left(\frac{1-p}{2}\right)^{5/3}\right].$$

The function $G(p)$ describing the normal state has been well-constrained by Monte-Carlo data [64] (see Fig. 9.9). As shown in Fig. 9.9, the function $G(p)$ is very well parametrized by a simple quadratic polynomial:

$$G(p) = 0.357 + 0.642p^2. \tag{9.91}$$

SYMMETRIC SUPERFLUID STATE $n_a = n_b$

As suggested in [127], by considering the calculated properties of the fully paired symmetric superfluid, one may determine the values of the functions $\alpha(p)$, $\tilde{C}(n_a,n_b)$, and $D(n_a,n_b)$ at the point $p = 0$ where the energy density functional depends only on the symmetric combination of parameters $n_a = n_b$ and $\tau_a = \tau_b$. For any value of the inverse effective mass $\alpha = \alpha_{p=0}$, one can uniquely determine the self-energy $\beta = \beta_{p=0}$ and pairing interaction γ by requiring that the energy and gap satisfy

$$\mathscr{E}_{SF} = \mathscr{E}(n,n) = \xi\mathscr{E}_{FG} = \xi\frac{\hbar^2}{m}\frac{(6\pi^2 n)^{5/3}}{10\pi^2}, \tag{9.92a}$$

$$\Delta = \eta\varepsilon_F = \eta\frac{\hbar^2}{m}\frac{(6\pi^2 n)^{2/3}}{2}. \tag{9.92b}$$

The parameters ξ and $\eta = \Delta/\varepsilon_F$ have been calculated using several Monte-Carlo techniques [18, 57, 59, 61, 45]. We take the following values in our estimates [57, 59]:

$$\xi = \frac{\mathscr{E}(n,n)}{\mathscr{E}_{FG}(n,n)} = 0.40(1), \qquad \eta = \frac{\Delta}{\varepsilon_F} = 0.504(24). \tag{9.93}$$

In order to determine the effective mass, we consider the quasiparticle dispersion relationship [57]. Within our density functional, this has the form

$$G(p) = \left(\frac{1+p}{2}g(p)\right)^{5/3} = \left(\frac{1+p}{2}\right)^{5/3} f(p), \qquad x = \frac{n_b}{n_a} \in [0,\infty].$$

The function $g(x) = g[p(x)]$ introduced in [101] has the necessary and sufficient requirement of convexity to satisfy the second law of thermodynamics; and the function $f(x) = f[p(x)]$ was introduced in [126] and has been tabulated using Monte-Carlo methods [64].

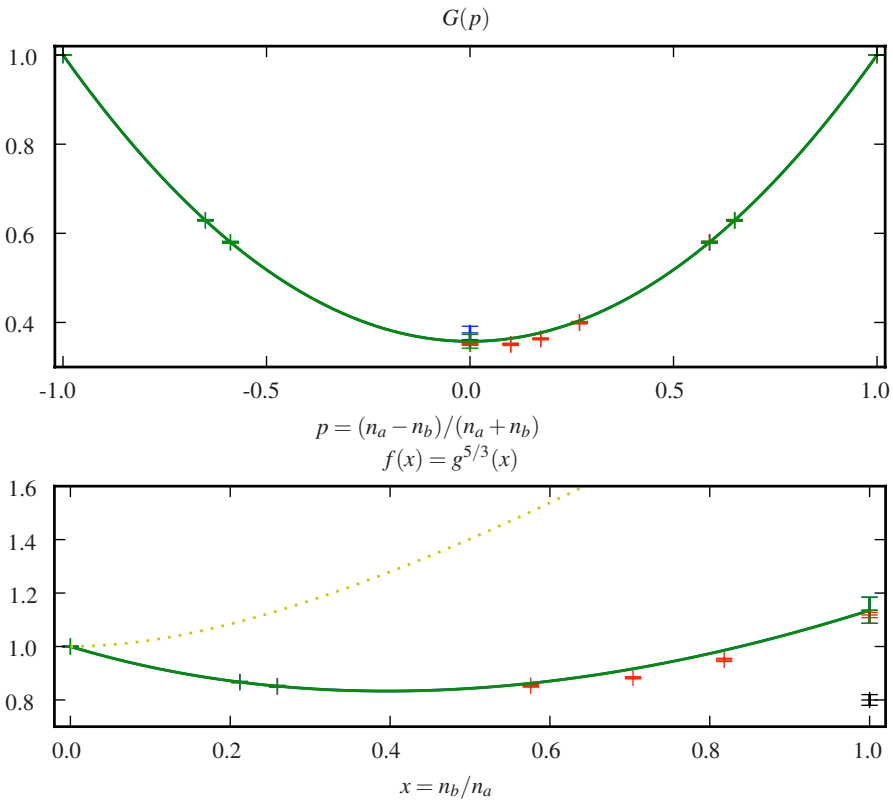

Fig. 9.9 Monte Carlo data used to fit the function $G(p)$ (top) and in its raw form $f(x) = g^{5/2}(x)$ (bottom) representing the energy of the normal state with respect to the energy of the free system. We excluded the red points from our fit because we suspect that they slightly contaminated by the superfluid state (and hence have a lower energy). Fitting these close to the superfluid state would require a double hump structure in $G(p)$ for which we do not yet see any physical motivation. To anchor the solution in the superfluid phase, we include a datum $\beta_{p=0}$ extracted from the symmetric state (9.95b). The value here depends slightly on whether or not we also extract an effective mass, or hold $\alpha = 1$ constant. Both fits are shown (but lie on top of each other). The present fit is the simple two-parameter quadratic given in (9.91). At the lower-right of the lower plot we have shown the values of $f_{x=1}$ for the superfluid state (black point). Finally, for comparison, we have included the function $f(x)$ obtained using the standard mean-field (Eagles-Leggett) approximation as a dotted yellow line to show that it bears little resemblance to the physical curves.

$$E_{qp}(k) = \sqrt{\left(\frac{\hbar^2 k^2}{2m_{\text{eff}}} - \mu_{\text{eff}}\right)^2 + \Delta^2} \tag{9.94}$$

where $n_a + n_b = k_F^3/3\pi^2$ is the Fermi wave-vector and μ_{eff} is the effective chemical potential. It turns out that μ_{eff} also depends on Δ/ε_F, so the quasiparticle dispersion relation is really a function of only two parameters: the effective mass and Δ/ε_F.

The fit to the Carlson-Reddy data [128] is shown in Fig. 9.10 and gives the following parameter values:[5]

$$\alpha_{p=0} = m_{\text{eff}}^{-1}/m^{-1} = \quad 1.094(17), \tag{9.95a}$$
$$\beta_{p=0} = -0.526(18), \tag{9.95b}$$
$$\gamma^{-1} = -0.0907(77), \tag{9.95c}$$
$$\eta = \Delta/\varepsilon_F = \quad 0.493(12), \tag{9.95d}$$
$$\xi_N = \alpha + \beta = \quad 0.567(24). \tag{9.95e}$$

where $\xi_N \mathscr{E}_{FG}$ is the energy of the interacting normal state predicted by the functional. Note that this agrees very well with the value given by $G(p)$ in Fig. 9.9 (we have used this parameter as an additional point in the fitting of $G(p)$).

In principle, one should use some form of ab initio calculation or experimental measurement for polarized systems to determine the dependence of the parameters α, β, and γ on the polarization $p = n_b/n_a$. Unfortunately, the fermion sign problem has made this difficult and there is presently insufficient quality data to perform such a fit. Instead, we simply fix

$$\gamma(p) = \gamma_{p=0} = -11.11(94). \tag{9.96}$$

If high quality data about polarized superfluid states become available, one might consider promoting this parameter to a polarization dependent function similarly to $\alpha(p)$ and $G(p)$. This fixes the pairing interaction:

$$\tilde{C}(n_a, n_b) = \frac{m}{\hbar^2} \frac{\alpha_+(p)(n_a + n_b)^{1/3}}{\gamma(p)}. \tag{9.97}$$

Effective Mass Parametrization: $\alpha(n_a, n_b)$

As discussed above, the effective mass cannot be determined solely from the properties of homogeneous matter. It is also clear in DFT's developed perturbatively [129, 130] that the effective mass is arbitrary. In the ASLDA, however, the only gradient terms that enter the functional are the kinetic terms τ whose coefficients are the effective masses. To allay the need for additional gradient corrections, one must

[5] We have performed a simple two-parameter non-linear least-squares fit which has a reduced $\chi^2_{\text{red}} = 1.1$, indicating a very good fit.

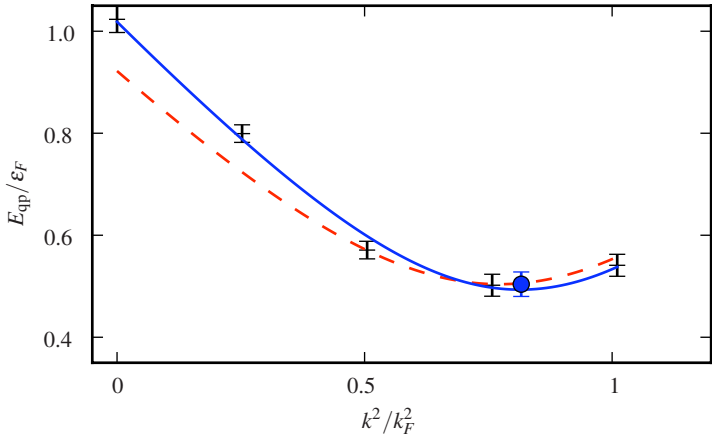

Fig. 9.10 Fit of the Monte-Carlo data for the quasiparticle dispersions from [57] with the BCS form (9.94). The solid blue curve is the full two-parameter fit including the mass as a parameter. This is used to determine the effective mass of the fully paired symmetric matter $m_{\rm eff} = 0.91(1)$. The dashed red curve is a one-parameter fit holding the mass fixed to $m = 1$.

provide a parametrization of the effective mass. Fortunately, three values are well determined: In a fully polarized system, the effective mass of the majority species remains unchanged, $m_{p=1} = 1.0m$, while in the minority species, the effective "polaron" mass $m_{p=-1} = 1.20m$ [131]. We use this value, but note that there are other estimates: Monte Carlo calculations give $m_{-1} = 1.04(3)$ [64] and $m_{-1} = 1.09(2)$ [132], and experiments measure $m_{-1} = 1.06$ (no error given) [133] and $m_{-1} = 1.17(10)$ [134]. The third value for symmetric matter $m_0 = m/\alpha_{p=0}$ is determined in (9.95a).

We now have three data-points constraining the effective mass parametrization of $\alpha(p)$. For numerical reasons, in order to ensure that the effective potentials $V_{a,b}$ approach zero as the density falls to zero, we impose the additional constraint that the first and second derivatives of $\alpha(p)$ vanish at the end-points $p = \pm 1$. Taken together, this fixes a sixth order, two parameter polynomial approximation for $\alpha(p)$:

$$\alpha(p) = 1.094 + 0.156p(1 - 2p^2/3 + p^4/5) - 0.532p^2(1 - p^2 + p^4/3). \quad (9.98)$$

9.3.2.2 Summary

Here we summarize the complete definition of the ASLDA functional. The SLDA functional follows by setting the local polarization

$$p(\mathbf{r}) = \frac{n_a(\mathbf{r}) - n_b(\mathbf{r})}{n_a(\mathbf{r}) + n_b(\mathbf{r})} \quad (9.99)$$

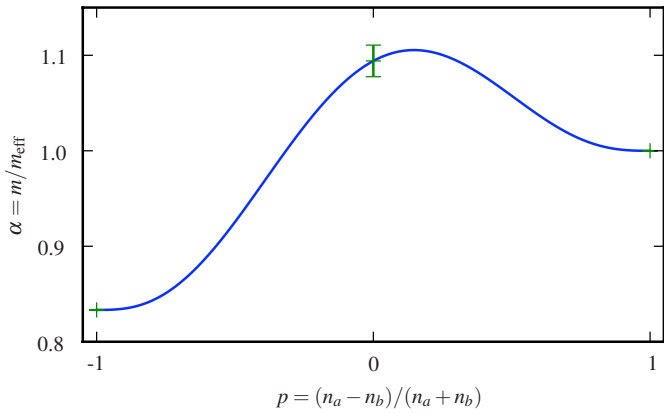

Fig. 9.11 Inverse effective mass $\alpha(p) = m/m_{\rm eff}(p)$ as a function of the polarization $p = (n_a - n_b)/(n_a + n_b)$. The functional fit is the polynomial (9.98).

to zero. First, fitting the quasiparticle dispersion relationships, gap and energy for the superfluid state gives the SLDA parameters at $p = 0$:

$$\alpha_{p=0} = 1.094(17), \quad \beta_{p=0} = -0.526(18), \quad \gamma_{p=0}^{-1} = -0.0907(77). \quad \text{(from (9.95))}$$

Using this derived effective mass, and the energy data for the normal state from Monte Carlo data we obtain the following polynomial fits defining the polarization dependence of the effective mass and self-energy:

$$\alpha(p) = 1.094 + 0.156p\left(1 - \frac{2p^2}{3} + \frac{p^4}{5}\right) - 0.532p^2\left(1 - p^2 + \frac{p^4}{3}\right), \quad \text{(from (9.98))}$$

$$G(p) = 0.357 + 0.642p^2, \quad \text{(from (9.91))}$$

$$\gamma(p) = \gamma_{p=0} = -11.11(94). \quad \text{(from (9.96))}$$

These fix the specification of the functional parameters

$$\alpha_a(n_a, n_b) = \alpha(p), \quad \alpha_b(n_a, n_b) = \alpha(-p), \quad \tilde{C}(n_a, n_b) = \frac{m}{\hbar^2}\frac{\alpha_+(p)(n_a + n_b)^{1/3}}{\gamma(p)},$$

$$D(n_a, n_b) = \frac{\left(6\pi^2(n_a + n_b)\right)^{5/3}}{20\pi^2}\left[G(p) - \alpha(p)\left(\frac{1+p}{2}\right)^{5/3} - \alpha(-p)\left(\frac{1-p}{2}\right)^{5/3}\right],$$

in terms of the densities

$$
\begin{aligned}
n_a(\mathbf{r}) &= \sum_{|E_n|<E_c} |u_n(\mathbf{r})|^2 f_\beta(E_n), \qquad n_b(\mathbf{r}) = \sum_{|E_n|<E_c} |v_n(\mathbf{r})|^2 f_\beta(-E_n), \\
\tau_a(\mathbf{r}) &= \sum_{|E_n|<E_c} |\nabla u_n(\mathbf{r})|^2 f_\beta(E_n), \quad \tau_b(\mathbf{r}) = \sum_{|E_n|<E_c} |\nabla v_n(\mathbf{r})|^2 f_\beta(-E_n), \\
\nu(\mathbf{r}) &= \frac{1}{2} \sum_{|E_n|<E_c} u_n(\mathbf{r}) v_n^*(\mathbf{r}) \Big(f_\beta(-E_n) - f_\beta(E_n) \Big), \\
\mathbf{j}_a(\mathbf{r}) &= \frac{\mathrm{i}}{2} \sum_{|E_n|<E_c} [u_n^*(\mathbf{r}) \nabla u_n(\mathbf{r}) - u_n(\mathbf{r}) \nabla u_n^*(\mathbf{r})] f_\beta(E_n), \\
\mathbf{j}_b(\mathbf{r}) &= \frac{\mathrm{i}}{2} \sum_{|E_n|<E_c} [v_n^*(\mathbf{r}) \nabla v_n(\mathbf{r}) - v_n(\mathbf{r}) \nabla v_n^*(\mathbf{r})] f_\beta(-E_n),
\end{aligned}
$$

in the form

$$
\mathscr{E}_{\mathrm{ASLDA}} = \frac{\hbar^2}{m} \left(\alpha_a(n_a, n_b) \frac{\tau_a}{2} + \alpha_b(n_a, n_b) \frac{\tau_b}{2} + D(n_a, n_b) \right) + g_{\mathrm{eff}} \nu^\dagger \nu
$$

together with the renormalization conditions

$$
\begin{aligned}
\Delta(\mathbf{r}) &= -g_{\mathrm{eff}}(\mathbf{r}) \nu_c(\mathbf{r}), \quad \frac{\alpha_+(\mathbf{r})}{g_{\mathrm{eff}}(\mathbf{r})} = \tilde{C}(\mathbf{r}) - \Lambda(\mathbf{r}) \\
\Lambda(\mathbf{r}) &= \frac{m}{\hbar^2} \frac{k_c(\mathbf{r})}{2\pi^2} \left\{ 1 - \frac{k_0(\mathbf{r})}{2k_c(\mathbf{r})} \ln \frac{k_c(\mathbf{r}) + k_0(\mathbf{r})}{k_c(\mathbf{r}) - k_0(\mathbf{r})} \right\}, \\
\frac{\hbar^2}{2m} \alpha_+(\mathbf{r}) k_0^2(\mathbf{r}) - \mu_+(\mathbf{r}) &= 0, \quad \frac{\hbar^2}{2m} \alpha_+(\mathbf{r}) k_c^2(\mathbf{r}) - \mu_+(\mathbf{r}) = E_c
\end{aligned}
$$

where $\alpha_+ = (\alpha_a + \alpha_b)/2$ and $\mu_+ = (\mu_a - V_a + \mu_b + V_b)/2$ is the average chemical potential defined through the equations:

$$
\begin{pmatrix} K_a - \mu_a + V_a & \Delta^\dagger \\ \Delta & -K_b + \mu_b - V_b \end{pmatrix} \begin{pmatrix} u_n \\ v_n \end{pmatrix} = E_n \begin{pmatrix} u_n \\ v_n \end{pmatrix}
$$

where

$$
\begin{aligned}
K_a u &= -\frac{\hbar^2}{2m} \nabla_i \big(\alpha_a(n_a, n_b) \nabla_i u \big) \\
K_b v &= -\frac{\hbar^2}{2m} \nabla_i \big(\alpha_b(n_a, n_b) \nabla_i v \big) \\
V_a &= \frac{\partial \alpha_-(n_a, n_b)}{\partial n_a} \frac{\hbar^2 \tau_-}{2m} + \frac{\partial \alpha_+(n_a, n_b)}{\partial n_a} \left(\frac{\hbar^2 \tau_+}{2m} - \frac{\Delta^\dagger \nu}{\alpha_+(n_a, n_b)} \right) \\
&\quad - \frac{\partial \tilde{C}(n_a, n_b)}{\partial n_a} \frac{\Delta^\dagger \Delta}{\alpha_+} + \frac{\hbar^2}{m} \frac{\partial D(n_a, n_b)}{\partial n_a} + U_a(\mathbf{r}), \\
\alpha_\pm(n_a, n_b) &= \tfrac{1}{2} [\alpha_a(n_a, n_b) \pm \alpha_b(n_a, n_b)], \\
\tau_\pm &= \tau_a \pm \tau_b.
\end{aligned}
$$

and similarly with $a \leftrightarrow b$.

9.3.3 Using the SLDA and ASLDA

Once the form of the DFT and its parameters have been fixed, the function needs to be tested and applied. Since we fit the parameters using QMC results for homogeneous matter, a non-trivial test is to compare it with ab initio results in inhomogeneous situations. This will asses the accuracy of the approximation we have made in neglecting gradient corrections beyond the kinetic term. In Sec. 9.3.3.1 we compare the predictions of the DFTs with QMC calculations of trapped systems. Next we show how the functionals can be used to explore mesoscopic physics inaccessible to QMC analysis techniques: we consider the structure of superfluid vortices in Sec. 9.3.3.2, and the prediction of a supersolid phase in the asymmetric case in Sec. 9.3.3.3.

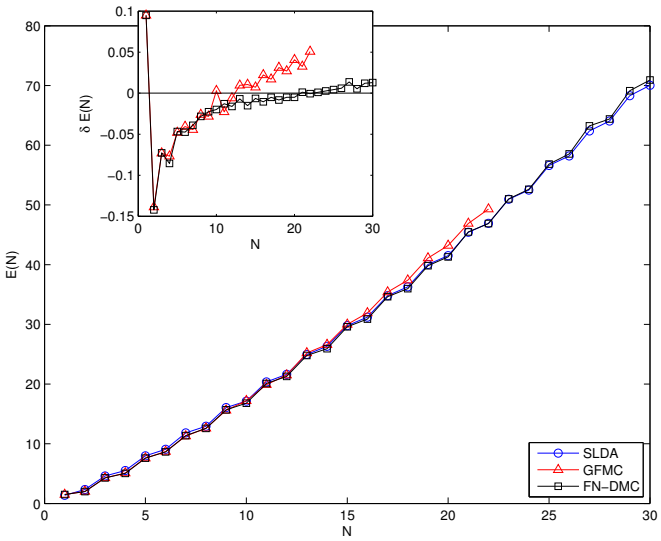

Fig. 9.12 The comparison between the GFMC [135], FN-DMC [136] and SLDA total energies $E(N)$. The clear odd-even staggering of the energies is due to the onset of the pairing correlations. The inset shows the discrepancy between the GFMC and FN-DMC and SLDA energies, $\delta E(N) = E_{MC}(N)/E_{\mathrm{SLDA}}(N) - 1$, where $E_{MC}(N)$ stands for the energies obtained in GFMC or FN-DMC respectively.

Normal State				Superfluid State			
(N_a,N_b)	E_{FNDMC}	E_{ASLDA}	(error)	(N_a,N_b)	E_{FNDMC}	E_{ASLDA}	(error)
$(3,1)$	6.6 ± 0.01	6.687	1.3%	$(1,1)$	2.002 ± 0	2.302	15%
$(4,1)$	8.93 ± 0.01	8.962	0.36%	$(2,2)$	5.051 ± 0.009	5.405	7%
$(5,1)$	12.1 ± 0.1	12.22	0.97%	$(3,3)$	8.639 ± 0.03	8.939	3.5%
$(5,2)$	13.3 ± 0.1	13.54	1.8%	$(4,4)$	12.573 ± 0.03	12.63	0.48%
$(6,1)$	15.8 ± 0.1	15.65	0.93%	$(5,5)$	16.806 ± 0.04	16.19	3.7%
$(7,2)$	19.9 ± 0.1	20.11	1.1%	$(6,6)$	21.278 ± 0.05	21.13	0.69%
$(7,3)$	20.8 ± 0.1	21.23	2.1%	$(7,7)$	25.923 ± 0.05	25.31	2.4%
$(7,4)$	21.9 ± 0.1	22.42	2.4%	$(8,8)$	30.876 ± 0.06	30.49	1.2%
$(8,1)$	22.5 ± 0.1	22.53	0.14%	$(9,9)$	35.971 ± 0.07	34.87	3.1%
$(9,1)$	25.9 ± 0.1	25.97	0.27%	$(10,10)$	41.302 ± 0.08	40.54	1.8%
$(9,2)$	26.6 ± 0.1	26.73	0.5%	$(11,11)$	46.889 ± 0.09	45	4%
$(9,3)$	27.2 ± 0.1	27.55	1.3%	$(12,12)$	52.624 ± 0.2	51.23	2.7%
$(9,5)$	30 ± 0.1	30.77	2.6%	$(13,13)$	58.545 ± 0.18	56.25	3.9%
$(10,1)$	29.4 ± 0.1	29.41	0.034%	$(14,14)$	64.388 ± 0.31	62.52	2.9%
$(10,2)$	29.9 ± 0.1	30.05	0.52%	$(15,15)$	70.927 ± 0.3	68.72	3.1%
$(10,6)$	35 ± 0.1	35.93	2.7%	$(1,0)$	1.5 ± 0.0	1.5	0%
$(20,1)$	73.78 ± 0.01	73.83	0.061%	$(2,1)$	4.281 ± 0.004	4.417	3.2%
$(20,4)$	73.79 ± 0.01	74.01	0.3%	$(3,2)$	7.61 ± 0.01	7.602	0.1%
$(20,10)$	81.7 ± 0.1	82.57	1.1%	$(4,3)$	11.362 ± 0.02	11.31	0.49%
$(20,20)$	109.7 ± 0.1	113.8	3.7%	$(7,6)$	24.787 ± 0.09	24.04	3%
$(35,4)$	154 ± 0.1	154.1	0.078%	$(11,10)$	45.474 ± 0.15	43.98	3.3%
$(35,10)$	158.2 ± 0.1	158.6	0.27%	$(15,14)$	69.126 ± 0.31	62.55	9.5%
$(35,20)$	178.6 ± 0.1	180.4	1%				

Table 9.2 Comparison between the ASLDA density functional as described in this section and the FN-DMC calculations [136, 137] for a harmonically trapped unitary gas at zero temperature. The normal state energies are obtained by fixing $\Delta = 0$ in the functional: In the FN-DMC calculations, this is obtained by choosing a nodal ansatz without any pairing. In the case of small asymmetry, the resulting "normal states" may be a somewhat artificial construct as there is no clear way of preparing a physical system in this "normal state" when the ground state is superfluid.

9.3.3.1 Trapped Systems

The functional form of both the SLDA and ASLDA have been completely fixed by considering only homogeneous matter. Hence, a non-trivial test of the theory is to compare the energy of trapped systems with Monte Carlo calculations. This was first done for the SLDA in [127] and the results are shown in Fig. 9.12. Even for systems with only a few particles—which have large gradients—the agreement is within 10%. This rapidly improves to the percent level as one move to larger systems.

The agreement is somewhat remarkable. In particular, we have included no gradient corrections in the theory beyond the Kohn-Sham kinetic energy. These gradient corrections will contribute at some level, but in the present system the coefficients are extremely tiny (the leading gradient correction $\sim (\nabla n)^2/n$ should give corrections that scale as $E \propto N^{2/3}$ for which there is no evidence in the Monte Carlo data). In any case, the agreement provides strong evidence that the SLDA captures the relevant energetics to provide a quantitative model of the unitary Fermi gas.

We should point out that the gradient terms in the SLDA are completely characterized by the kinetic terms. Thus, finite size effects are highly sensitive to the inverse effective mass parameter α. As mentioned in Sec. 9.3.2.1, the energy and gap can be fit with $\alpha = 1$, but the resulting parametrization demonstrates a marked systematic deviation from the trap energies shown in Fig. 9.12. It is reassuring that the agreement is restored when the effective mass is chosen (9.95a) to reproduce the quasiparticle spectrum.

We have validated the ASLDA in a similar manner for trapped systems in Table 9.2. Again, the agreement is at the few percent level in virtually all cases. In general, the formulation of the unitary DFT has a remarkable ability to capture the finite size effects in systems down to even a few particles [138], lending credence to the approximation of neglecting further gradients beyond the standard kinetic terms. This was somewhat anticipated since the kinetic terms completely describe finite size (shell) effects in the non-interacting system, but is non-trivial in the strongly interacting case of the unitary gas.

Note that the BdG and SLDA functionals have also been considered in larger trapped systems [139, 140].

9.3.3.2 Vortex Structure

The first use of the SLDA was to determine the structure of superfluid vortices [60]. In this work, two forms of SLDA (slightly different parameter values) were considered, and the solution for an axial symmetric vortex with unit circulation was found. The method of solution uses a technique that properly treats the infinite boundary conditions without truncating the physical space and introducing finite-size artifacts (see [141, 142] for details). The profile for this vortex is shown in Fig. 9.13. In particular, it was predicted that the vortices should have a significant density depletion in the core—something that is not observed in the weak-coupling limit where pairing is exponentially suppressed. This predicted core depletion allows for the direct imaging of vortices in rotating trapped gasses [143], providing direct evidence for superfluidity in these systems.

9.3.3.3 FFLO/LOFF

The first application of the ASLDA was to consider the energetic stability of a Larkin-Ovchinnikov–Fulde-Ferrell (LOFF) [146, 147] polarized superfluid state [125]. The density functional as constructed naturally supports a strong first-order phase transition between the fully paired superfluid state and the interacting normal state (dashed line in Fig. 9.14). We seed the functional with a periodic solution of the form shown in Fig. 9.15 with a node in the gap $\Delta(z)$. Allowing the system to relax to the optimal period L we find that this Larkin-Ovchinnikov type of solution has significantly lower energy than the competing pure and mixed phases over a large range of the phase diagram.

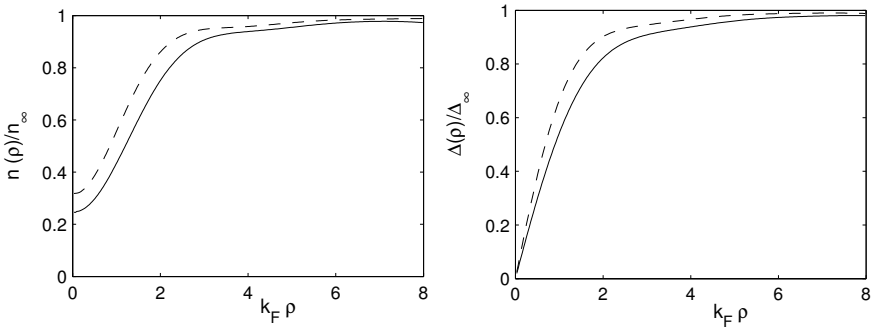

Fig. 9.13 Density profile (left) and gap parameter (right) from [60] for a superfluid vortex in the symmetric $n_a = n_b$ unitary Fermi gas with unit circulation. The solid curve corresponds to a parametrization of the SLDA with no self-energy $\beta = 0$ but including an effective mass correction. The dotted curve corresponds to a version with unit effective mass $\alpha = 1$. The other two parameters were fixed to reproduce the best approximation to energies of the normal and superfluid states known at the time: $\xi_N = 0.54$ and $\xi_{SF} = 0.44$. The current parameter set (9.95) should be preferred, but gives similar results. Note: The solid curve does not have the required currents to restore Galilean invariance (see Sec. 9.4.2), but the effect should be small here. Since the dotted curve has no effective mass correction, Galilean corrections are not required.

This is a qualitatively new prediction of the ASLDA: such states are only metastable in the BdG. The effect of the self-energy corrections is to reduce the energy of these states to favor them over the homogeneous phases. It is interesting to note that the density contrast of these states is comparable to the density contrast in vortices (see Fig. 9.13). Such states have yet to be observed in experiments: this may be because the physical region in which the LO state is favoured exists only in a thin shell. Also, the one-dimensional structure discussed here will be unstable at any finite temperature [148] (see also [149]) but might be stabilized in traps. The ground state will most likely be some sort of three-dimensional lattice structure (see for example [150]) which will likely require a fairly large physical volume to exists without significant frustration. The ideal situation would be a very flat trap tuned so that the LO region occupies a large physical space at the center of this trap, however, the construction of such traps presently poses some experimental difficulties that we hope will be overcome in the near future.

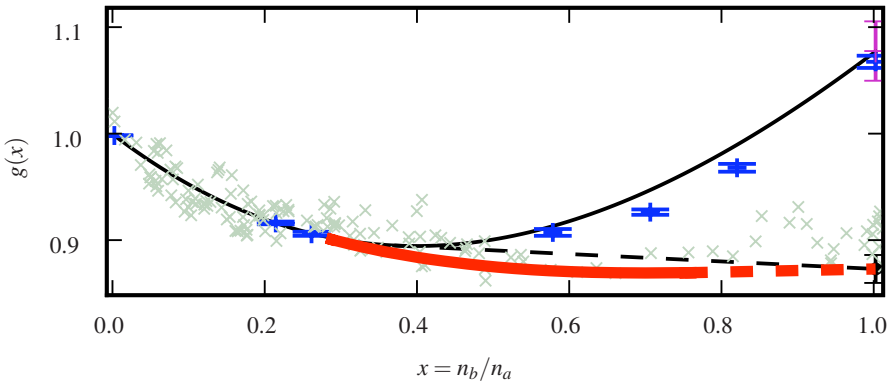

Fig. 9.14 The dimensionless convex function $g(x)$ [101] that defines the energy density $\mathscr{E}(n_a,n_b) = \frac{3}{5}\frac{\hbar^2}{2m}(6\pi^2)^{2/3}\left[n_a g(x)\right]^{5/3}$ as a function of the asymmetry $x = n_b/n_a$ (this plot is very similar to Fig. 9.9). The points with error-bars (blue online) are the Monte Carlo data from [132, 144, 64]. The fully-paired solution $g(1) = (2\xi)^{3/5}$ is indicated to the bottom right, and the recent MIT data [133] is shown (light $\times$) for comparison. The phase separation discussed in [132, 144, 64, 101] is shown by the Maxwell construction (thin black dashed line) of the first-order transition. The LO state (thick red curve) has *lower energy* than all pure states and phase separations previously discussed. The Maxwell construction of the weakly first-order transition between the superfluid and LOFF phase is shown by the thick dashed line (red).

9.4 Time-Dependent Superfluid Local Density Approximation

9.4.1 Time-Dependent Equations for the Quasiparticle Wave Functions

The equations for the time-dependent quasiparticle wave functions $u_{n,\sigma}(\mathbf{r},t)$, $v_{n,\sigma}(\mathbf{r},t)$ have the time-dependent Bogoliubov-de Gennes form

$$\mathrm{i}\hbar\frac{\partial}{\partial t}\begin{pmatrix} u_a \\ u_b \\ v_a \\ v_b \end{pmatrix} = \begin{pmatrix} h_a + U_a & 0 & 0 & \Delta \\ 0 & h_b + U_b & -\Delta & 0 \\ 0 & -\Delta^* & -h_a^* - U_a & 0 \\ \Delta^* & 0 & 0 & -h_b^* - U_b \end{pmatrix}\begin{pmatrix} u_a \\ u_b \\ v_a \\ v_b \end{pmatrix}. \tag{9.100}$$

For the sake of simplicity, we have dropped the arguments $(\mathbf{r},t)$ for all functions in these equations. Note also that the external potentials $U_\sigma(\mathbf{r},t)$ are real. The only difference with the static SLDA in the structure of $h_\sigma(\mathbf{r},t)$ are the contributions arising from the variation of the current density correction to the kinetic energy density $\tilde{\tau}(\mathbf{r},t)$ (9.104,9.110), which are required by Galilean invariance to be discussed in Sec. 9.4.2. The chemical potentials $\mu_{a,b}$, which can always be thought of as external constraints, are implicitly included in $U_\sigma(\mathbf{r},t)$. The chemical potentials can also be removed by a simple gauge transformation of the quasi-particle wave functions. It is straightforward to show that these equations conserve the total particle number for

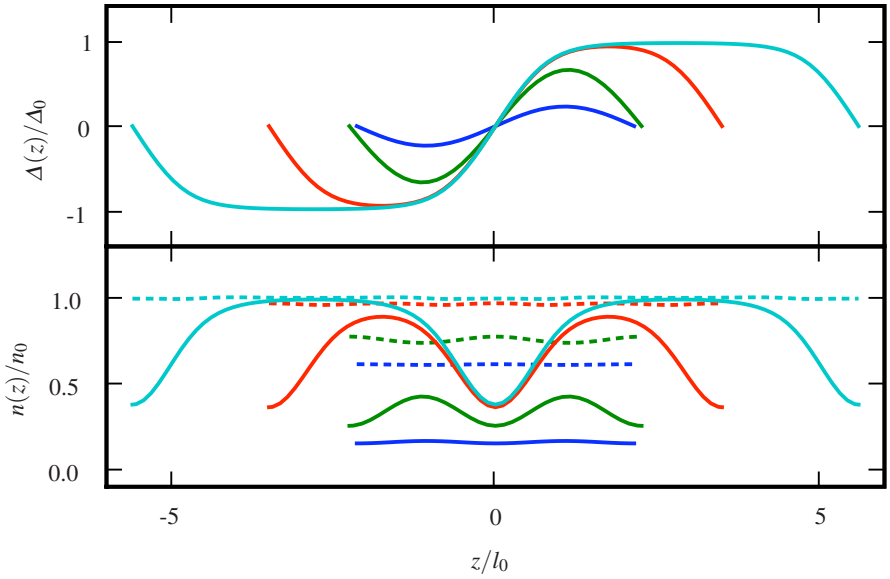

Fig. 9.15 A single LO period showing the spatial dependence of the pairing field $\Delta(z)$ (top) and the number densities of the majority (dotted) and minority (solid) species (bottom) at the values. Units are fixed so that $\mu_- = \mu_a - \mu_b$ is held fixed as it is for trapped systems. We normalize everything in terms of the density $n_0 = n_a = n_b$, interparticle spacing $l_0 = {n_0}^{-1/3}$, and superfluid pairing gap Δ_0 of the fully paired superfluid at the superfluid/LO transition point close to the center of the cloud. At the superfluid/LO transition, the character of the solution is that of widely spaced domain walls (see for example [145]). As one proceeds outward in the trap, the period and amplitude of the solution decreases until it is almost sinusoidal at the transition point to the interacting normal phase.

arbitrary time-dependent external fields and also for arbitrary time variations of the coupling constant $g(t)$. As expected however, in the presence of an external pairing field, particle number is not conserved: particles can be exchanged with the coupled system implied by the source of the external pairing field.

9.4.2 Galilean Invariance

The functionals as expressed in Sec. 9.3 are not manifestly covariant under Galilean transformation (a subset of the general coordinate invariance discussed in [151] which restrict the form of higher-order gradient terms). To restore this covariance, the currents currents $\mathbf{j}_a(\mathbf{r})$ and $\mathbf{j}_b(\mathbf{r})$ described in (9.72) must be included. These vanish in time-reversal invariant ground states, but are crucial for discussing states that break time reversal and for the general time-dependent analysis. In nuclear physics Galilean covariance have been considered for quite some time [152, 153, 154, 155],

and the contribution of these currents is often essential for describing the properties of excited states.

We start by expressing the Galilean invariance of the Lagrangian density for a single Fermi species (see [151] for a more general discussion)

$$\mathscr{L} = \psi^\dagger \left(\mathrm{i}\hbar\partial_t - \frac{(-\mathrm{i}\hbar\nabla)^2}{2m} \right) \psi. \tag{9.101}$$

This is invariant under the following Galilean transformation:

$$\psi(\mathbf{x},t) \to \exp\left[-\mathrm{i}\left(\tfrac{1}{2}m|\mathbf{v}|^2 t + m\mathbf{v}\cdot\mathbf{x}\right)/\hbar\right] \psi(\mathbf{x}+\mathbf{v}t,t). \tag{9.102}$$

From this, we see that the currents and kinetic densities transform as

$$\mathbf{j} = \tfrac{\mathrm{i}}{2}\psi^\dagger\nabla\psi + \text{h.c.} \to \mathbf{j} + m\mathbf{v}n, \tag{9.103a}$$

$$\tau = \tfrac{1}{2m}\nabla\psi^\dagger\nabla\psi \to \tau + \mathbf{v}\cdot\mathbf{j} + \tfrac{1}{2}m|\mathbf{v}|^2 n. \tag{9.103b}$$

It follows directly that for a two-component system, the following combinations are Galilean invariant:

$$\tilde{\tau}_\sigma = \tau_\sigma - \frac{|\mathbf{j}_\sigma|^2}{2m_\sigma n_\sigma}, \qquad\qquad \frac{\mathbf{j}_b}{m_b n_b} - \frac{\mathbf{j}_a}{m_a n_a}. \tag{9.104}$$

We would like to separate out the center of mass motion from the intrinsic functional, so we introduce the total mass current and density:

$$\mathbf{j}_+ = \mathbf{j}_a + \mathbf{j}_b, \qquad\qquad \rho_+ = m_a n_a + m_b n_b. \tag{9.105}$$

We may then write the functional in the following way:

$$\mathscr{E} = \frac{|\mathbf{j}_+|^2}{2\rho_+} + \tilde{\mathscr{E}}. \tag{9.106}$$

The first term captures the energy of the center of mass motion and $\tilde{\mathscr{E}}$ describes the remaining intrinsic energy of the system, and should be strictly Galilean invariant.

Excited states may be described by an extension of the DFT method commonly referred to as Time-Dependent Density Functional Theory (TDDFT) [156, 157, 158, 159]. This theory describes the evolution of the one-body number density in the presence of an arbitrary one-body external field. As in the case of static DFT, one can prove an existence theorem [156, 157, 158]. This states that a functional exists from which one can determine the exact time-dependent number density for a given quantum system, and can be expressed in the form

$$\mathscr{S} = \frac{\mathrm{i}\hbar}{2}\int \mathrm{d}t\mathrm{d}^3r \sum_{n,\sigma}\left\{ v_{n,\sigma}(\mathbf{r},t)\frac{\partial v^*_{n,\sigma}(\mathbf{r},t)}{\partial t} - v^*_{n,\sigma}(\mathbf{r},t)\frac{\partial v_{n,\sigma}(\mathbf{r},t)}{\partial t}\right\}$$
$$- \int \mathrm{d}t\mathrm{d}^3r \Bigg\{ \frac{\hbar^2}{2m}\sum_\sigma \tau_\sigma(\mathbf{r},t) + \sum_\sigma U_\sigma(\mathbf{r},t) n_\sigma(\mathbf{r},t)$$
$$+ \mathscr{E}\left[n_a(\mathbf{r},t), \tilde{\tau}_a(\mathbf{r},t), n_b(\mathbf{r},t), \tilde{\tau}_b(\mathbf{r},t), |\nu(\mathbf{r},t)|^2, g(\mathbf{r},t)\right]\Bigg\}. \quad (9.107)$$

Here $\sigma = a,b$ labels the two fermion species. The existence proof for superfluid systems is analogous to the proof for normal systems [156, 157, 158]. Here $U_\sigma(\mathbf{r},t)$ are arbitrary time-dependent one-body external fields, which couple to the conserved number densities of the fermion species $n_\sigma(\mathbf{r},t)$. These external fields can represent couplings to the laboratory environment, such as a trapping potential, which can be used to manipulate and study these systems.

The direct coupling of an external gauge field to the electric charge and magnetic moments of the particles can also be incorporated in a straightforward manner, by the usual process of converting the global particle number symmetry to a local symmetry by invoking the principle of gauge invariance. We can also couple an arbitrary time-dependent external pairing field as well to represent interactions with another superfluid system brought into the proximity of the system under study. As mentioned above, this will violate the conservation of particle number as particles are now able to be exchanged with the other system. Finally, the last argument $g(\mathbf{r},t)$ of the interaction term $\mathscr{E}$ represents the possibility of varying the coupling constants in space and time. In particular, as discussed in Sec. 9.2.1, by means of a Feshbach resonance an external magnetic field can be used to directly control the scattering length, providing yet another handle to manipulate and study these systems.

In the functional $\mathscr{S}$ we have separated the kinetic energy $\hbar^2\sum_\sigma \tau_a(\mathbf{r},t)/2m$ from the interaction energy in order to disentangle the dependence on the reference frame. The interaction energy encoded in the functional $\mathscr{E}$ should be independent of the motion of the system as a whole. By default, the properties of the ground states of a physical system are typically discussed in the center of mass reference frame. When the system is excited by various external probes, inevitably currents appear. In the LDA it is natural to assume that the energy density separates into the kinetic energy of center of mass (which depends only on its local center of mass velocity and its corresponding mass) and the internal energy (which should not depend on the local center of mass velocity). The energy density $\mathscr{E}\left[n_a(\mathbf{r},t), \tilde{\tau}_a(\mathbf{r},t), n_b(\mathbf{r},t), \tilde{\tau}_b(\mathbf{r},t), |\nu(\mathbf{r},t)|^2, g(\mathbf{r},t)\right]$ is the same as in the static SLDA, with the only difference that the dependence on the modified kinetic energy density $\tilde{\tau}_\sigma(\mathbf{r},t)$ now includes the current densities (9.72b) to satisfy Galilean invariance

$$\mathbf{j}_\sigma(\mathbf{r},t) = \frac{\mathrm{i}\hbar}{2}\sum_n \left[\nabla v_{n,\sigma}(\mathbf{r},t) v^*_{n,\sigma}(\mathbf{r},t) - v_{n,\sigma}(\mathbf{r},t)\nabla v^*_{n,\sigma}(\mathbf{r},t)\right]. \quad (9.108)$$

Here we will describe a slightly different philosophy in implementing the Galilean invariance than discussed at the beginning of this section, which leads to a somewhat

different definition of the modified kinetic energy densities $\tilde{\tau}_\sigma(\mathbf{r},t)$ than those introduced in (9.104) above. This ambiguity illustrates the freedom one has in introducing currents and using no other restriction except Galilean invariance.

Upon boosting the system to a frame with a velocity $\mathbf{V}$, the current density changes $\mathbf{j}_\sigma(\mathbf{r},t) \to \mathbf{j}_\sigma(\mathbf{r},t) + mn(\mathbf{r},t)\mathbf{V}$. We introduce the velocity of the local center of mass frame ($m_a = m_b = m$)

$$\mathbf{V}(\mathbf{r},t) = \frac{\mathbf{j}_+(\mathbf{r},t)}{\rho_+(\mathbf{r},t)}, \tag{9.109}$$

where we have introduced the total current $\mathbf{j}_+$ and density ρ_+ from (9.105). Consequently, the following combination of the kinetic energy density, current density and number density

$$\tilde{\tau}_\sigma(\mathbf{r},t) = \tau_\sigma(\mathbf{r},t) - \mathbf{j}_\sigma(\mathbf{r},t)\cdot\mathbf{V}(\mathbf{r},t) + \frac{mn_\sigma(\mathbf{r},t)\mathbf{V}^2(\mathbf{r},t)}{2}, \tag{9.110}$$

renders the energy density locally Galilean invariant [127]. $\tilde{\tau}_\sigma(\mathbf{r},t)$ is therefore the internal kinetic energy density in the local center of mass frame, which is different from the form of modified kinetic energy introduced in (9.104). The difference between the two approaches to enforcing the Galilean invariance amounts to terms proportional to $|\mathbf{j}_b/m_b n_b - \mathbf{j}_a/m_a n_a|^2$, see (9.104).

It is worth noticing that because the Galilean invariance is built in, one of the famous relations in the Landau's Fermi liquid theory linking the effective mass of the quasiparticles with the p-wave interaction (denoted F_1) is automatically satisfied (see [12]).

Note also that if terms arise of the form $\mathbf{j}_a(\mathbf{r},t)\cdot\mathbf{j}_b(\mathbf{r},t)$, a new physical effect appears whereby the local velocity of one species depends also on the velocity of the other species. In other words, the inverse mass becomes a tensor in the spin ("isospin") space. By including terms of the form $|(\mathbf{j}_a(\mathbf{r},t)\cdot\nabla n_\sigma(\mathbf{r},t))|^2$, the effective mass becomes a tensor in real space. This was discussed in [160] in connection with the construction of the optimal local Schrödinger equation to represent a non-local equation. In particular, it seems that, in order to describe some rather subtle level orderings of the single-particle spectrum found in the a non-local Schrödinger equation, one needs a tensor effective mass in the local equations. This is also related to the discussion of superfluid mixtures, where it was observed long ago that one superfluid can drag the other one without any dissipation: the Andreev-Bashkin effect [161]. Similar effects arise when one considers the terms induced by Galilean invariance (9.110) or $\mathbf{j}_a(\mathbf{r},t)\cdot\mathbf{j}_b(\mathbf{r},t)$, when the presence of a current of one species induces a current of the other species.

9.4.3 The Excitation of the Pairing Higgs Mode

We shall illustrate the power of the Time-Dependence SLDA(TD-SLDA) by examining the response of a superfluid unitary gas to the time variation of the scattering

length [162]. This problem has been studied extensively in the weak coupling regime when $k_F|a| \ll 1$ and $a < 0$, see [163, 164, 165, 166, 167, 168, 169, 170, 171, 172, 173, 174, 175, 176, 177, 178, 179, 180, 181]. The initial state of the system will be the ground state, and at subsequent times, the evolution will be adiabatic in the sense that no entropy production is allowed. To some extent this is a rather strong limitation of this time-dependent description of the quantum evolution, a restriction which can be lifted if one would consider a further extension of the formalism, the Stochastic TD-SLDA [182] which will not be discussed here.

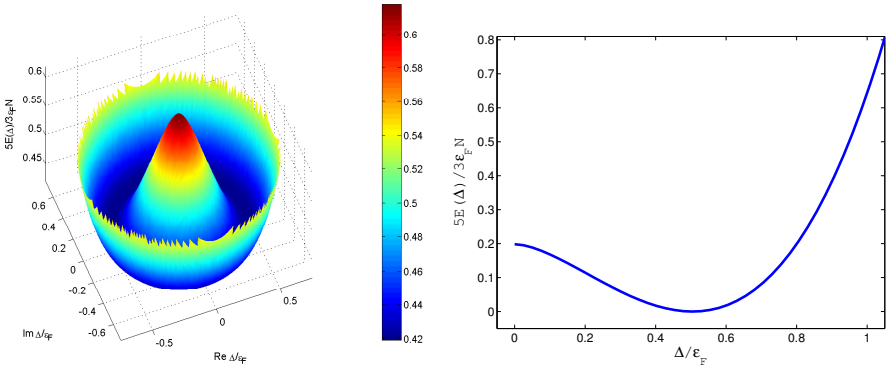

Fig. 9.16 The profile of the energy of a unitary Fermi gas as a function of the pairing gap with respect to the energy of the ground state. One would naïely expect that this system if released from a point almost at the tip of the "Mexican hat" will roll down along the radial direction, past the equilibrium value $\Delta_0 = 0.5\varepsilon_F$ and oscillate indefinitely back and forth.

Consider the following scenario [162]: start with a homogeneous unitary Fermi gas in its ground state. At first slowly reduce the coupling constant γ from its unitary value to a very small but still negative value. If this change is slow enough, then the system tracks the ground state into the ground state of the system with an exponentially small pairing gap. Now rapidly ramp the coupling γ back to its unitary value and let the system evolve. This essentially looks at the evolution of an almost normal system with the unitary DFT. The behavior shown in Fig. 9.17 is rather surprising.

Many approaches have been developed to describe the dynamics of a fermionic superfluid at or near $T = 0$ including superfluid hydrodynamics, a Landau-Ginzburg or Gross-Pitaevskii (LG/GP) like description, and effective field theory, see [183, 184, 185, 31, 151, 115, 186, 26, 187]. The common thread in all these approaches is the desire to identify a significantly smaller set of relevant degrees of freedom, and achieve an accurate description of the phenomena within a reduced framework. As a rule, when reducing the number of the degrees of freedom, one assumes that the system evolves through states where local equilibrium is maintained. In this instance, one would naïvely expect that the system dynamics are governed by an effective "Mexican hat" potential, Fig. 9.16, representing the energy of the system as a function

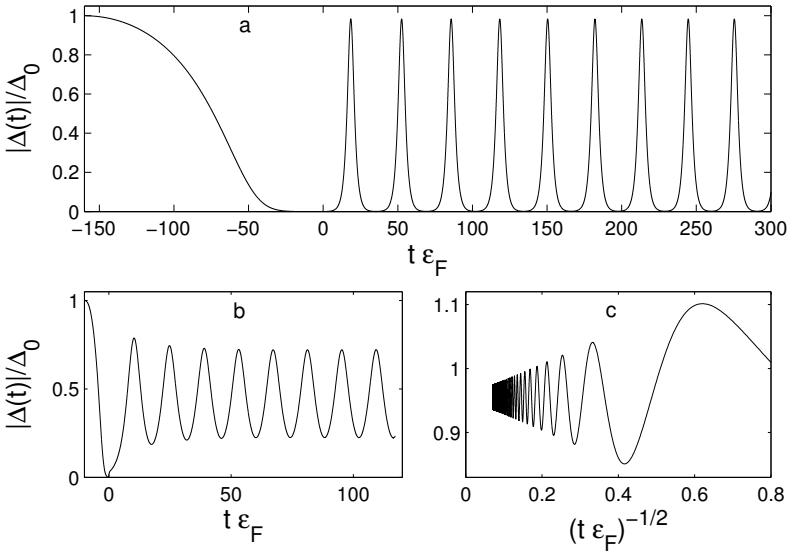

Fig. 9.17 The panels a,b and c display response of the homogeneous system to an initial switching time interval $t_0\varepsilon_F = 160, 10$ and 160 and values of the gap corresponding to γ_s are $\gamma_s/\gamma = 0.005, 0.005$ and 0.5 respectively, where γ is the coupling constant controlling the magnitude of the pairing gap and $\Delta_0 \approx 0.5\varepsilon_F$ is the gap equilibrium value, both at unitarity. The panels a and b show that when the system is released from the neighborhood of the tip of the "Mexican hat" potential the pairing gap oscillates back and forth, but never past the equilibrium value Δ_0. At the same time the system will rotate around the origin as the phase of the pairing field (not shown here) will monotonically evolve in time as well. However, when the system is released from an initial position closer to the minimum at Δ_0 the oscillation is damped, $\Delta(t) = \Delta_\infty + A\sin(2\Delta_\infty t + \phi)/\sqrt{\Delta_\infty t}$, with a mean frequency $2\Delta_\infty$ and around a value smaller than the equilibrium $\Delta_\infty < \Delta_0$, a behavior which was first studied in [163] in the BCS limit, when the coupling is weak.

of the complex pairing field. The system is brought adiabatically from the minimum of the potential to almost the "tip of the Mexican hat", and released with zero initial "velocity". The naïve picture is that the system will "roll" down along the radial direction accelerating until it reaches the minimum of the potential, pass through the minimum, and oscillate back and forth along the "radial" direction without damping.

One might also inspect the LG/GP description of the dynamics of the system using the nonlinear Schrödinger equation

$$i\hbar\frac{\partial\Psi(\mathbf{r},t)}{\partial t} = -\frac{\hbar^2\Delta\Psi(\mathbf{r},t)}{4m} + \mathscr{U}(|\Psi(\mathbf{r},t)|^2)\Psi(\mathbf{r},t). \tag{9.111}$$

Since there are no spatial gradients in this system (we have changed the coupling in a uniform manner so as not to break the translational invariance), only the second term on the right hand side of this equation contributes, and the solution is a simple monotonic evolution of the condensate phase $\Psi(\mathbf{r},t)$ in time and the magnitude of

"wave function" $\Psi(\mathbf{r},t)$ remains constant. In lieu of a better simple alternative, many authors have used this approach to characterize dynamics of Fermi superfluids at essentially zero temperatures, even though the LG/GP description is only justified near the critical temperature.

Another approach is to use the zero-temperature limit of Landau's two fluid hydrodynamics, which reduces to the following two equations at zero temperature

$$\dot{n}(\mathbf{r},t)+\nabla\cdot[\mathbf{v}(\mathbf{r},t)n(\mathbf{r},t)]=0,\qquad m\dot{\mathbf{v}}(\mathbf{r},t)+\nabla\left\{\frac{m\mathbf{v}^2(\mathbf{r},t)}{2m}+\mu[n(\mathbf{r},t)]\right\}=0. \tag{9.112}$$

Here $\mathbf{v}(\mathbf{r},t)$ is the hydrodynamic velocity and $\mu[n(\mathbf{r},t)]$ is the local thermodynamic potential. Since there are no spatial gradients, these two equation simply predict that the number density will remain constant and nothing else will happen.

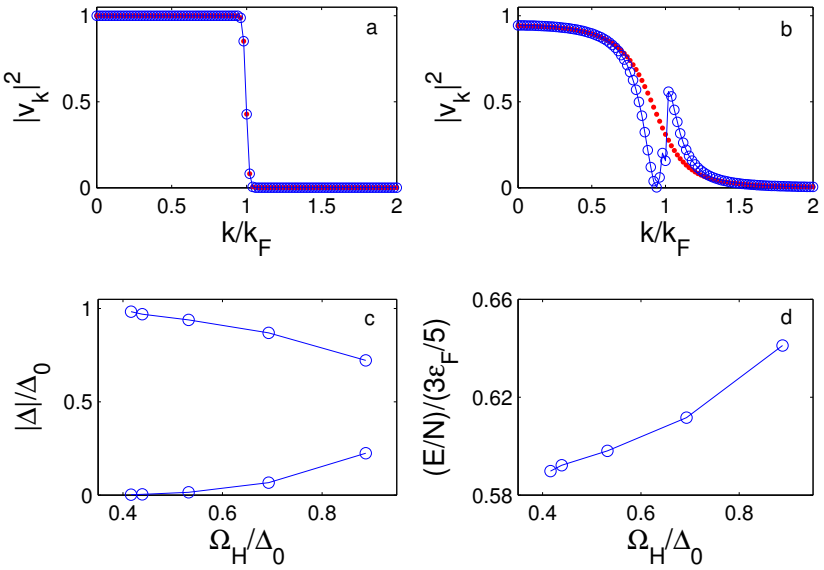

Fig. 9.18 Panels *a* and *b* display the instantaneous occupation probabilities of the mode shown in upper panel of Fig. 9.17 corresponding to times $t>0$ when the pairing field is at its minimum and maximum values respectively with circles joined by a solid (blue with circles) line. With (red) dots we plotted the equilibrium occupation probabilities corresponding to the same instantaneous values of the pairing gap. In panels *c* and *d* we show the maximum and minimum values of the oscillating pairing field and the corresponding excitation energy as a function of the frequency of the Higgs-like modes, see Fig. 9.17 *a* and *b*.

Apart from the fact that the number density will remain constant and spatially uniform, these three different naïve pictures lead to drastically different predictions.

The actual time evolution of the system, shown in Fig. 9.17, is qualitatively different from any individual picture, but demonstrates a combination of the expected features. The pairing gap does increase from almost zero towards the equilibrium value, and it oscillates, but it never crosses the minimum equilibrium value Δ_0 of the "Mexican hat" potential. At the same time, the phase of the pairing gap increases monotonically in time and the number density is constant.

By preparing the initial state slightly differently one can excite different types of these modes that have been dubbed "Higgs" modes of the pairing field. One can vary the upper and the lower values between which the pairing field oscillates, and also adjust the period of these oscillations. It is remarkable, however, that the frequencies of these modes are always smaller than $2\Delta_0$, where Δ_0 is the equilibrium value of the pairing gap at unitarity, even though the excitation energy is large. These are indeed very collective excitations of the system, of extremely low frequency, but with an excitation energy per particle significantly less than pairing gap.

It is still an unresolved question of how these modes will eventually decay and how the system will thermalize. It is also instructive to examine the time dependent population of the various single-particle momentum states of these collective modes as shown in Fig. 9.18. When the value of the pairing gap is very small the occupation probabilities are essentially those of a system in equilibrium. However, when the system reaches a pairing gap essentially equal to the equilibrium value Δ_0, the occupation probabilities are clearly very different from those in the ground state, which clearly points to a non-equilibrium state. This aspect should clarify why neither LG/GP nor quantum hydrodynamics are valid as both assume local equilibrium is maintained.

9.4.4 Generation and Dynamics of Vortices

A number of results concerning the generation and dynamics of vortices in a unitary Fermi gas by an external time-dependent perturbation can be found at [188]. As far as we are aware, this problem has been studied in one paper for a pure 2D systems [189]. As in the previous example, we do not yet consider entropy production in these simulations.

In order to illustrate further the power of the TD-SLDA as well as the limitations of traditional approaches such as superfluid hydrodynamics or a LG/GP analysis, we now consider the quantum dynamics of a stirred unitary Fermi gas [188]. We start with the gas in its ground state in a cylindrical trap, uniform and with periodic boundary conditions in the third spatial direction. We then subject the system to a time-dependent external stirring field which breaks the cylindrical symmetry. When implemented numerically [190], if one places the system on a spatial lattice with N_s spatial lattice points in one direction, one can show that the size of the problem scales as $\propto N_s^5$. When the limitation of spatial homogeneity in the z-direction is lifted the size of the problem scales as $\propto N_s^6$, which as a rule requires an implementation on the largest leadership class supercomputers available. For example, if $N_s = 50$ an

efficient solution of the TD-SLDA equations becomes possible only on the JaguarPF Cray XT5,[6] which we are currently utilizing to its full extent.

When homogeneity along the z-direction is enforced, the quasiparticle wave functions have the structure $(u_n(x,y,t)\exp(\mathrm{i}kz), v_n(x,y,t)\exp(\mathrm{i}kz))$ while self-energy $U(x,y,t)$ and the pairing potential $\Delta(x,y,t)$ are translationally invariant along z. We adiabatically introduce a vertical rod into this "soup can" and stir the gas with a constant angular velocity. One can vary both the stirring radius R and stirring angular frequency ω to control the speed $v_{\rm rod} = R\omega$ of the rod.

One might expect that if $v_{\rm rod} \ll v_c$, where v_c is the critical velocity of a unitary Fermi gas, then the system will return to its initial state after the stirring is turned off. However, if $v_{\rm rod} > v_c$, then one might destroy the superfluid order, resulting in a normal Fermi gas. If $v_1 < v_{\rm rod} < v_c$, where v_1 is some minimal stirring velocity, one expects that vortices will be created. Unfortunately, none of the simple theories can shed much light on the outcome: superfluid hydrodynamics cannot describe quantum vortices as there is no intrinsic quantization or Planck's constant in its formulation: vortex quantization must be imposed by hand, and there is nothing in principle to prevent decay of a quantized vortex into two fractionally quantized vortices. The time dependent LG/GP approach will also fail to describe the normal state and the transition from superfluid to normal state, as it is formulated explicitly in terms of the order parameter alone, which vanishes in the normal state. Thus, it seems that the only viable solution is to forgo a reduction in the degrees of freedom and deal directly with the quasiparticles included in the DFT.

A unitary Fermi gas is a special system in quite a number of ways: in particular, it appears to have the highest critical velocity of all known superfluids [191, 192]. On the BCS side of the Feshbach resonance, if stirred fast enough, the system can loose superfluidity by the breaking of the Cooper pairs $v_{qp} = \min(E_k, k)$. On the BEC side of the Feshbach resonance, the dominant mechanism for the loss of superfluidity is the excitation of the Anderson-Bogoliubov sound modes $c = v_F\sqrt{\xi/3}$. In the a unitary Fermi gas, these two different critical velocities appear to be essentially identical, and exactly at unitarity one obtains

$$v_c = \min(c, v_{qp}) = v_F \min\left(\sqrt{\frac{\xi}{3}}, \sqrt{\alpha\sqrt{(\overline{\beta}-\xi)^2+\eta^2}+(\overline{\beta}-\xi)}\right) \approx 0.365 v_F .$$

Since the amount of information one extracts in a TD-SLDA simulation of this type is very large, it is not sufficient to display only a few pictures such as those in Figs. 9.19 and 9.20. We invite the interested reader to explore some of the movies made of these simulations [188]. We shall comment here only on a few selected aspects of these results, most of which will be prepared for a publication at a later time.

Our expectation that, under gentle stirring, the unitary Fermi gas will return to its initial superfluid state is supported by the simulations [188], and is in line with how one would expect a superfluid to respond to such an external probe. The other expectation, that vigorous stirring can destroy the superfluid order is also confirmed.

[6] JaguarPF is a Cray XT5 supercomputer with 224,256 processing cores, see http://ww.nccs.gov.

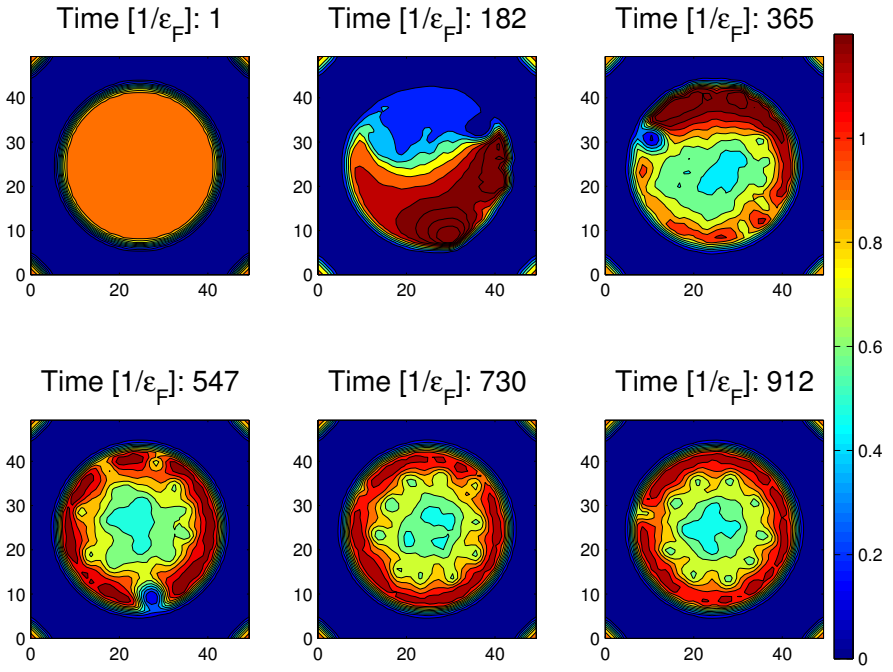

Fig. 9.19 The contour density profiles of a unitary Fermi gas in a cylindrical container, stirred with a uniformly rotating rod, which is inserted and extracted adiabatically from the system. The position (and intensity) of the rod can be inferred as the deepest density depletion in the system, and it is actually visible only in panels 2-4. Initialy the gas shows an almost uniform density distribution, and subsequently it is gathered almost entirely in front of the stirring rod. The magnitude of the density is in units of the unperturbed central initial density of the cloud and the colorbar on the right decodes the meaning of each color used. By the end of the simulation there are 13 vortices forming an almost perfect triangular Abrikosov lattice in this confined geometry.

Within TD-SLDA, the dynamic generation of vortices as well as formation of the celebrated Abrikosov vortex lattice are also readily demonstrated. By varying shape, the number and the stirring velocity we generated a plethora of quantized vortices in this "soup can" of superfluid unitary Fermi gas [188].

While we expected to generate a relatively small number of vortices at low stirring velocity, and that the number of vortices will increase with more vigorous stirring, many of the features of dynamic vortex generation are quite surprising. The fact that this system is compressible results in surprisingly large time-dependent variations of the local number density. Often the entire mass of the system is gathered in front of the stirrer, leaving little matter behind it: The gas can occupy less than half of the available volume, even though the volume excluded by the stirrer is quite small. It also comes as a great surprise that the system does not loose quantum coherence under such a violent perturbation. Moreover, it organizes itself in an almost perfect vortex lattice after the stirring is turned off. Even more surprising is

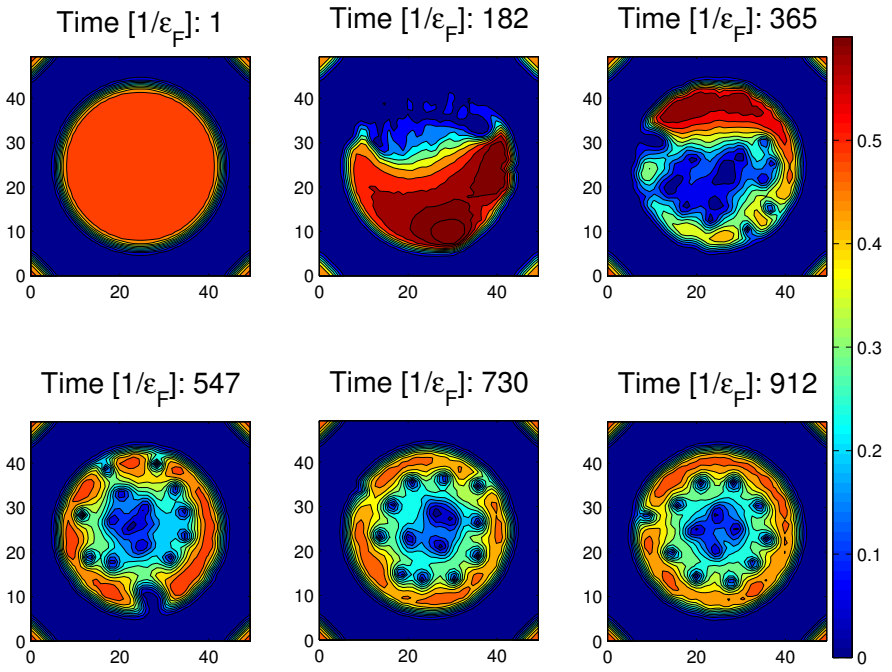

Fig. 9.20 The corresponding contour profiles of the pairing field $|\Delta(x,y,t)|$ a unitary Fermi gas in a cylindrical container, stirred with a uniformly rotating rod. A plot (not shown here) of the phase of the pairing field $\arg\Delta(x,y,t)$ shows that as one circles a vortex core the phase changes by 2π, thus each of these vortices carries exactly $\hbar/2$ units of angular momentum per particle and both the number (normal) density and the pairing field are significantly depleted in the core of the vortex [60].

that the system remains superfluid, *even when stirred at supercritical speeds!* We have observed that the system forms a vortex lattice even if stirred with speeds up to $v_s = 0.60v_F > v_c \approx 0.365v_F$ (see the case of 7 vortices with a large radius stirrer at [188]). We attribute this behavior to the fact that an increased density of the cloud during the stirring process corresponds to an increased local critical velocity, since the local Fermi velocity increases as well accordingly.

These two cases of exciting and monitoring the unitary Fermi gas by two drastically different methods illustrate both the power and flexibility of this framework, as well as the richness of the phenomena waiting to be fully explored. One potential topic to be explored by these techniques that has mesmerized the low temperature community during the past few decades is quantum turbulence [193, 194, 195]. Hopefully this can also be replicated in experiments with cold atomic fermionic gases. Due to the complexity of the full 3D time-dependent Bogoliubov-de Gennes equations, this aspect has never been theoretically addressed for fermionic systems. The TD-SLDA appears as a framework of choice in this respect. In particular one can address on a fully microscopic basis for vortex reconnection dynamics, which

is likely at the heart of quantum turbulence at zero temperature, where dissipative processes are greatly inhibited.

9.5 Concluding Remarks

We have reviewed here three methods to describe the properties of many-body systems starting from the bare Hamiltonian, and building a practical framework for studying nontrivial properties of mesoscopic systems and quantum dynamics.

The QMC method is particularly suited to calculate properties of the homogeneous phase of matter in an unbiased fashion. It also can be used for inhomogeneous systems, but is limited by system size and can not handle large number of Fermions. It is also generally plagued by the infamous sign problem (except in exceptionally symmetric contexts) and so far has not been used to describe systems in the time dependent domain.

The complimentary approach of density functional theory (DFT) through the use of the SLDA and ASLDA can be applied to extend these results to mesoscopic systems with larger number of particles and a wide variety of geometries. The time dependent TDDFT (TD-SLDA) extension brings these techniques to bear on time-dependent quantum dynamics. The main difficulty with the DFT is that there is no well defined procedure to construct the functional. However, in the particular case of a unitary Fermi gas, the form of the SLDA and ASLDA functionals is sufficiently restricted by dimensional analysis, QMC results, and Galilean invariance as to be able to make testable predictions with relatively small uncertainties. This has been validated with both ab initio theoretical and experimental results.

The next step is to use such tools to make predictions about the properties of the unitary gas under various conditions: by changing the geometry and even the Hamiltonian as a function of time, by probing the system with a variety of external probes and exciting a plethora of modes—both linear and nonlinear—and by studying both the equilibrium and non-equilibrium dynamics. We have illustrated a few of these applications, but it is clear that we have barely scratched the surface of this subject.

The Fermi gas in the unitary regime proves to be an extraordinarily rich physical system to study, not only because one can both theoretically and experimentally address many of its properties with both precision and accuracy, but because it has so many truly unexpected phases and dynamical phenomena.

Many fascinating features of this systems are still waiting to be revealed in experiments in their full glory, including: the pseudogap phase, the supersolid LOFF phase, p-wave superfluidity [196, 197], the Higgs mode of the pairing field, the behavior and response to various spatial and time varying trapping fields and probes, the dynamics of vortices which opens a window to quantum turbulence both theoretically and experimentally, the existence of supercritical superflow, and its kinetic properties—in particular its viscosity. One can safely state that the most extraordinary features of the unitary gas are still waiting to be demonstrated.

Perhaps the most captivating part of the story of the unitary Fermi gas is that it provides a link to an abundance of widespread fields of physics, from optics and atomic physics, to condensed matter physics, to nuclear physics and the physics of neutron stars, color superconductivity in QCD and dark matter, relativistic heavy ion collisions, and the AdS/CFT approaches in quantum field theory.

We would like to thank our collaborators J. E. Drut, Y. -L. Luo, K. J. Roche, G. Wlazłowski, S. Yoon, and Y. Yu for their invaluable contributions during various stages of the work reviewed here, some of which has not been published yet. We thank D. Blume, J. Carlson, S. Giorgini, L. Luo, S. Reddy, C. Salomon, Y. Shin, and G. E. Thomas for providing their numerical results. Support is acknowledged from the DOE under grants DE-FG02-97ER41014, DE-FC02-07ER41457, and DE-FG02-00ER41132, from the Polish Ministry of Science under contracts No. N N202 328234 and N N202 128439, and from the LDRD program at Los Alamos. Calculations reported here have been in part performed on the UW Athena cluster, on NERSC Franklin Cray XT4 supercomputer under grant B-AC02-05CH11231 and at the Interdisciplinary Centre for Mathematical and Computational Modelling (ICM) at Warsaw University. This document is unclassified with LANL release number LA-UR 10-05509.

References

[1] D. M. Eagles, Phys. Rev. **186**, 456 (1969).
[2] A. J. Leggett, in *Modern Trends in the Theory of Condensed Matter*, edited by A. Pekalski and J. Przystawa (Springer, Berlin, 1980), Lecture Notes in Physics, pp. 13 – 27, proc. XVI Karpacz Winter School of Theoretical Physics.
[3] P. Nozières and S. Schmitt-Rink, J. Low Temp. Phys. **59**, 195 (1985).
[4] C. A. R. Sá de Melo, M. Randeria, and J. R. Engelbrecht, Phys. Rev. Lett. **71**, 3202 (1993).
[5] J. R. Engelbrecht, M. Randeria, and C. A. R. Sá de Melo, Phys. Rev. B **55**, 15153 (1997).
[6] M. Randeria, in *Bose–Einstein Condensation*, edited by A. Griffin, D. W. Snoke, and S. Stringari (Cambridge University Press, Cambridge, UK, 1995), chap. 15, pp. 355–392.
[7] R. Haussmann, Zeitschrift fur Physik B Condensed Matter **91**, 291 (1993).
[8] R. Haussmann, Phys. Rev. B **49**, 12975 (1994).
[9] F. Pistolesi and G. C. Strinati, Phys. Rev. B **49**, 6356 (1994).
[10] F. Pistolesi and G. C. Strinati, Phys. Rev. B **53**, 15168 (1996).
[11] P. Pieri and G. C. Strinati, Phys. Rev. B **61**, 15370 (2000).
[12] A. A. Abrikosov, L. P. Gorkov, and I. E. Dzyaloshinski, *Methods of Quantum Field Theory in Statistical Physics* (Dover, 1975).
[13] L. P. Gorkov and T. K. Melik-Barkhudarov, Sov. Phys.–JETP **13**, 1018 (1961).
[14] D. S. Petrov, C. Salomon, and G. V. Shlyapnikov, Phys. Rev. Lett. **93**, 090404 (2004).

[15] A. Bulgac, P. F. Bedaque, and A. C. Fonseca, *A dilute atomic fermi system with a large positive scattering length* (2003), cond-mat/0306302.
[16] I. V. Brodsky, M. Y. Kagan, A. V. Klaptsov, R. Combescot, and X. Leyronas, Phys. Rev. A **73**, 032724 (2006).
[17] J. Levinsen and V. Gurarie, Phys. Rev. A **73**, 053607 (2006).
[18] J. Carlson, S.-Y. Chang, V. R. Pandharipande, and K. E. Schmidt, Phys. Rev. Lett. **91**, 050401 (2003), physics/0303094.
[19] A. Bulgac, J. E. Drut, and P. Magierski, Phys. Rev. Lett. **96**, 090404 (2006), cond-mat/0505374.
[20] *The Many-Body Challenge Problem (*MBX*) formulated by G. F. Bertsch in 1999*, See also [22, 23].
[21] T.-L. Ho, Phys. Rev. Lett. **92**, 090402 (2004).
[22] G. A. Baker, Jr., Phys. Rev. C **60**, 054311 (1999).
[23] G. A. Baker, Jr., Int. J. Mod. Phys. B **15**, 1314 (2001).
[24] H. Heiselberg, Phys. Rev. A **63**, 043606 (2001).
[25] K. M. O'Hara, S. L. Hemmer, M. E. Gehm, S. R. Granade, and J. E. Thomas, Science **298**, 2179 (2002), cond-mat/0212463.
[26] S. Giorgini, L. P. Pitaevskii, and S. Stringari, Rev. Mod. Phys. **80**, 1215 (2008), 0706.3360.
[27] I. Bloch, J. Dalibard, and W. Zwerger, Rev. Mod. Phys. **80**, 885 (2008), 0704.3011.
[28] W. Ketterle and M. W. Zwierlein, in [198], pp. 95–287, 0801.2500.
[29] L. Luo and J. E. Thomas, J. Low Temp. Phys. **154**, 1 (2009).
[30] R. Grimm, in [198], pp. 413–462, cond-mat/0703091.
[31] Y. Nishida and D. T. Son, Phys. Rev. Lett. **97**, 050403 (2006).
[32] D. T. Son, Phys. Rev. D **78**, 046003 (2008).
[33] H. T. C. Stoof, J. M. V. A. Koelman, and B. J. Verhaar, Phys. Rev. B **38**, 4688 (1988).
[34] E. Tiesinga, S. J. M. Kuppens, B. J. Verhaar, and H. T. C. Stoof, Phys. Rev. A **43**, 5188 (1991).
[35] E. Tiesinga, A. J. Moerdijk, B. J. Verhaar, and H. T. C. Stoof, Phys. Rev. A **46**, R1167 (1992).
[36] E. Tiesinga, B. J. Verhaar, and H. T. C. Stoof, Phys. Rev. A **47**, 4114 (1993).
[37] A. J. Moerdijk, B. J. Verhaar, and A. Axelsson, Phys. Rev. A **51**, 4852 (1995).
[38] T. Köhler, K. Góral, and P. S. Julienne, Rev. Mod. Phys. **78**, 1311 (2006).
[39] R. A. Duine and H. T. C. Stoof, Phys. Rep. **396**, 115 (2004), cond-mat/0312254.
[40] E. Timmermans, P. Tommasini, M. Hussein, and A. Kerman, Phys. Rep. **315**, 199 (1999), ISSN 0370-1573.
[41] H. A. Forbert and S. A. Chin, Int. J. Mod. Phys. B **15**, 1752 (2001), nucl-th/0009068.
[42] M. Suzuki, Phys. Lett. A **146**, 319 (1990), ISSN 0375-9601.
[43] H. Yoshida, Phys. Lett. A **150**, 262 (1990), ISSN 0375-9601.
[44] M. Creutz and A. Gocksch, Phys. Rev. Lett. **63**, 9 (1989).

[45] A. Bulgac, J. E. Drut, and P. Magierski, Phys. Rev. A **78**, 023625 (2008), 0803.3238.
[46] J. W. Negele and H. Orland, *Quantum Many-particle Systems* (Westview Press, Reading, MA, 1998), ISBN 0738200522 : 9780738200521.
[47] J. E. Hirsch, Phys. Rev. B **28**, 4059 (1983).
[48] S. E. Koonin, D. J. Dean, and K. Langanke, Phys. Rep. **278**, 1 (1997), ISSN 0370-1573.
[49] Y. Alhassid, Int. J. Mod. Phys. B **15**, 1447 (2001), nucl-th/0009005.
[50] G. Wlazłowski and P. Magierski, Int. J. Mod. Phys. E **18**, 919 (2009), 0812.0883.
[51] A. Bulgac, J. E. Drut, and P. Magierski, Int. J. Mod. Phys. B **20**, 5165 (2006), cond-mat/0602091.
[52] M. N. Barber, in *Phase Transitions and Critical Phenomena*, edited by C. Domb and J. L. Lebowitz (Academic Press, 1983), vol. 8 of *Phase Transitions and Critical Phenomena*, p. 146, ISBN 0122203143 : 9780122203145.
[53] S. Tan, Ann. Phys. (NY) **323**, 2971 (2008), cond-mat/0508320.
[54] E. Braaten and L. Platter, Phys. Rev. Lett. **100**, 205301 (2008).
[55] S.-Y. Chang, V. R. Pandharipande, J. Carlson, and K. E. Schmidt, Phys. Rev. A **70**, 043602 (2004), physics/0404115.
[56] G. E. Astrakharchik, J. Boronat, J. Casulleras, and S. Giorgini, Phys. Rev. Lett. **93**, 200404 (2004), cond-mat/0406113.
[57] J. Carlson and S. Reddy, Phys. Rev. Lett. **95**, 060401 (2005), cond-mat/0503256.
[58] A. Gezerlis and J. Carlson, Phys. Rev. C **77**, 032801 (pages 4) (2008), 0711.3006.
[59] S. Zhang, K. E. Schmidt, and J. Carlson, private communication.
[60] A. Bulgac and Y. Yu, Phys. Rev. Lett. **91**, 190404 (2003), cond-mat/0303235.
[61] P. Magierski, G. Wlazłowski, A. Bulgac, and J. E. Drut, Phys. Rev. Lett. **103**, 210403 (2009).
[62] H. Heiselberg, C. J. Pethick, H. Smith, and L. Viverit, Phys. Rev. Lett. **85**, 2418 (2000), cond-mat/0004360.
[63] J. Carlson, J. Morales, V. R. Pandharipande, and D. G. Ravenhall, Phys. Rev. C **68**, 025802 (2003).
[64] C. Lobo, A. Recati, S. Giorgini, and S. Stringari, Phys. Rev. Lett. **97**, 200403 (pages 4) (2006), cond-mat/0607730.
[65] A. J. Leggett, J. Phys. Colloques **41**, C7 (1980).
[66] A. Perali, P. Pieri, L. Pisani, and G. C. Strinati, Phys. Rev. Lett. **92**, 220404 (2004).
[67] L. D. Carr, G. V. Shlyapnikov, and Y. Castin, Phys. Rev. Lett. **92**, 150404 (2004).
[68] L. Luo, B. Clancy, J. Joseph, J. Kinast, and J. E. Thomas, Phys. Rev. Lett. **98**, 080402 (2007).
[69] A. Bulgac, J. E. Drut, and P. Magierski, Phys. Rev. Lett. **99**, 120401 (2007), cond-mat/0701786.

[70] A. L. Fetter and J. D. Walecka, *Quantum Theory of Many-Particle Systems* (McGraw-Hill, San Fransisco, 1971).
[71] E. T. Jaynes, in *Maximum Entropy Formalism*, edited by R. D. Levine and M. Tribus (MIT Press, Cambridge, Mass., 1979), pp. 15–118, ISBN 0262120801 : 9780262120807.
[72] R. N. Silver, D. S. Sivia, and J. E. Gubernatis, Phys. Rev. B **41**, 2380 (1990).
[73] R. N. Silver, J. E. Gubernatis, D. S. Sivia, and M. Jarrell, Phys. Rev. Lett. **65**, 496 (1990).
[74] S. R. White, Phys. Rev. B **44**, 4670 (1991).
[75] M. Bertero, C. D. Mol, and E. R. Pike, Inverse Problems **1**, 301 (1985).
[76] M. Bertero, C. D. Mol, and E. R. Pike, Inverse Problems **4**, 573 (1988).
[77] C. E. Creffield, E. G. Klepfish, E. R. Pike, and S. Sarkar, Phys. Rev. Lett. **75**, 517 (1995).
[78] G. D. de Villiers, B. McNally, and E. R. Pike, Inverse Problems **15**, 615 (1999).
[79] P. Magierski and G. Wlazłowski, in preparation.
[80] E. Burovski, N. Prokof'ev, B. Svistunov, and M. Troyer, Phys. Rev. Lett. **96**, 160402 (2006).
[81] E. Burovski, N. Prokof'ev, B. Svistunov, and M. Troyer, New Journal of Physics **8**, 153 (2006), cond-mat/0605350.
[82] E. Burovski, E. Kozik, N. Prokof'ev, B. Svistunov, and M. Troyer, Phys. Rev. Lett. **101**, 090402 (2008), 0805.3047.
[83] J. Stajic, J. N. Milstein, Q. Chen, M. L. Chiofalo, M. J. Holland, and K. Levin, Phys. Rev. A **69**, 063610 (2004).
[84] Q. Chen, J. Stajic, S. Tan, and K. Levin, Phys. Rep. **412**, 1 (2005).
[85] K. Levin and Q. Chen, in [198], pp. 751–778.
[86] Y. He, C.-C. Chien, Q. Chen, and K. Levin, Phys. Rev. B **76**, 224516 (2007).
[87] C. Chin, M. Bartenstein, A. Altmeyer, S. Riedl, S. Jochim, J. H. Denschlag, and R. Grimm, Science **305**, 1128 (2004), cond-mat/0405632.
[88] M. Greiner, C. A. Regal, and D. S. Jin, Phys. Rev. Lett. **94**, 070403 (2005).
[89] C. H. Schunck, Y. Shin, A. Schirotzek, M. W. Zwierlein, and W. Ketterle, Science **316**, 867 (2007), cond-mat/0702066.
[90] J. Kinnunen, M. Rodríguez, and P. Törmä, Science **305**, 1131 (2004), cond-mat/0405633.
[91] Y. He, Q. Chen, and K. Levin, Phys. Rev. A **72**, 011602 (2005).
[92] Z. Yu and G. Baym, Phys. Rev. A **73**, 063601 (2006).
[93] G. Baym, C. J. Pethick, Z. Yu, and M. W. Zwierlein, Phys. Rev. Lett. **99**, 190407 (2007).
[94] M. Punk and W. Zwerger, Phys. Rev. Lett. **99**, 170404 (2007).
[95] A. Perali, P. Pieri, and G. C. Strinati, Phys. Rev. Lett. **100**, 010402 (2008).
[96] J. P. Gaebler, J. T. Stewart, T. E. Drake, D. S. Jin, A. Perali, P. Pieri, and G. C. Strinati, Nature Physics **6**, 569 (2010), 1003.1147.
[97] J. T. Stewart, J. P. Gaebler, and D. S. Jin, Nature **454**, 744 (2008), 0805.0026.

[98] E. D. Kuhnle, P. Dyke, M. Mark, P. Hannaford, , and C. J. Vale, *Bragg spectroscopy of the BEC-BCS crossover in lithium-6*, poster at BEC 2009 (2009).
[99] P. Magierski, G. Wlazłowski, and A. Bulgac, work in progress.
[100] J. E. Thomas, J. Kinast, and A. Turlapov, Phys. Rev. Lett. **95**, 120402 (2005).
[101] A. Bulgac and M. M. Forbes, Phys. Rev. A **75**, 031605(R) (2007), cond-mat/0606043.
[102] M. Bartenstein, A. Altmeyer, S. Riedl, R. Geursen, S. Jochim, C. Chin, J. H. Denschlag, R. Grimm, A. Simoni, E. Tiesinga, et al., Phys. Rev. Lett. **94**, 103201 (2005), cond-mat/0408673.
[103] J. Kinast, A. Turlapov, J. E. Thomas, Q. Chen, J. Stajic, and K. Levin, Science **307**, 1296 (2005), cond-mat/0502087.
[104] S. Nascimbène, N. Navon, K. J. Jiang, F. Chevy, and C. Salomon, Nature **463**, 1057 (2010), 0911.0747v1.
[105] M. Horikoshi, S. Nakajima, M. Ueda, and T. Mukaiyama, Science **327**, 442 (2010).
[106] S. Nascimbène, N. Navon, F. Chevy, and C. Salomon, New J. Phys. **12**, 103026 (2010), 1006.4052.
[107] P. Hohenberg and W. Kohn, Phys. Rev. **136**, B864 (1964).
[108] W. Kohn and L. J. Sham, Phys. Rev. **140**, A1133 (1965).
[109] R. M. Dreizler and E. K. U. Gross, *Density Functional Theory: An Approach to the Quantum Many–Body Problem* (Springer-Verlag, Berlin, 1990), ISBN 9780387519937.
[110] R. G. Parr and Y. Weitao, *Density-Functional Theory of Atoms and Molecules*, no. 16 in International Series of Monographs on Chemistry (Oxford University Press, New York, 1989), ISBN 9780195092769.
[111] J. E. Drut, R. J. Furnstahl, and L. Platter, Prog. Part. Nucl. Phys. **64**, 120 (2010), 0906.1463.
[112] F. Chevy, Phys. Rev. A **74**, 063628 (pages 4) (2006), cond-mat/0605751.
[113] W. Kohn, Rev. Mod. Phys. **71**, 1253 (1999).
[114] T. Papenbrock, Phys. Rev. A **72**, 041603 (2005), cond-mat/0507183.
[115] G. Rupak and T. Schaefer, Nucl. Phys. **A816**, 52 (2009), 0804.2678.
[116] A. Bulgac and Y. Yu, Phys. Rev. Lett. **88**, 042504 (2002), nucl-th/0106062v3.
[117] P. G. de Gennes, *Superconductivity of metals and alloys* (Benjamin, New York, 1966).
[118] T. Papenbrock and G. F. Bertsch, Phys. Rev. C **59**, 2052 (1999), nucl-th/9811077.
[119] S. Tan, Ann. Phys. (NY) **323**, 2952 (2008), cond-mat/0505200.
[120] J. M. Blatt and V. F. Weisskopf, *Theoretical Nuclear Physics* (Wiley, New York, 1952), pp. 74–76, ISBN 978-0486668277.
[121] K. Huang, *Statistical Mechanics* (Wiley, New York, 1987), pp. 230–238.
[122] K. Huang and C. N. Yang, Phys. Rev. **105**, 767 (1957).
[123] T. D. Lee and C. N. Yang, Phys. Rev. **105**, 1119 (1957).
[124] A. Bulgac and M. M. Forbes (2008), 0808.1436.

[125] A. Bulgac and M. M. Forbes, Phys. Rev. Lett. **101**, 215301 (2008), 0804.3364.
[126] T. D. Cohen, Phys. Rev. Lett. **95**, 120403 (2005), cond-mat/0501080.
[127] A. Bulgac, Phys. Rev. A **76**, 040502 (2007), cond-mat/0703526.
[128] J. Carlson and S. Reddy, Phys. Rev. Lett. **100**, 150403 (pages 4) (2008), 0711.0414.
[129] A. Bhattacharyya and R. J. Furnstahl, Phys. Lett. B **607**, 259 (2005), nucl-th/0410105.
[130] A. Bhattacharyya and R. J. Furnstahl, Nucl. Phys. A **747**, 268 (2005), nucl-th/0408014.
[131] R. Combescot and S. Giraud, Phys. Rev. Lett. **101**, 050404 (2008), 0804.2638.
[132] S. Pilati and S. Giorgini, Phys. Rev. Lett. **100**, 030401 (pages 4) (2008), 0710.1549.
[133] Y. Shin, Phys. Rev. A **77**, 041603 (2008), 0801.1523.
[134] S. Nascimbène, N. Navon, K. J. Jiang, L. Tarruell, M. Teichmann, J. McKeever, F. Chevy, and C. Salomon, Phys. Rev. Lett. **103**, 170402 (2009), 0907.3032.
[135] S.-Y. Chang and G. F. Bertsch, Phys. Rev. A **76**, 021603 (pages 4) (2007), physics/0703190.
[136] D. Blume, J. von Stecher, and C. H. Greene, Phys. Rev. Lett. **99**, 233201 (pages 4) (2007), 0708.2734.
[137] D. Blume, Phys. Rev. A **78**, 013635 (2008), 0805.2130.
[138] M. M. Forbes, S. Gandolfi, and A. Gezerlis, Phys. Rev. Lett. **106**, 235303 (2011), 1011.2197.
[139] L. O. Baksmaty, H. Lu, C. J. Bolech, and H. Pu, Phys. Rev. A **83**, 023604 (2010), 1003.4488.
[140] J. C. Pei, J. Dukelsky, and W. Nazarewicz, Phys. Rev. A **82**, 021603 (2010), 1005.3239.
[141] S. T. Belyaev, A. V. Smirnov, S. V. Tolokonnikov, and S. A. Fayans, Sov. J. Nucl. Phys. **45**, 783 (1987).
[142] S. A. Fayans, S. V. Tolokonnikov, E. L. Trykov, and D. Zawischa, Nucl. Phys. A **676**, 49 (2000), ISSN 0375-9474.
[143] M. W. Zwierlein, J. R. Abo-Shaeer, A. Schirotzek, C. H. Schunck, and W. Ketterle, Nature **435**, 1047 (2005), ISSN 7045.
[144] R. Combescot, A. Recati, C. Lobo, and F. Chevy, Phys. Rev. Lett. **98**, 180402 (pages 4) (2007), cond-mat/0702314.
[145] N. Yoshida and S.-K. Yip, Phys. Rev. **A75**, 063601 (pages 6) (2007), cond-mat/0703205.
[146] P. Fulde and R. A. Ferrell, Phys. Rev. **135**, A550 (1964).
[147] A. I. Larkin and Y. N. Ovchinnikov, Sov. Phys.–JETP **20**, 762 (1965), zh. Eksper. Teoret. Fiz. **47**, 1136 (1964).
[148] G. Dewel, P. Borckmans, and D. Walgraef, J. Phys. C **12**, L491 (1979).
[149] L. Radzihovsky and A. Vishwanath, Phys. Rev. Lett. **103**, 010404 (2009), 0812.3945.

[150] J. A. Bowers and K. Rajagopal, Phys. Rev. D **66**, 065002 (2002), hep-ph/0204079.
[151] D. T. Son and M. B. Wingate, Ann. Phys. (NY) **321**, 197 (2006), cond-mat/0509786.
[152] Y. M. Engel, D. M. Brink, K. Goeke, S. J. Krieger, and D. Vautherin, Nucl. Phys. A **249**, 215 (1975), ISSN 0375-9474.
[153] J. Dobaczewski and J. Dudek, Phys. Rev. C **52**, 1827 (1995).
[154] V. O. Nesterenko, W. Kleinig, J. Kvasil, P. Vesely, and P.-G. Reinhard, Int. J. Mod. Phys. E **17**, 89 (2008), 0711.1090.
[155] M. Bender, P.-H. Heenen, and P.-G. Reinhard, Rev. Mod. Phys. **75**, 121 (2003).
[156] A. K. Rajagopal and J. Callaway, Phys. Rev. B **7**, 1912 (1973).
[157] V. Peuckert, Journal of Physics C: Solid State Physics **11**, 4945 (1978).
[158] E. Runge and E. K. U. Gross, Phys. Rev. Lett. **52**, 997 (1984).
[159]
[160] A. Bulgac, C. Lewenkopf, and V. Mickrjukov, Phys. Rev. B **52**, 16476 (1995).
[161] A. F. Andreev and E. P. Bashkin, Sov. Phys.–JETP **42**, 164 (1975), zh. Éksp. Teor. Fiz. **69**, 319 (1975).
[162] A. Bulgac and S. Yoon, Phys. Rev. Lett. **102**, 085302 (2009).
[163] A. F. Volkov and S. M. Kogan, Sov. Phys.–JETP **38**, 1018 (1974), zh. Éksp. Teor. Fiz. **65**, 2038 (1973).
[164] R. A. Barankov, L. S. Levitov, and B. Z. Spivak, Phys. Rev. Lett. **93**, 160401 (2004).
[165] R. A. Barankov and L. S. Levitov, Phys. Rev. Lett. **96**, 230403 (2006).
[166] A. V. Andreev, V. Gurarie, and L. Radzihovsky, Phys. Rev. Lett. **93**, 130402 (2004).
[167] M. H. Szymańska, B. D. Simons, and K. Burnett, Phys. Rev. Lett. **94**, 170402 (2005).
[168] A. Tomadin, M. Polini, M. P. Tosi, and R. Fazio, Phys. Rev. A **77**, 033605 (2008).
[169] R. A. Barankov and L. S. Levitov, Phys. Rev. A **73**, 033614 (2006).
[170] G. L. Warner and A. J. Leggett, Phys. Rev. B **71**, 134514 (2005).
[171] W. Yi and L.-M. Duan, Phys. Rev. A **73**, 013609 (2006).
[172] A. Nahum and E. Bettelheim, Phys. Rev. B **78**, 184510 (2008).
[173] R. Teodorescu, J. Phys. A **39**, 10363 (2006), nlin/0512060.
[174] A. Robertson, L. Jiang, H. Pu, W. Zhang, and H. Y. Ling, Phys. Rev. Lett. **99**, 250404 (2007).
[175] E. A. Yuzbashyan, B. L. Altshuler, V. B. Kuznetsov, and V. Z. Enolskii, J. Phys. A **38**, 7831 (2005), cond-mat/0407501.
[176] M. Dzero, E. A. Yuzbashyan, B. L. Altshuler, and P. Coleman, Phys. Rev. Lett. **99**, 160402 (2007).
[177] E. A. Yuzbashyan, B. L. Altshuler, V. B. Kuznetsov, and V. Z. Enolskii, Phys. Rev. B **72**, 220503 (2005).
[178] E. A. Yuzbashyan and M. Dzero, Phys. Rev. Lett. **96**, 230404 (2006).
[179] E. A. Yuzbashyan, Phys. Rev. B **78**, 184507 (2008).

[180] E. A. Yuzbashyan, O. Tsyplyatyev, and B. L. Altshuler, Phys. Rev. Lett. **96**, 097005 (2006).
[181] M. Dzero, E. A. Yuzbashyan, and B. L. Altshuler, Europhysics Letters **85**, 20004 (2009), 0805.2798.
[182] A. Bulgac, J. Phys. G **37**, 064006 (2010), 1001.0396.
[183] E. Babaev, Phys. Rev. B **79**, 104506 (2009).
[184] E. Babaev, Phys. Rev. Lett. **103**, 231101 (2009).
[185] E. Babaev, J. Jäykkä, and M. Speight, Phys. Rev. Lett. **103**, 237002 (2009).
[186] G. Rupak, T. Schäfer, and A. Kryjevski, Phys. Rev. A **75**, 023606 (2007).
[187] I. M. Khalatnikov, *An introduction to the theory of superfluidity* (Advanced Book Program, Perseus Pub., Cambridge, Mass., 2000), ISBN 0738203009 (pbk.).
[188] A. Bulgac, Y.-L. Luo, P. Magierski, K. J. Roche, and Y. Yu, Science **332**, 1288 (2011).
[189] G. Tonini, F. Werner, and Y. Castin, European Physical Journal D **39**, 283 (2006), cond-mat/0504612.
[190] A. Bulgac and K. J. Roche, Journal of Physics: Conference Series **125**, 012064 (2008).
[191] R. Sensarma, M. Randeria, and T.-L. Ho, Phys. Rev. Lett. **96**, 090403 (2006).
[192] R. Combescot, M. Y. Kagan, and S. Stringari, Phys. Rev. A **74**, 042717 (2006).
[193] W. F. Vinen and R. J. Donnelly, Physics Today **60**, 43 (2007).
[194] W. F. Vinen, J. Low Temp. Phys. **145**, 7 (2006).
[195] M. Tsubota, Journal of the Physical Society of Japan **77**, 111006(1 (2008), 0806.2737.
[196] A. Bulgac, M. M. Forbes, and A. Schwenk, Phys. Rev. Lett. **97**, 020402 (2006), cond-mat/0602274.
[197] A. Bulgac and S. Yoon, Phys. Rev. A **79**, 053625 (2009), 0901.0348.
[198] M. Inguscio, W. Ketterle, and C. Salomon, eds., *Ultra-cold Fermi Gases*, vol. 164 of *International School of Physics "Enrico Fermi"* (IOS Press, Amsterdam, 2007), ISBN 978-1-58603-846-5.
[199] A. Baran, A. Bulgac, M. M. Forbes, G. Hagen, W. Nazarewicz, N. Schunck, and M. V. Stoitsov, Phys. Rev. C **78**, 014318 (pages 10) (2008), 0805.4446.

9.6 Appendix

9.6.1 Formal Description of the DFT

Here we present a somewhat formal derivation of the variational property of the Kohn-Sham equations. Consider a general free-energy functional of the following form

$$F = E(n_A, n_B, \cdots) + T\,\mathrm{Tr}\,(\rho \ln \rho) \tag{9.113}$$

where

$$\begin{aligned} n_A &= \mathrm{Tr}\left(\rho \mathbf{A}^T\right), \\ n_B &= \mathrm{Tr}\left(\rho \mathbf{B}^T\right), \\ &\vdots \end{aligned}$$

are the various densities, anomalous densities, etc. expressed linearly in terms of the one-body density matrix ρ. By varying the functional with respect to the density matrix ρ subject to the appropriate constraints on density matrix form (discussed in section 9.6.1.1), one obtains a solution of the form

$$\rho = f_\beta(\mathbf{H}[\rho]) \tag{9.114}$$

where $f_\beta(E)$ is the appropriate thermal distribution for the particles of interest, and $\mathbf{H}$ is a single-particle Hamiltonian that depends on ρ:

$$\mathbf{H}[\rho] = \frac{\partial E}{\partial n_A}\mathbf{A} + \frac{\partial E}{\partial n_B}\mathbf{B} + \cdots . \tag{9.115}$$

The typical Kohn-Sham equations follow by diagonalizing the self-consistency condition (9.114) with a set of normalized Kohn-Sham eigenfunctions of definite energy:

$$\mathbf{H}\left|n\right\rangle = E_n \left|n\right\rangle . \tag{9.116}$$

The density matrix is diagonal in this basis and expressed in terms of the appropriate distribution functions $f_\beta(E)$:

$$\rho = \sum_n f_\beta(E_n) \left|n\right\rangle \left\langle n\right| . \tag{9.117}$$

All of the functionals considered in this chapter may be expressed in this form. Once the appropriate matrix structures $\mathbf{A}$, $\mathbf{B}$ etc. are described, the form of the Kohn-Sham equations and potentials follows directly from these expressions.

9.6.1.1 Fermions

The only remaining complication is to impose the appropriate constraint on the density matrix ρ. This ensures that the appropriate statistics of the particles is enforces. As we shall be interested in Fermions, the relevant constraint on the density matrix (dictated by the canonical commutation relationships) is

$$\rho + \mathbf{C}\rho^T\mathbf{C} = \mathbf{1} \tag{9.118}$$

where $\mathbf{C} = \mathbf{C}^T$ is the charge conjugation matrix:

$$\mathbf{C}\left|\psi\right\rangle = \left|\psi\right\rangle^* . \tag{9.119}$$

This follows from the anti-commutation relationship for fermions and is discussed further in the Section 9.6.2. The constrained minimization of the functional $F(\rho)$ results in the standard Fermi distribution[7]

$$\rho = \frac{1}{1+e^{\beta\left(\mathbf{H}[\rho]-\mathbf{C}\mathbf{H}^T[\rho]\mathbf{C}\right)}}, \tag{9.120}$$

which is the fermionic form of the self-consistency condition (9.114) for the density matrix ρ. In practise, one does not iterate the entire density matrix. Instead, one stores only the densities n_A, n_B, etc. Through (9.115), these define the Kohn-Sham Hamiltonian $\mathbf{H}$, which is then diagonalized to form the new density matrix and finally the new densities. If, for example, symmetries allow the Hamiltonian $\mathbf{H}$ to be block diagonalized, then one can construct and accumulate the densities in parallel over each block. Finally, the densities represent far fewer parameters than the full density matrix. Thus, more sophisticated root-finding techniques such as Broyden's method [199] may be efficiently employed: Applying these techniques to the full density matrix would be significantly more expensive.

9.6.2 Single Particle Hamiltonian

It is convenient to express these concepts in the language of second quantization. The Hamiltonian will appear as a quadratic operator of the form

$$H_s = \tfrac{1}{2}\Psi^\dagger \mathscr{H}_s \Psi \tag{9.121}$$

where Ψ has several components and $\mathscr{H}_s$ is a matrix. The factor of $1/2$ accounts for the double counting to be discussed below. For a two component system, the most general Ψ that allows for all possible pairings has four components:

$$\Psi = \begin{pmatrix} a \\ b \\ a^\dagger \\ b^\dagger \end{pmatrix}. \tag{9.122}$$

In terms of components of the wavefunction, we will write $\mathscr{H}_s \psi = E\psi$ where:

$$\psi = \begin{pmatrix} u_a \\ u_b \\ v_a \\ v_b \end{pmatrix}. \tag{9.123}$$

[7] Formally, this constraint can be implemented using a Lagrange multiplier, but it is much easier to see the results by letting $\rho = \mathbf{1}/2 + \mathbf{x} - \mathbf{C}\mathbf{x}^T\mathbf{C}$ where $\mathbf{x}$ is unconstrained, and then performing the variation with respect to $\mathbf{x}$.

The naming of these components is conventional (see for example [117]) and the functions u and v are typically called "Coherence Factors". Note that the convention is that $v^*_{a,b}(\mathbf{r},t)$ are the wavefunctions of the particles. In this formulation the Hamiltonian has the form presented in (9.100):

$$\mathscr{H}_s = \begin{pmatrix} h_a + U_a & 0 & 0 & \Delta \\ 0 & h_b + U_b & -\Delta & 0 \\ 0 & -\Delta^* & -h_a^* - U_a & 0 \\ \Delta^* & 0 & 0 & -h_b^* - U_b \end{pmatrix} \tag{9.124}$$

9.6.2.1 Four-component Formalism

We shall start with this full four-component formalism but soon utilized a reduction: If the superfluid pairing $\Delta \sim \langle ab \rangle$ channel is attractive, then often the "Fock" channel is repulsive so we can take $\langle a^\dagger b \rangle = 0$. In combination with the double-counting discussed below, this will allow us to fully express the system in terms of two components.

The four-component formalism double counts the degrees of freedom: Ψ contains both a and $a^\dagger$. This degeneracy is described in terms of the charge conjugation matrix $\mathscr{C}$:

$$\Psi^\dagger = \mathscr{C}\Psi \qquad \text{where} \qquad \mathscr{C} = \begin{pmatrix} \mathbf{0} & \mathbf{1} \\ \mathbf{1} & \mathbf{0} \end{pmatrix}. \tag{9.125}$$

The operator Ψ will satisfy the single-particle Shrödinger equations

$$H_s |\Psi\rangle = E |\Psi\rangle \tag{9.126}$$

where the Hamiltonian $H_s = \Psi^\dagger \mathscr{H}_s \Psi$ can be chosen to satisfy (the sign implements Fermi statistics)

$$\mathscr{C}\mathscr{H}_s^T\mathscr{C} = -\mathscr{H}_s. \tag{9.127}$$

In this form, the charge conjugation symmetry ensures that the eigenstates will appear in $\pm E$ pairs.[8] Keeping only one set of pairs will ensure that we do not double count. Using this symmetry, we can formally diagonalize the Hamiltonian by a unitary transformation $\mathscr{U}$ such that:

$$\mathscr{U}^\dagger \mathscr{H}_s \mathscr{U} = \tfrac{1}{2} \begin{pmatrix} \mathbf{E} & \mathbf{0} \\ \mathbf{0} & -\mathbf{E} \end{pmatrix} \tag{9.128}$$

where $\mathbf{E} = \mathrm{diag}(E_i)$ is diagonal. The columns of the matrix $\mathscr{U}$ are the (ortho)normalized wave-functions and describe the "coherence" factors. To determine the correct expres-

[8] Suppose $\mathscr{H}_s\psi = \varepsilon\psi$. Applying (9.127), using $\mathscr{C}^2 = \mathbf{1}$, and taking the transpose imply that $\psi^T\mathscr{C}^T\mathscr{H}_s = -\varepsilon\psi^T\mathscr{C}^T$. Since left and right eigenvalues are the same, this implies that there is some other state such that $\mathscr{H}_s\tilde{\psi} = -\varepsilon\tilde{\psi}$. For Hermitian Hamiltonians, $\mathscr{H}_s = \mathscr{H}_s^\dagger$, hence, the other state can be directly constructed as $\tilde{\psi} = \mathscr{C}\psi^*$.

sions for the densities in terms of the wavefunctions we form them in the diagonal basis and then transform back to the original basis using $\mathscr{U}$.

Despite this formal degeneracy of eigenstates, we are not aware of a general technique to block-diagonalize the original Hamiltonian in the presence of non-zero terms of the form $\langle a^\dagger b\rangle$, though perhaps the symmetry might be incorporated into the eigensolver.

9.6.2.2 Two-component Formalism

If $\langle a^\dagger b\rangle = 0$, however, then the Hamiltonian is naturally block diagonal:

$$\mathscr{H}_s = \frac{1}{2}\begin{pmatrix} \mathbf{H}_s & \mathbf{0} \\ \mathbf{0} & -\mathbf{H}_s^T \end{pmatrix}, \qquad H_s = \psi^\dagger \mathbf{H}_s \psi + \text{const}, \tag{9.129}$$

and one may consider only a single block in terms of the reduced set of operators

$$\psi = \begin{pmatrix} a \\ b^\dagger \end{pmatrix}. \tag{9.130}$$

This directly avoids any double counting issues. This system may be diagonalized:

$$\mathbf{H}_s \mathbf{U} = \mathbf{U}\mathbf{E}. \tag{9.131}$$

The matrix $\mathbf{U}$ defines the single "quasi"-particle operators ϕ as linear combination of the physical particle operators contained in ψ:

$$\phi = \mathbf{U}^\dagger \psi. \tag{9.132}$$

The Hamiltonian is diagonal in this basis

$$H_s = \phi^\dagger \cdot \mathbf{E} \cdot \phi \tag{9.133}$$

and hence expectation values may be directly expressed

$$\langle \phi \phi^\dagger \rangle = \theta_\beta(\mathbf{E}) = \begin{pmatrix} \theta_\beta(E_0) & & & \\ & \theta_\beta(E_1) & & \\ & & \ddots & \\ & & & \theta_\beta(E_n) \end{pmatrix}$$

where $1 - \theta_\beta(E) = f_\beta(E)$ is the appropriate distribution function: For fermions we have

$$\theta_\beta(E) = \frac{1}{1 + e^{-\beta E}}. \tag{9.134}$$

At $T = 0$ this reduces to $\theta_0(E) = \theta(E)$ and is equivalent to the zero-temperature property that negative energy states are filled while positive energy states are empty.

This may be simply transformed back into the original densities (on the diagonal) and anomalous densities (off-diagonal):

$$\mathbf{F}_+ = \langle \psi \psi^\dagger \rangle = \begin{pmatrix} \langle aa^\dagger \rangle & \langle ab \rangle \\ \langle b^\dagger a^\dagger \rangle & \langle b^\dagger b \rangle \end{pmatrix} = \mathbf{U} \theta_\beta(\mathbf{E}) \mathbf{U}^\dagger,$$
$$\mathbf{F}_-^T = \langle \psi^* \psi^T \rangle = \begin{pmatrix} \langle a^\dagger a \rangle & \langle a^\dagger b^\dagger \rangle \\ \langle ba \rangle & \langle bb^\dagger \rangle \end{pmatrix} = \mathbf{U}^* \theta_\beta(-\mathbf{E}) \mathbf{U}^T.$$

Fermi statistics demands $\mathbf{F}_- + \mathbf{F}_+ = \mathbf{1}$ but we may have to relax this requirement somewhat in order to regulate the theory in terms of an energy cutoff $\theta_c(E)$. The columns of $\mathbf{U}_n$ of $\mathbf{U}$ correspond to the single-particle "wavefunctions" for the state with energy E_n. We partition these into two components sometimes referred to as "coherence factors"

$$\mathbf{U}_n = \begin{pmatrix} \mathbf{u}_n \\ \mathbf{v}_n \end{pmatrix}. \tag{9.135}$$

The unitarity of $\mathbf{U}$ imposes the conditions that

$$\mathbf{u}_m^\dagger \mathbf{u}_n + \mathbf{v}_m^\dagger \mathbf{v}_n = \delta_{mn}, \tag{9.136a}$$
$$\sum_n \mathbf{u}_n \mathbf{u}_n^\dagger = \sum_n \mathbf{v}_n \mathbf{v}_n^\dagger = \mathbf{1}, \tag{9.136b}$$
$$\sum_n \mathbf{u}_n \mathbf{v}_n^\dagger = \sum_n \mathbf{v}_n \mathbf{u}_n^\dagger = \mathbf{0}. \tag{9.136c}$$

From this we may read off the expressions for the densities

$$\mathbf{n}_a = \langle a^\dagger a \rangle = \sum_n \mathbf{u}_n^* \mathbf{u}_n^T \theta_\beta(-E_n), \tag{9.137a}$$
$$\mathbf{n}_b = \langle b^\dagger b \rangle = \sum_n \mathbf{v}_n \mathbf{v}_n^\dagger \theta_\beta(E_n), \tag{9.137b}$$
$$\nu = \langle ab \rangle = \sum_n \mathbf{u}_n \mathbf{v}_n^\dagger \theta_\beta(E_n) \tag{9.137c}$$
$$= -\sum_n \mathbf{u}_n \mathbf{v}_n^\dagger \theta_\beta(-E_n) \tag{9.137d}$$
$$= \sum_n \mathbf{u}_n \mathbf{v}_n^\dagger \frac{\theta_\beta(E_n) - \theta_\beta(-E_n)}{2}. \tag{9.137e}$$

The last form for ν must be used if the regulator is implemented such that $\theta_c(E) + \theta_c(-E) \neq 1$, in particular, if $\theta_c(E) = 0$ for $|E| > E_c$. Note that these expressions are basis independent, e.g. in position space:

$$n_a(\mathbf{r}, \mathbf{r}') = \sum_n u_n(\mathbf{r})^* u_n(\mathbf{r}')^T \theta_\beta(-E_n). \tag{9.138}$$

The energy E_n here is the energy determined by solving these equations and will contain both positive and negative energies.